NASA TECHNICAL REPORT

NASA TR R-386

NASA TR R-386

CONVECTION IN THE TANKS OF A ROTATING SPACECRAFT

by Computational Fluid Dynamics Branch

Ames Research Center

Moffett Field, Calif. 94035

NATIONAL AERONAUTICS AND SPACE ADMINISTRATION • WASHINGTON, D. C. • JUNE 1972

1. Report No. NASA TR R- 386	2. Government Accession No.	3. Recipient's Catalog No.
4. Title and Subtitle CONVECTION IN THE TANKS OF A ROTATING SPACECRAFT		5. Report Date June 1972 6. Performing Organization Code
7. Author(s) Computational Fluid Dynamics Branch		8. Performing Organization Report No. A–4224 10. Work Unit No. 129–04–20–01–00–21
9. Performing Organization Name and Address NASA Ames Research Center Moffett Field, Calif., 94035		11. Contract or Grant No.
12. Sponsoring Agency Name and Address National Aeronautics and Space Administration Washington, D. C. 20546		13. Type of Report and Period Covered Technical Report 14. Sponsoring Agency Code
15. Supplementary Notes		

16. Abstract

This collection of papers describes a general study of convection and mixing of a stratified fluid in a rotating container, with application to the special problem of fluid heating and convection in a spacecraft tank. The analysis is based on a set of approximate equations for the Navier-Stokes description of fluid convection with small density variations in a rotating system including effects of body forces due to temperature stratification (caused by a heater) and arbitrary time-dependent rotation of the tank about a noncentral axis. A highly efficient numerical finite-difference scheme and computational method are described for the convection of vorticity and energy in a two-dimensional tank. For a fluid such as oxygen in a supercritical cryogenic state near the critical point, the thermodynamic properties must be accurately represented. Efficient methods are developed for these evaluations. Special procedures are developed for analysis of the thermodynamic states resulting from the approximate flow equations derived for small density variations. Results of the numerical simulation are presented for studying the effectiveness of rotation maneuvers in mixing stratified oxygen in the tanks of an Apollo spacecraft. Significant effects of the rotation maneuvers are discussed, including in particular the reduction of the potential for pressure collapse.

STAR Categories and Key Words for Individual Chapters:

Chapter 1: STAR Category 12, Fluid Mechanics; Key words – convection, stratified fluids, spacecraft, Apollo, pressure collapse.

Chapter 2: STAR Category 12, Fluid Mechanics; Key words – convection, stratified fluid, rotating system, compressible, viscous.

Chapter 3: STAR Category 19, Mathematics, Key words – numerical analyses, convection, dissipation, Navier-Stokes, Poisson equation, finite difference.

Chapter 4: STAR Category 23, Physics, General; Key words – cryogenic, equations of state, oxygen, volume averages.

Chapter 5: STAR Category 12, Fluid Mechanics; Key words – Apollo, oxygen tank, cryogenic, stratified fluid, natural convection, computational methods.

Chapter 6: STAR Category 12, Fluid Mechanics; Key words – Apollo, oxygen tank, cryogenic, stratified fluid, natural convection.

17. Key Words (Suggested by Author(s)) (Overall report)	18. Distribution Statement
Convection Stratified fluid Computational methods Cryogenic thermodynamics Apollo Pressure collapse	Unclassified – Unlimited

19. Security Classif. (of this report)	20. Security Classif. (of this page)	21. No. of Pages	22. Price*
Unclassified	Unclassified	147	$3.00

* For sale by the National Technical Information Service, Springfield, Virginia 22151

TABLE OF CONTENTS

TABLE OF CONTENTS - Continued

PRINCIPAL NOTATION

$A_i^{(1)}(T), A_i^{(2)}(T)$	coefficients in modified virial formulation of the thermal equation of state (ch. 4)
a	van der Waals parameter (ch. 5)
$\underset{\sim}{a}$	linear acceleration of noninertial system (may be taken to include any body forces)
a_1, a_2	x and y components of $\underset{\sim}{a}$ (dimensional or dimensionless; see eqs. (2.95))
b	van der Waals parameter (ch. 5)
c_p	specific heat at constant pressure, $(\partial h/\partial T)_p$
c_v	specific heat at constant volume (or density), $(\partial e/\partial T)_\rho$
E	total internal energy in the tank; also displacement operator in chapter 3
e	specific internal energy
$\underset{\sim}{e}_1, \underset{\sim}{e}_2, \underset{\sim}{e}_3$	Cartesian unit base vectors in the directions of x, y, z (with $\underset{\sim}{e}_3$ along the rotation axis)
$\underset{\sim}{e}_r, \underset{\sim}{e}_\theta, \underset{\sim}{e}_z$	unit vectors, respectively, in the directions of increasing r, θ, z in cylindrical coordinates
$\underset{\sim}{e}_r, \underset{\sim}{e}_\phi, \underset{\sim}{e}_\theta$	unit vectors, respectively, in the directions of increasing r, φ, θ in spherical coordinates (fig. 2.3)
$F(\tau)$	continuous temperature distribution function (ch. 4)
F_N	discrete temperature distribution function (ch. 5 and 6)
G_1, G_2	dimensionless forms of apparent-body-force components (ch. 2)
Gr	Grashof number (eqs. (2.95b))
$\underset{\sim}{g}$	total apparent body force per unit mass in the noninertial system
g_1, g_2	x and y components of $\underset{\sim}{g}$
$g_i^{(1)}(\rho), g_i^{(2)}(\rho)$	functions in the modified virial formulation of the equations of state (ch. 4)

g_r, g_θ	r and θ components of $\underset{\sim}{g}$ in cylindrical coordinates
H	dimensionless temperature (eqs. (2.95) in ch. 2)
h	specific enthalpy
$\underset{\sim}{I}$	unit tensor in chapter 2; unit matrix in chapter 3
i	$\sqrt{-1}$
JH	JM-1 in chapter 3
JM,KM	maximum values of the indices j,k
j	index for finite differencing in x direction
k	thermal conductivity; also index for finite differencing in y direction
L	arbitrary reference length; also an integer in chapter 3
ℓ	length of side of square tank; also a recursion index in chapter 3
M	mass of oxygen in the tank; also integer equal to JM-2 in chapter 3
N	index for discrete temperature distribution function and corresponding thermodynamic variables (see ch. 4 and 5)
n	index for finite differencing in time (ch. 3 and 5)
Pr	Prandtl number, $\rho_o \nu c_p / k$
p	thermodynamic pressure
p_a	pressure calculated from an analytical representation in chapter 4
p_p	pressure p_a modified to give a true physical representation when p_a is multivalued (ch. 4)
$p_v(T)$	vapor pressure
$\underset{\sim}{q}$	heat flux vector
$\underset{\sim}{R}$	perpendicular vector from axis of rotation to point of interest (ch. 2)
$\underset{\sim}{R}^*$	position vector from fixed point on axis of rotation to a point in the noninertial (rotating) system (ch. 2)
R	gas constant; also magnitude of vector $\underset{\sim}{R}$ in chapter 2

R_c	distance from axis of rotation to center of tank
R_1, R_2	x and y components of $\underset{\sim}{R}$
Re	Reynolds number, $\Omega_o L^2/\nu$
r, θ, z	cylindrical coordinates fixed relative to tank, with origin at tank center and with θ measured from perpendicular to R_c
r, ϕ, θ	spherical coordinates fixed in a rotating system, depicted in figure 2.3
S	unit step function
T	temperature of fluid
$\overline{T}$	temperature of fluid averaged over space
T_R	reference temperature (see ch. 5)
t	time
U	dimensionless velocity in x direction (eqs. (2.95)); also internal energy function in chapter 4
u, v, w	x, y, z components of $\underset{\sim}{V}$
$\underset{\sim}{V}$	fluid velocity relative to noninertial system fixed on the tank
$\underset{\sim}{V}^*$	velocity projection defined in various ways in chapter 2
V	dimensionless velocity in y direction (eqs. (2.95)); also volume in chapter 5
V_T	volume of oxygen tank
v_r, v_θ, v_z	r, θ, z components of $\underset{\sim}{V}$
v_r, v_ϕ, v_θ	r, ϕ, θ components of $\underset{\sim}{V}$
W_{jk}	computational weighting function (ch. 4 and 5)
x, y, z	Cartesian coordinates fixed relative to the tank, with origin at one corner
Z	compressibility factor in thermal equation of state
α	isothermal compressibility coefficient at state p_o, T_o in chapter 2; also Courant number in chapter 3
β	thermal-expansion coefficient at state p_o, T_o in chapter 2; also $\mu\Delta\tau/(\Delta\xi)^2$ in chapter 3

δ $(\rho - \rho_o)/\rho_o$

η dimensionless coordinate, y/L

κ bulk viscosity coefficient

λ second viscosity coefficient in chapter 2; also ratio $\phi(\tau+\Delta\tau)/\phi(\tau)$ in chapter 3

λ_j eigenvalue of a matrix in chapter 3

μ coefficient of shear viscosity in chapter 2; also a model diffusivity in chapter 3

ν kinematic viscosity coefficient, $(\mu/\rho)_o$

ξ dimensionless coordinate, x/L

ρ density of fluid

$\overline{\rho}$ density of fluid averaged over space

$\underset{\sim}{\sigma}$ total stress tensor

$\underset{\sim}{\tau}$ viscous stress tensor

τ dimensionless time (eqs. (2.95)); also dimensionless temperature in chapter 4, eq. (4.25)

Φ viscous dissipation function, $(1/\mu)\underset{\sim}{\tau}:\underset{\sim}{\nabla}\underset{\sim}{V}$

ϕ time-dependent scalar potential of acceleration $\underset{\sim}{a}$ in chapter 2; also a model dependent variable in chapter 3

Ψ dimensionless stream function (eqs. (2.95))

ψ stream function representing $\underset{\sim}{V}^*$ in chapter 2

$\underset{\sim}{\Omega}, \Omega$ vector and magnitude of time-dependent angular velocity of noninertial system relative to inertial system; $\underset{\sim}{\Omega} = \underset{\sim}{e}_3\Omega$; (either dimensional or dimensionless; eqs. (2.95))

$\dot{\underset{\sim}{\Omega}}, \dot{\Omega}$ respectively, $d\underset{\sim}{\Omega}/dt$ and $d\Omega/dt$

Ω_o constant reference value of Ω

$\underset{\sim}{\omega}$ vorticity vector, curl $\underset{\sim}{V}$

ω z component of vorticity (either dimensional or dimensionless; eqs. (2.95))

Subscripts

c	thermodynamic state at the critical point
col	collapse state (ch. 4 and 5)
j	index for finite differencing in x direction
k	index for finite differencing in y direction
N	index for discrete temperature distribution function and corresponding thermodynamic variables (ch. 4 and 5)
n	index for finite differencing in time
SL	saturated liquid
SV	saturated vapor
o	slowly varying value of a thermodynamic variable averaged over all space (except for Ω); also a value corresponding to a reference temperature of 55° K^{o} in eq. (4.5b); also an initial value in chapter 5

Superscripts

n	index for finite differencing in time
$(\bar{\ })$	slowly varying value of a thermodynamic variable averaged over all space
$(\tilde{\ })$	value computed from "predictor" in chapter 3

1. AN OVERVIEW OF THE ROTATING SPACECRAFT-TANK CONVECTION PROBLEM

E. Dale Martin

SUMMARY

This introductory article provides the background for the succeeding articles comprising a study of convection in the tanks of a rotating spacecraft. The discussion relates the analysis of mixing of a stratified fluid in a supercritical cryogenic state (e.g., oxygen, in which mixing fans may not be used) to spacecraft such as Apollo and orbiting space stations.

INTRODUCTION

This report describes a general study of convection and mixing of a stratified fluid in a rotating container and its application to the special problem of fluid heating and convection in a spacecraft tank. In a rotating container, spatial variations of temperature and density lead to "natural convection" under the action of the effective body forces induced by the rotation. Simultaneously, time-dependent rotation of the container may induce "forced convection" coupled with the effects of stratification (see ch. 2).

The study reported here began with the need to analyze the oxygen storage system used in an Apollo spacecraft, as outlined in the next section. Therefore, although the study applies to spacecraft fluid storage systems in general (including, e.g., orbiting space stations), the following conditions are imposed (at certain stages in the study) in the specific application to an Apollo oxygen tank: the fluid considered is oxygen in a supercritical cryogenic state, near the critical point (where the fluid is not distinguishable as being either a gas or a liquid); the system is free of gravitational forces; and the container is rotating about a noncentral axis.

In a near-critical thermodynamic state, a fluid such as oxygen may undergo a phenomenon known as "pressure collapse," which is a local rapid decrease in pressure resulting from the sudden mixing of a thermally stratified fluid. The potential pressure drop (also called "potential pressure decay" and "potential for pressure collapse") is defined as the difference between the pressure in a thermally stratified environment and the pressure that would be present if the stratified fluid were suddenly mixed adiabatically into a uniform state. Thus, because of the nature of the state relations in the near-critical region (where the state is highly sensitive to changes in temperature), sudden mixing of a significantly stratified supercritical fluid results in a substantial pressure drop. From many state points, such an occurrence would drive the fluid into the undesirable two-phase state, where vapor and liquid can coexist. The sudden decrease in pressure may render inoperative the systems (such as fuel cells and life support) intended to be supplied by the oxygen-storage system. This phenomenon of pressure collapse can be prevented by limiting the stratification, which is done by keeping the fluid sufficiently mixed. (Slow mixing limits the possibility of sudden mixing.)

From the above description, one can surmise that results of calculations of flow of a near-critical fluid may be highly dependent on accurate

representation of the thermodynamic properties (cf. ch. 4 and 6). Near-critical fluids also have low viscosity coefficients and high thermal expansion coefficients (ref. 1, p. 660 ff) so there will be strong coupling between the natural convection and the forced convection due to time-dependent rotation (cf. ch. 2).

The goals of the study reported here are to simulate - by numerical analysis and computation - the fluid motion, the energy transfer, and the mixing of a fluid under the above conditions, and to determine in particular the effectiveness of the mixing resulting from rotation maneuvers in reducing the potential pressure drop in the cryogenic oxygen-storage system used in spacecraft such as the Apollo.

BACKGROUND FROM APOLLO

In spacecraft such as Apollo, supercritical cryogenic storage of oxygen and hydrogen is highly desirable because a large mass of the fluid can be stored at very high density, and therefore in a small volume, at pressures low enough for reasonably lightweight tanks.

The Apollo oxygen tanks are located in the service module as shown in figure 1.1 for Apollo 13. The tanks are spheres with inside diameters of 25 in. and with distances from the spacecraft axis to the sphere centers of 3 ft (tank 1) and about 5 ft (tank 2). With the assumption that the center of mass of the vehicle is on the central axis, these distances are then the "rotation arms" of the spheres when the vehicle rotates in space. Each tank is loaded initially with 330 lb of liquid oxygen. The oxygen is then heated by an internal electrical heater (see fig. 1.2) to completely vaporize the oxygen. Subsequently, the heater is operated periodically to maintain a system design pressure of 900 ±35 psia. The maintenance of system pressure by the heater operation is required because pressure is changed both by "heat leak" (heat conduction into the tank) at the imperfectly insulated wall and by withdrawal of fluid from the tank. Pressure sensors switch on the heater when the pressure drops to the desired lower limit and switch off the heater at the upper pressure limit. These "heater cycles" and corresponding "pressure cycles" are discussed in chapter 6.

If there were no convection of the fluid (in zero gravity) during heater operation, strong temperature and density gradients would develop because of the inefficiency of pure heat conduction for energy transfer. Each heater cycle results in increasingly severe gradients; therefore, a significant potential pressure drop would develop so that a small subsequent acceleration could result in pressure collapse. Adequate slow mixing of the fluid therefore is required to prevent severe stratification.

In manned space missions prior to Apollo 14, electrically driven fans inside the oxygen tanks (see fig. 1.2) were used to ensure sufficient circulation of the fluid. A series of incidents resulted in electric arcing of the fan wiring in the no. 2 oxygen tank of Apollo 13, with combustion of Teflon

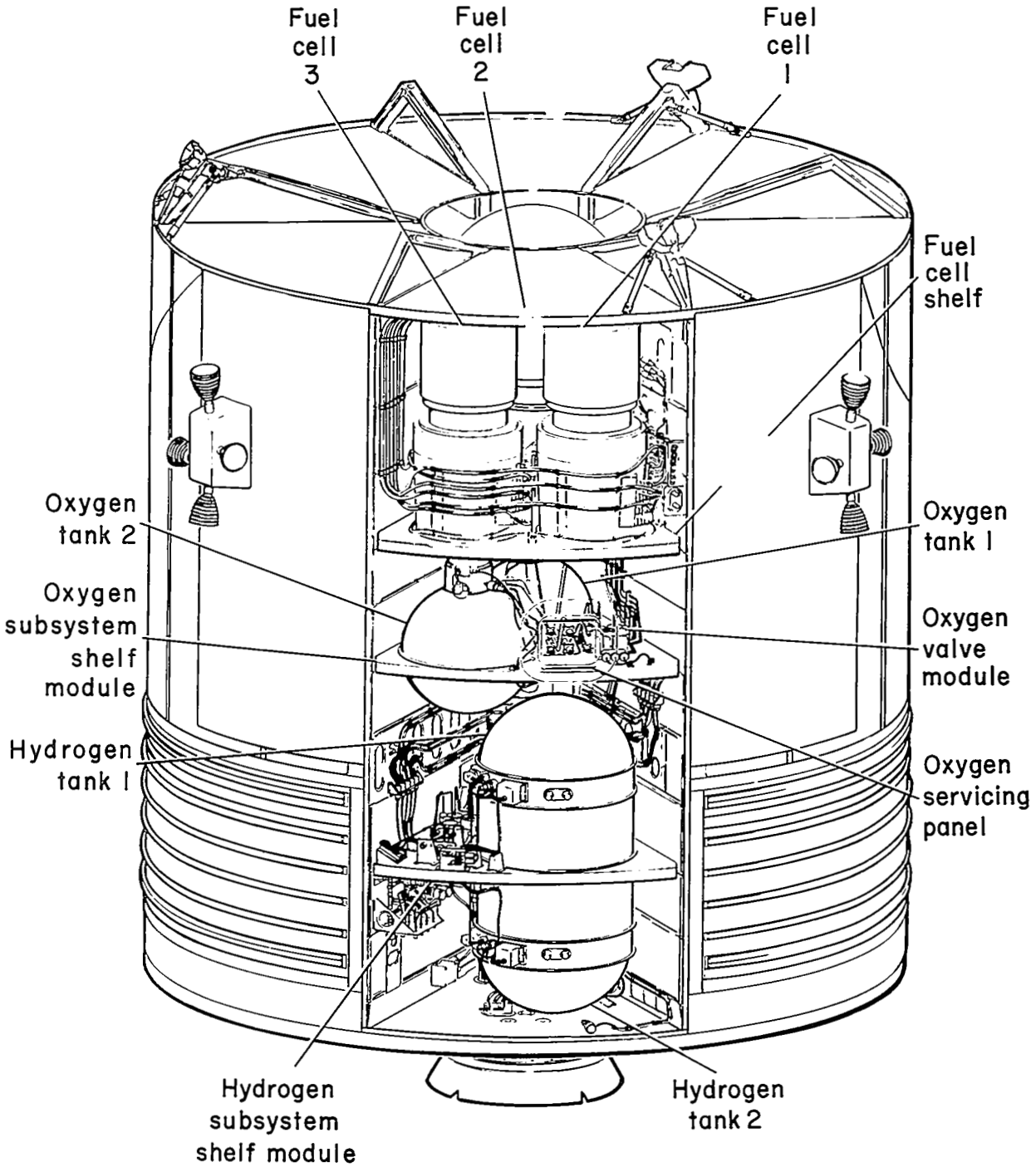

Figure 1.1– Arrangement of fuel cells and cryogenic systems in bay 4 of Apollo 13 service module.

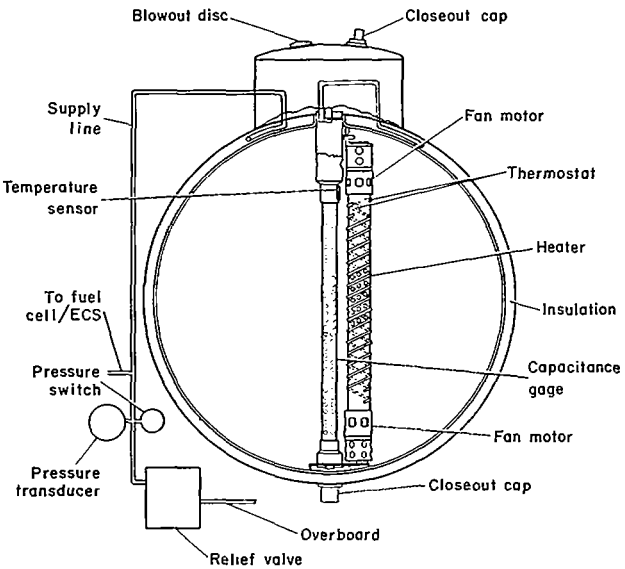

Figure 1.2.– Oxygen tank no. 2 internal components (Apollo 13).

wire insulation leading to failure of the conduit-entry plug, a sudden release of pressure from the tank, and ultimate abortion of the mission.

In June 1970, the Apollo 13 Review Board recommended removal of the wiring and fan motors, and also suggested further investigation of the need for stirring in the cryogenic oxygen-storage system. In the redesign effort by NASA Manned Spacecraft Center, an Apollo Cryogenic Oxygen Tank Analysis Team was established, with one function being to analyze the stratification problem. Various investigators contributed to that team effort. With the stratification established as possibly crucial by the team, one problem was to determine the adequacy of vehicle rotation and maneuvers to produce sufficient convection for the required mixing in the oxygen tanks, without fans. The contributions by Ames Research Center were based on the studies described in this report; preliminary results were reported at a meeting of the analysis team by B. Baldwin and Y. Sheaffer in January 1971 and at the NASA-MSC Cryogenics Symposium by B. Baldwin, E. D. Martin, W. A. Reinhardt, and Y. Sheaffer in May 1971.

APPROACH AND SCOPE OF THE STUDY

The format of this report, a collection of separate but related articles as chapters, is used because each article makes contributions both to the overall subject of the report and to general knowledge in separate specialized fields.

In chapter 2, Martin and Baldwin develop a set of approximate equations for the Navier-Stokes description of fluid convection in a rotating system, including the influence both of effective buoyancy body forces due to temperature and density stratifications and of arbitrary time-dependent rotation and acceleration of the tank. The equations represent a small-density-variation approximation that is valid under conditions of low relative velocity but with significant density and temperature variations. All relevant terms representing effects of rotation and changes in rotation are included. For example, the analysis includes the Coriolis terms known to be significant in the three-dimensional flow, as shown by experiments with dye injected into a water-filled rotating sphere (unpublished results by J. F. Lands, Jr., and R. C. Ried, Jr., reported at a meeting of the Apollo Tank Analysis Team in January 1971). The equations are valid for combined forced and contained natural convection, whereas previous treatments of convection in rotating systems had

dealt with either pure natural convection or pure forced convection. For subsequent computations, the two-dimensional square-tank problem is formulated.

In chapter 3, Lomax and Bailey describe a numerical finite-differencing scheme for computing the convection of vorticity and energy in a two-dimensional rotating tank, starting with the partial differential equations derived in chapter 2. The highly efficient computational method employs at each time step a Buneman Poisson solver for the Poisson equation relating the stream function to vorticity, and uses MacCormack's method for the transport equations for vorticity and energy.

Reinhardt then develops efficient and versatile methods for the numerical evaluation of thermodynamic properties of cryogenic oxygen from semiempirical equations (ch. 4). For reasons discussed above, accurate thermodynamic-property representations are needed for computations in the near-critical region. In the efficient methods developed, an arbitrary choice of independent state variables is allowed. A procedure for the rapid evaluation of volume integrals of spatially dependent quantities is introduced that depends on temperature distribution functions. By this method, insignificant losses in accuracy are accepted in exchange for significant savings in computation time.

In chapter 5, Baldwin, Reinhardt, and Sheaffer discuss how the results based on the small-density-variation approximation (with density considered only as a function of temperature and with pressure as a slowly varying parameter) can be interpreted to determine the thermodynamic quantities. The latter include the slowly varying average pressure, the actual density distribution, and the potential pressure drop. The problem of evaluating the time-dependent thermodynamic state of stratified fluid is considered based on (1) van der Waals equations of state, and (2) more exact thermodynamic relations.

In chapter 6, Baldwin, Reinhardt, and Sheaffer present results of the numerical simulation for studying the effectiveness of rotation reversal and spinup from rest on mixing stratified oxygen in the Apollo storage tanks. The computations are two-dimensional simulations based on the complete equations developed in chapter 2, with use of the methods from chapters 4 and 5 for the accurate thermodynamics and efficient evaluations, and with use of the computational method described in chapter 3. The significant effects of the rotation maneuvers on the potential pressure drop are discussed.

Each chapter concludes with a list of references.

REFERENCE

1. Ostrach, S.: Laminar Flows with Body Forces. Section F in Theory of Laminar Flows, F. K. Moore, ed., Vol. IV of High Speed Aerodynamics and Jet Propulsion, Princeton Univ. Press, 1964, pp. 528-718.

2. FLOW EQUATIONS GOVERNING COMBINED FORCED AND NATURAL CONVECTION FOR APPLICATION IN A ROTATING TANK

E. Dale Martin and Barrett S. Baldwin

SUMMARY

A set of simplified equations is derived that represents a small-density-variation approximation of the Navier-Stokes equations for combined forced and contained natural convection of a stratified fluid. These equations reduce to a generalization of the Boussinesq approximation in the special case of steady rotation with (variable) buoyancy body forces, but also properly represent the forced convection due to time-dependent rotation. For use in subsequent numerical computations, the problem of convection in a rotating square tank with temperature and density stratifications is formulated.

INTRODUCTION

In this chapter, equations for fluid convection in a tank with arbitrary time-dependent rotation are developed from the Navier-Stokes equations. Simplified forms of these equations are obtained for use in numerical computation of the fluid convection in noninertial coordinate systems. Conditions assumed to exist in the rotating tank are small temperature and density variations and small apparent body forces.

To clarify the relationship of the present problem to other convection problems, consider the terminology of, and conditions for, various classes of convection. Two special cases of convection (flow) are forced convection and natural convection (see Prandtl, ref. 1, pp. 396 and 412). Natural convection is further divided into cases of free convection and contained natural convection. Natural convection implies that no causes of the motion exist other than effective body forces acting on portions of the fluid with density variations due to thermal expansion. In that case, effects of pressure and apparent body forces can be expressed entirely in terms of *buoyancy* forces. The fluid convection associated with the present problem is generally a combination of natural and forced convection. In the special (or limiting) case of steady rotation it reduces to the state of contained natural convection.

Whenever a fluid flow is at low velocity relative to boundaries, with relatively small accompanying temperature and density variations, one usually considers the highly simplifying assumption of "constant density" of the fluid flow. A complication arises, however, when temperature differences, producing density variations that are acted upon by body forces, are a significant cause of the convection. Obviously, density variations must be accounted for in the body-force terms (the momentum *production*), if not in other aspects of compressibility of the fluid flow. The usual approximate method of treating problems of nearly constant-density flow with "buoyancy" body forces (cf. ref. 1, p. 412; ref. 2, p. 320; ref. 3, p. 248) is commonly known as the Boussinesq approximation (e.g., ref. 4, p. 506; ref. 5, p. 684; ref. 6, p. 29), and has been applied to natural convection driven by constant body forces. That approximation has recently been generalized to include spatially varying body forces in a uniformly rotating container (see, e.g., refs. 7-9).

The Boussinesq approximation and its generalization to variable body forces apply only to pure natural convection, and are not sufficiently general for present purposes (with time-varying rotation rates producing forced convection). Forced convection in rotating flows of homogeneous fluids has been studied extensively (e.g., refer to ref. 8), especially with reference to the "spinup" and "spindown" problems. The early fundamental treatments by von Kármán and Cochran and by Bödewadt (see ref. 10, pp. 157-162) showed fundamental differences between the spinup and spindown problems in three dimensions because of instabilities. A recent study by Briley and Walls (ref. 11) indicates that these effects also occur in a tank rotating about its center and lead to Taylor vortices in the spindown problem at some Reynolds numbers. The rotating forced-convection flows that have been studied did not include stratification effects, that is, body forces due to density variations.

In the present study, a small-density-variation approximation is developed in a manner analogous to the Boussinesq approximation, including both variable buoyancy body forces in a stratified fluid and the allowance for forced convection produced by time-varying rotation. Thus, the formulation is developed both to be consistent with the physics of the time-varying rotation (forced convection) and to reduce to a formulation for pure natural convection in the limiting case of steady rotation that is analogous to the Boussinesq approximation.

The development procedure is to first write the compressible Navier-Stokes system of equations in vector form in an arbitrary noninertial frame of reference. Then the set of equations is reduced to an approximate form for nearly constant density flow, accounting properly for all body-force terms in the limit as the temperature and density variations vanish. (It will be seen that both the momentum and energy conservation equations require special consideration for the present problem.) For convenience in numerical analysis, the equations are then cast in terms of the vorticity and stream functions. The special case of a constant inertial axis of rotation and the further specialization to two-dimensional flow are formulated. The two-dimensional equations in rectangular coordinates are presented for use in computation of convection in a square tank.

Although three-dimensional effects such as axial flow due to Ekman-layer suction (see, e.g., ref. 8) and development of Taylor vortices (e.g., ref. 11) cannot be represented in the two-dimensional formulation, the first numerical treatments of this problem in two dimensions are expected to yield significant information regarding the adequacy of vehicle rotation to produce sufficient convection. Because additional convection mechanisms are supplied by three-dimensional effects, the results from the two-dimensional formulation are believed to be conservative.

COMPRESSIBLE NAVIER-STOKES EQUATIONS IN A TIME-VARYING ROTATING REFERENCE FRAME

The Navier-Stokes set of equations for compressible flow in a noninertial (rotating and accelerating) reference frame is

$$\frac{D\rho}{Dt} + \rho \nabla \cdot \underset{\sim}{V} = 0 \tag{2.1}$$

$$\rho \frac{D\underset{\sim}{V}}{Dt} = -\nabla p + \nabla \cdot \underset{\sim}{\tau} + \rho \underset{\sim}{g} \tag{2.2}$$

$$\rho \frac{De}{Dt} = -p \nabla \cdot \underset{\sim}{V} - \nabla \cdot \underset{\sim}{q} + \mu \Phi \tag{2.3a}$$

where D/Dt is the substantial-derivative operator

$$\frac{D}{Dt} = \frac{\partial}{\partial t} + \underset{\sim}{V} \cdot \nabla$$

and where, for later use, equation (2.3a) may also be written in an equivalent form, in terms of specific enthalpy (ref. 2, p. 322), as

$$\rho \frac{Dh}{Dt} = \frac{Dp}{Dt} - \nabla \cdot \underset{\sim}{q} + \mu \Phi \tag{2.3b}$$

The set of equations must be supplemented by appropriate equations of state:

$$\left.\begin{aligned} \rho &= \rho(p,T) \\ e &= e(p,T) = \int c_v \, dT \\ h &= h(p,T) = \int c_p \, dT \end{aligned}\right\} \tag{2.4}$$

In the above equations, the Navier-Stokes expression for the viscous stress tensor $\underset{\sim}{\tau}$, defined by

$$\underset{\sim}{\sigma} = -p\underset{\sim}{I} + \underset{\sim}{\tau} \tag{2.5}$$

(where p is the thermodynamic pressure, $\underset{\sim}{I}$ is the unit tensor, and $\underset{\sim}{\sigma}$ is the total stress tensor), is

$$\underset{\sim}{\tau} = \lambda(\nabla \cdot \underset{\sim}{V})\underset{\sim}{I} + \mu[\nabla\underset{\sim}{V} + (\nabla\underset{\sim}{V})_t] \tag{2.6}$$

where

μ	shear viscosity coefficient
$\lambda \equiv \kappa - \frac{2}{3}\mu$	"second viscosity coefficient"
$\kappa \equiv \frac{-(1/3)\underset{\sim}{I} : \underset{\sim}{\sigma} - p}{\nabla \cdot \underset{\sim}{V}}$	bulk viscosity coefficient
$(\nabla\underset{\sim}{V})_t$	"transpose" of the dyadic $\nabla\underset{\sim}{V}$

Also in equations (2.3), the viscous dissipation function Φ is defined by

$$\mu\Phi \equiv \underset{\sim}{\tau} : \underset{\sim}{\nabla}\underset{\sim}{V} \tag{2.7}$$

and the heat-flux vector $\underset{\sim}{q}$ is given by the Fourier heat-conduction law:

$$\underset{\sim}{q} = -k\underset{\sim}{\nabla}T \tag{2.8}$$

Of primary concern here is the apparent body force per unit mass in the noninertial system $\underset{\sim}{g}$, which is given by

$$\underset{\sim}{g} = -[\underset{\sim}{a} + \dot{\underset{\sim}{\Omega}} \times \underset{\sim}{R}^* + 2\underset{\sim}{\Omega} \times \underset{\sim}{V} + \underset{\sim}{\Omega} \times (\underset{\sim}{\Omega} \times \underset{\sim}{R}^*)] \tag{2.9}$$

where

$\underset{\sim}{\Omega}$ time-dependent angular velocity of the noninertial system relative to the inertial system

$\dot{\underset{\sim}{\Omega}} \equiv d\underset{\sim}{\Omega}/dt$

$\underset{\sim}{R}^*$ position vector from a fixed point (0* on fig. 2.1) on the axis of rotation of the noninertial system to a point of interest in the rotating system

$\underset{\sim}{\Omega} \times (\underset{\sim}{\Omega} \times \underset{\sim}{R}^*)$ centripetal acceleration due to rotation of the system

$2\underset{\sim}{\Omega} \times \underset{\sim}{V}$ Coriolis acceleration

$\dot{\underset{\sim}{\Omega}} \times \underset{\sim}{R}^*$ *linear* acceleration due to the angular acceleration $\dot{\underset{\sim}{\Omega}}$

$\underset{\sim}{a} = \underset{\sim}{a}(t)$ (time-dependent) *linear* acceleration of the noninertial system, in excess of $\dot{\underset{\sim}{\Omega}} \times \underset{\sim}{R}^*$

As an effective body force per unit mass, $\underset{\sim}{a}$ may be taken to include any body forces acting on the gas in the inertial reference frame.

Equations (2.1) through (2.3) are derived directly from the corresponding equations in an *inertial* reference frame by substituting for the term $\rho(D\underset{\sim}{V}/Dt)$, measured relative to the inertial system, the terms

$$\rho\left[\frac{D\underset{\sim}{V}}{Dt} + \dot{\underset{\sim}{\Omega}} \times \underset{\sim}{R}^* + 2\underset{\sim}{\Omega} \times \underset{\sim}{V} + \underset{\sim}{\Omega} \times (\underset{\sim}{\Omega} \times \underset{\sim}{R}^*) + \underset{\sim}{a}\right]$$

(cf. Becker, ref. 12, p. 251). The term $\rho(D\underset{\sim}{V}/Dt)$ is the *only* term in the inertial system affected by the transformation to a noninertial reference frame because it is the only time derivative of a vector function (ref. 12).

At this point it is convenient to define a position vector $\underset{\sim}{R}$ as the perpendicular vector from the axis of rotation to any point of interest determined by $\underset{\sim}{R}^*$ (see fig. 2.1), such that

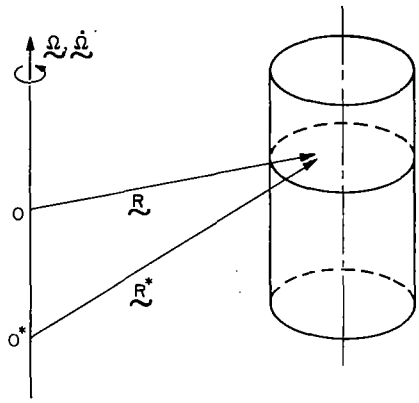

Figure 2.1.– Position vectors in a rotating system.

$$\underset{\sim}{\Omega} \cdot \underset{\sim}{R} = 0 \qquad (2.10)$$

The vector $\underset{\sim}{R}$ always lies in a plane of rotation. Its origin O moves along the axis of rotation as the point of interest inside the tank is varied. Note that

$$\underset{\sim}{\Omega} \times \underset{\sim}{R}^* = \underset{\sim}{\Omega} \times \underset{\sim}{R} \qquad (2.11a)$$

$$\dot{\underset{\sim}{\Omega}} \times \underset{\sim}{R}^* = \dot{\underset{\sim}{\Omega}} \times \underset{\sim}{R} \qquad (2.11b)$$

where the axis of rotation is taken to be constant in inertial space. With equations (2.11), $\underset{\sim}{R}^*$ may be replaced by $\underset{\sim}{R}$ everywhere in equation (2.9), or

$$\underset{\sim}{g} = -[\underset{\sim}{a} + \dot{\underset{\sim}{\Omega}} \times \underset{\sim}{R} + 2\underset{\sim}{\Omega} \times \underset{\sim}{V} + \underset{\sim}{\Omega} \times (\underset{\sim}{\Omega} \times \underset{\sim}{R})] \qquad (2.12)$$

REDUCTION OF EQUATIONS FOR SMALL-DENSITY-VARIATION APPROXIMATION

Equations of State and Small-Perturbation Theory

It is assumed that pressure and temperature variations, and therefore all fluid property variations, are small over the space of the tank and relatively slow in time. The thermal equation of state $\rho = \rho(p,T)$ is then written as a Taylor series about the nearly constant average state defined by $\rho_o = \rho(p_o,T_o)$:

$$\rho = \rho_o + \left[\left(\frac{\partial \rho}{\partial T}\right)_p\right]_o \Delta T + \left[\left(\frac{\partial \rho}{\partial p}\right)_T\right]_o \Delta p + O[(\Delta T)^2,(\Delta p)^2]$$

$$= \rho_o\{1 - \beta\, \Delta T + \alpha\, \Delta p + O[(\Delta T)^2,(\Delta p)^2]\} \qquad (2.13)$$

where

$$\beta \equiv \left[\frac{-1}{\rho}\left(\frac{\partial \rho}{\partial T}\right)_p\right]_o \qquad (2.14a)$$

is the thermal expansion coefficient at the state p_o, T_o,

$$\alpha \equiv \left[\frac{1}{\rho}\left(\frac{\partial \rho}{\partial p}\right)_T\right]_o \qquad (2.14b)$$

is the compressibility of the fluid at the state p_o, T_o, and

$$\Delta T = T - T_o \tag{2.15a}$$

$$\Delta p = p - p_o \tag{2.15b}$$

As is customary in convection problems involving buoyancy forces due to thermal expansion, when pressure gradients are expected to be very small, we neglect not only terms of $O[(\Delta T)^2,(\Delta p)^2]$ in equation (2.13), but also neglect $\alpha\ \Delta p$ in comparison to $\beta\ \Delta T$:

$$\rho \approx \rho_o(1 - \beta\ \Delta T) \tag{2.16}$$

From the resulting flow computations made using equation (2.16), one can always check that $\alpha\ \Delta p/\beta\ \Delta T$ is small everywhere to justify á posteriori the use of (2.16).

By the same procedure as in equations (2.13) through (2.16), the caloric equations of state in (2.4) are simplified by assuming the pressure dependence of e and h to be negligible, so that the differentials de and dh can be written simply as

$$de = c_v\ dT \equiv \left(\frac{\partial e}{\partial T}\right)_\rho dT \tag{2.17a}$$

$$dh = c_p\ dT \equiv \left(\frac{\partial h}{\partial T}\right)_p dT \tag{2.17b}$$

The coefficients α, β, c_v, and c_p must be determined from thermodynamics and are not considered further in the present article.

The formulation involving the flow equations above with equation (2.16) substituted everywhere for ρ can be regarded as a *small-perturbation theory* with

$$\rho \equiv \rho_o(1 + \delta) \tag{2.18a}$$

or

$$\delta \equiv \frac{\rho - \rho_o}{\rho_o} \approx -\beta\ \Delta T \tag{2.18b}$$

where

$$|\delta| \ll 1 \tag{2.19}$$

so that δ can be neglected in comparison to unity. It will be important in formulating the theory *not* to neglect $\rho_o\delta$ in those instances where after substitution of (2.18a) the term ρ_o effectively cancels out of the equations.

Along with the general assumption of small temperature, pressure, and density variations, the transport properties μ and k are taken to be constants at a given time.

If desired, the small-perturbation theory can be extended formally to higher approximations that supply higher-order corrections for significant ΔT and Δp in the Taylor expansions (about the state ρ_o, p_o, T_o) of ρ, h, and the transport properties. The formal small-perturbation theory (with appropriate emphasis on buoyancy effects to make them of lowest order) yields a first-order formulation equivalent to that derived below in a less formal way.

Mass-Conservation and Momentum Equations

In the limit as $\delta \to 0$, one finds conservation of mass (eq. (2.1)), to be approximated by

$$\underline{\nabla} \cdot \underline{V} = 0 \tag{2.20}$$

This equation can henceforth be used in the flow calculation to represent conservation of mass and can be combined with the other equations wherever appropriate.

In deriving the approximation for the momentum-conservation equation as $\delta \to 0$, one could proceed in a manner equivalent to that for the Boussinesq approximation *only if* the angular velocity of the tank were constant. In the present problem, however, we must allow for time-varying angular velocity. Thus, convection in a rotating tank, with fluid-density variations caused by temperature variations, falls essentially into two categories:

1. If the angular velocity of the tank is *constant*, then the conditions are met for the limiting state referred to as "contained natural convection." For that case, in the limit as $\delta \to 0$, the fluid approaches a state in equilibrium with the walls (no relative motion), which is equivalent to a rigid body rotation. If, then, there are small temperature and density variations in the tank, the resulting flow is entirely a small perturbation on the "rigid-body" rotation. In that case, no causes of the motion exist (in the reference frame of the tank) other than the effective body forces acting on portions of the fluid with density differences due to thermal expansion. Then the effects of pressure and apparent body forces can be expressed entirely in terms of *buoyancy* forces, with essentially constant density of the fluid assumed in all other respects. These are the assumptions of the Boussinesq approximation used frequently in special cases of natural convection.

2. If only the *axis* of the angular velocity is constant (in inertial space), but the *magnitude* of rotation changes significantly with time (e.g., a steady rotation is stopped or reversed), then there are factors producing the convection *other than* simply the apparent body forces acting on density differences due to thermal expansion. Sudden changes in the boundary rotation from a previously steady rotation produce boundary layers, with significant velocities at the boundary relative to the internal core. The rotational inertia of the core tends to keep it rotating without substantial change, except for factors such as buoyancy body forces and slight axial flow due to Ekman-layer suction (e.g., see ref. 8), until affected by diffusion of the viscous forces from the boundary. In this case, the assumptions of natural

convection are violated, and a more general formulation must be used. It should, however, for present purposes, include the valid approximate formulation of natural convection in the special case where the rotational velocity is held constant for a period of time.

In the limit as $\delta \to 0$ ($\rho \sim \rho_o$), μ and k approach constant values at a given time, and from (2.6) and (2.20),

$$\begin{aligned} \nabla \cdot \tau &\approx \mu[\nabla \cdot \nabla\nabla + \nabla \cdot (\nabla\nabla)_t] \\ &= \mu[\nabla^2\nabla + \nabla(\nabla \cdot \nabla)] \approx \mu\nabla^2\nabla \end{aligned} \tag{2.21}$$

Assuming that only the apparent-body-force term in (2.2) may be affected by small density variations, we therefore retain δ only in that term and write (2.2) as

$$\frac{D\nabla}{Dt} = -\frac{1}{\rho_o}\nabla p + \nu\nabla^2\nabla + (1 + \delta)g \tag{2.22}$$

By manipulating equation (2.22) in various ways, one can determine in what sense δ must be retained in (2.22) in the limit as $\delta \to 0$. For this, various terms in the quantity g, given by equation (2.12), can be expressed as gradients of scalar quantities. Those portions of $(1 + \delta)g$ that can be so expressed can then be regarded simply as modifications to the pressure gradient term, $(-1/\rho_o)\nabla p$ (which is ultimately to be eliminated from the problem). The various forms equivalent to (2.22) are derived in this and following sections.

First consider the centripetal acceleration, $\Omega \times (\Omega \times R)$. For arbitrary vectors A and B the following vector identity holds (ref. 13, p. 270):

$$A \times (B \times C) \equiv (A \cdot C)B - (A \cdot B)C \tag{2.23}$$

Therefore

$$\Omega \times (\Omega \times R) \equiv (\Omega \cdot R)\Omega - \Omega^2 R \tag{2.24}$$

One can write

$$\Omega = e_3\Omega(t) \tag{2.25}$$

where e_3 is a unit vector in the direction of the axis of rotation, so that with (2.10), equation (2.24) becomes

$$\Omega \times (\Omega \times R) = -\Omega^2 R = -\nabla[(1/2)\Omega^2 R^2] \tag{2.26}$$

Further, consider the fact that since a is, at most, a function of time, $a = a(t)$, then

$$\nabla \times a(t) = 0 \tag{2.27a}$$

so that a scalar potential $\phi = \underset{\sim}{R}^* \cdot \underset{\sim}{a}(t)$ can be defined such that

$$\underset{\sim}{a} = \underset{\sim}{\nabla}\phi \tag{2.27b}$$

satisfies the vector identity

$$\underset{\sim}{\nabla} \times \underset{\sim}{\nabla}\phi = 0 \tag{2.27c}$$

Then equation (2.22), with (2.12), (2.26), and (2.27b), becomes

$$\frac{D\underset{\sim}{V}}{Dt} = -\frac{1}{\rho_o}\underset{\sim}{\nabla}P_1 + \nu\nabla^2\underset{\sim}{V} + \underset{\sim}{g}\delta - (\dot{\underset{\sim}{\Omega}} \times \underset{\sim}{R} + 2\underset{\sim}{\Omega} \times \underset{\sim}{V}) \tag{2.28}$$

where

$$P_1 = p + \rho_o[\phi - (1/2)\Omega^2R^2] \tag{2.29}$$

(with ϕ and Ω both depending on time), which may be called the "reduced pressure" (cf. ref. 8, p. 6, for constant Ω).

On the Use of Stream Functions to Reduce the Coriolis Term

Under some conditions, the following procedure introduces further simplification:

For any arbitrary scalar functions ψ_1 and ψ_2 the vector identity holds (ref. 13, p. 278):

$$\underset{\sim}{\nabla} \cdot (\underset{\sim}{\nabla}\psi_1 \times \underset{\sim}{\nabla}\psi_2) = 0 \tag{2.30}$$

To satisfy (2.30), a vector $\underset{\sim}{V}^*$ (to be defined for special cases) can be written in terms of ψ_1 and ψ_2 as

$$\underset{\sim}{V}^* = \underset{\sim}{\nabla}\psi_1 \times \underset{\sim}{\nabla}\psi_2 \tag{2.31}$$

(The vector $\underset{\sim}{V}^*$ is normal to both $\underset{\sim}{\nabla}\psi_1$ and $\underset{\sim}{\nabla}\psi_2$, and is therefore along the intersection of the two surfaces $\psi_1 = C_1(t)$ and $\psi_2 = C_2(t)$. In cases where one defines $\underset{\sim}{V}^*$ to be $\underset{\sim}{V}$, equation (2.20) is satisfied by (2.30); the surface intersection is then a streamline and ψ_1 and ψ_2 are "stream functions."

With equation (2.31) and use of the identity (2.23), the Coriolis acceleration can be written as

$$\begin{aligned} 2\underset{\sim}{\Omega} \times \underset{\sim}{V} &= 2\underset{\sim}{\Omega} \times (\underset{\sim}{\nabla}\psi_1 \times \underset{\sim}{\nabla}\psi_2) + 2\underset{\sim}{\Omega} \times (\underset{\sim}{V} - \underset{\sim}{V}^*) \\ &= 2[(\underset{\sim}{\Omega} \cdot \underset{\sim}{\nabla}\psi_2)\underset{\sim}{\nabla}\psi_1 - (\underset{\sim}{\Omega} \cdot \nabla\psi_1)\nabla\psi_2] + 2\underset{\sim}{\Omega} \times (\underset{\sim}{V} - \underset{\sim}{V}^*) \end{aligned} \tag{2.32}$$

Use of this expression is convenient only in some special cases.

Case 1. No special restrictions—With no special restrictions, it is just as well to use (2.28) without (2.32) because use of ψ_1 and ψ_2 in (2.32) appears to offer no simplification.

One considers then in (2.28) (in the limit as $\delta \to 0$) omitting the parts of $\underset{\sim}{g}$ in the term $\underset{\sim}{g}\delta$ that are the same as the remaining body forces: $-\dot{\underset{\sim}{\Omega}} \times \underset{\sim}{R} - 2\underset{\sim}{\Omega} \times \underset{\sim}{V}$. However, if it should happen (as is true in some cases) that the Coriolis force term $(-2\underset{\sim}{\Omega} \times \underset{\sim}{V})$ is exactly balanced by part of the pressure gradient and is effectively eliminated from the problem, then that part of $\underset{\sim}{g}$ should *not* be omitted from the term $\underset{\sim}{g}\delta$ for small δ. Therefore, if the effects of $2\underset{\sim}{\Omega} \times \underset{\sim}{V}$ are unknown, it is better to leave $2\underset{\sim}{\Omega} \times \underset{\sim}{V}$ *in* $\underset{\sim}{g}$ in the term of order δ, as well as in the body force term without the factor δ.

Case 2. No flow changes in z direction—Let $\underset{\sim}{e}_3$ be a unit vector in the z direction, also the direction of $\underset{\sim}{\Omega}(t)$ (eq. (2.25)). Call the plane $z = 0$ the xy plane (although other coordinates may be used in the plane). Let $\underset{\sim}{V}^*$ be the velocity projection in the xy plane, so that

$$\underset{\sim}{V} = \underset{\sim}{V}^*(x,y,t) + \underset{\sim}{e}_3 w(x,y,t) \tag{2.33a}$$

Note that $\underset{\sim}{\nabla} \cdot \underset{\sim}{V} = \underset{\sim}{\nabla} \cdot \underset{\sim}{V}^* = 0$. Then let

$$\psi_2 = z \ , \quad \psi_1 = \psi(x,y,t) \tag{2.33b}$$

so that (for use in (2.32)):

$$\underset{\sim}{\nabla}\psi_2 = \underset{\sim}{e}_3, \quad \underset{\sim}{\Omega} \cdot \underset{\sim}{\nabla}\psi_2 = \Omega(t) \tag{2.33c}$$

In rectangular coordinates (x,y,z):

$$\left.\begin{aligned} \underset{\sim}{\nabla}\psi_1 &= \underset{\sim}{e}_1 \frac{\partial \psi}{\partial x} + \underset{\sim}{e}_2 \frac{\partial \psi}{\partial y} \\ \underset{\sim}{V}^* &= \underset{\sim}{\nabla}\psi_1 \times \underset{\sim}{\nabla}\psi_2 = \underset{\sim}{e}_1 \frac{\partial \psi}{\partial y} - \underset{\sim}{e}_2 \frac{\partial \psi}{\partial x} \end{aligned}\right\} \tag{2.33d}$$

But, by definition, $\underset{\sim}{V}^* = \underset{\sim}{e}_1 u + \underset{\sim}{e}_2 v$ so that if the flow is two-dimensional, ψ is the conventional stream function. In cylindrical coordinates (r,θ,z) with unit vectors $\underset{\sim}{e}_r$, $\underset{\sim}{e}_\theta$, $\underset{\sim}{e}_3$:

$$\left.\begin{aligned} \underset{\sim}{\nabla}\psi_1 &= \underset{\sim}{e}_r \frac{\partial \psi}{\partial r} + \underset{\sim}{e}_\theta \frac{\partial \psi}{\partial \theta} \\ \underset{\sim}{V}^* &= \underset{\sim}{\nabla}\psi_1 \times \underset{\sim}{\nabla}\psi_2 = \underset{\sim}{e}_r \frac{1}{r} \frac{\partial \psi}{\partial \theta} - \underset{\sim}{e}_\theta \frac{\partial \psi}{\partial r} \\ &= \underset{\sim}{e}_r v_r + \underset{\sim}{e}_\theta v_\theta \end{aligned}\right\} \tag{2.33e}$$

Also

$$\left.\begin{aligned} &\underset{\sim}{\Omega} \cdot \nabla\psi_1 = 0 \\ &\underset{\sim}{V} - \underset{\sim}{V}^* = \underset{\sim}{e}_3 w \quad \text{and} \quad \underset{\sim}{\Omega} \times (\underset{\sim}{V} - \underset{\sim}{V}^*) = 0 \end{aligned}\right\} \tag{2.33f}$$

With equations (2.33), equation (2.32) becomes

$$2\underset{\sim}{\Omega} \times \underset{\sim}{V} = \nabla[2\Omega(t)\psi] \tag{2.34}$$

and (2.28) becomes

$$\frac{D\underset{\sim}{V}}{Dt} = -\frac{1}{\rho_o}\nabla P_2 + \nu\nabla^2\underset{\sim}{V} + \underset{\sim}{g}\delta - (\dot{\underset{\sim}{\Omega}} \times \underset{\sim}{R}) \tag{2.35}$$

where

$$P_2 = p + \rho_o[\phi - (1/2)\Omega^2 R^2 + 2\Omega\psi] \tag{2.36}$$

with ϕ and Ω time dependent; see reference 14, p. 177, for ϕ and Ω independent of time.

For the case where the rotational speed is constant ($\dot{\underset{\sim}{\Omega}} \equiv 0$), equation (2.35) is analogous to the Boussinesq approximation, with pure natural convection caused by "buoyancy" body forces.

The case where the z component of velocity $w(x,y,t)$ is zero (*two-dimensional flow*) is included in case 2, equations (2.33) through (2.36).

Case 3. Rotational symmetry[1] *in cylindrical coordinates*—Consider cylindrical coordinates (r,θ,z), with the unit vector $\underset{\sim}{e}_z = \underset{\sim}{e}_3 = \underset{\sim}{\Omega}/\Omega$ defining the z direction and the coordinates r and θ being in the xy plane (fig. 2.2). Let $\underset{\sim}{e}_r$ and $\underset{\sim}{e}_\theta$ be unit vectors in the respective directions of increasing r and θ. Assume that the flow is invariant in θ. (This would be true in the rotating tank only if the axis of rotation is at the center of the tank and only for those ranges of the parameters for which such a flow is stable.)

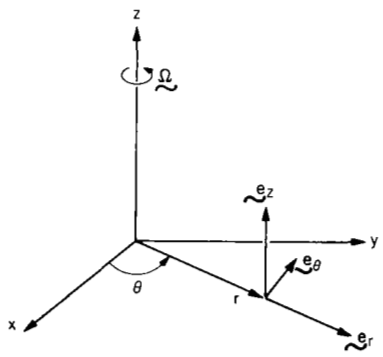

Figure 2.2.– Cylindrical coordinates for rotational symmetry.

Let any plane through the axis (constant θ) be called the rz plane. In this case, let $\underset{\sim}{V}^*$ be the projection in the rz plane of the velocity $\underset{\sim}{V}$ at a point in that plane, so that

$$\underset{\sim}{V} = \underset{\sim}{V}^*(r,z,t) + \underset{\sim}{e}_\theta v_\theta(r,z,t) \tag{2.37}$$

[1]A distinction is made between rotational and axial symmetry ($v_\theta = 0$) following Synge (ref. 15) and reference 16.

Note that with rotational symmetry

$$\nabla \cdot \underset{\sim}{V} = \nabla \cdot \underset{\sim}{V}^* = \frac{1}{r}\frac{\partial}{\partial r}(rv_r) + \frac{\partial v_z}{\partial z} = 0 \tag{2.38}$$

where v_r and v_z are the respective velocity components in the r and z directions, and do not depend on θ.

Then let

$$\psi_2 = \theta \quad \text{and} \quad \psi_1 = \psi(r,z,t) \tag{2.39a}$$

so that, for use in (2.32):

$$\left.\begin{aligned} \nabla\psi_2 &= \underset{\sim}{e}_\theta \frac{1}{r}\frac{\partial \psi_2}{\partial \theta} = \frac{1}{r}\underset{\sim}{e}_\theta \\ \underset{\sim}{\Omega} \cdot \nabla\psi_2 &= 0 \\ \nabla\psi_1 &= \underset{\sim}{e}_r \frac{\partial \psi}{\partial r} + \underset{\sim}{e}_z \frac{\partial \psi}{\partial z} \\ \underset{\sim}{V}^* \equiv \nabla\psi_1 \times \nabla\psi_2 &= \underset{\sim}{e}_r\left(-\frac{1}{r}\frac{\partial \psi}{\partial z}\right) + \underset{\sim}{e}_z\left(\frac{1}{r}\frac{\partial \psi}{\partial r}\right) \\ &= \underset{\sim}{e}_r v_r + \underset{\sim}{e}_z v_z \\ \underset{\sim}{\Omega} \cdot \nabla\psi_1 &= -\Omega r v_r \\ \underset{\sim}{\Omega} \times (\underset{\sim}{V} - \underset{\sim}{V}^*) &= -\underset{\sim}{e}_r \Omega v_\theta \end{aligned}\right\} \tag{2.39b}$$

Therefore, from (2.32), with (2.39b),

$$2\underset{\sim}{\Omega} \times \underset{\sim}{V} = 2\Omega(v_r \underset{\sim}{e}_\theta - v_\theta \underset{\sim}{e}_r) \tag{2.40}$$

It is seen from this special case of rotational symmetry that the Coriolis force $2\underset{\sim}{\Omega} \times \underset{\sim}{V}$ in equation (2.28) is in general not negligible in three-dimensional flow, either when $\delta \to 0$ with forced convection ($\dot{\Omega} \neq 0$ at some time in the problem) or for steady rotation ($\dot{\Omega} \equiv 0$) with $\delta \neq 0$. Thus, if the flow is restricted to be two-dimensional, then (see case 2 above) the Coriolis force can be included in ∇p and eliminated in the limit as $\delta \to 0$; but if the flow is three-dimensional, the Coriolis force is not balanced by pressure gradients, and so cannot in general be eliminated when $\delta \to 0$.

Case 4. Rotational symmetry[2] *in spherical coordinates*—Following a procedure similar to that in case 3 above, consider spherical coordinates (r,ϕ,θ), with the unit vector $\underset{\sim}{e}_3 = \underset{\sim}{\Omega}/\Omega$ defining the axis of symmetry from which the

[2]See footnote 1.

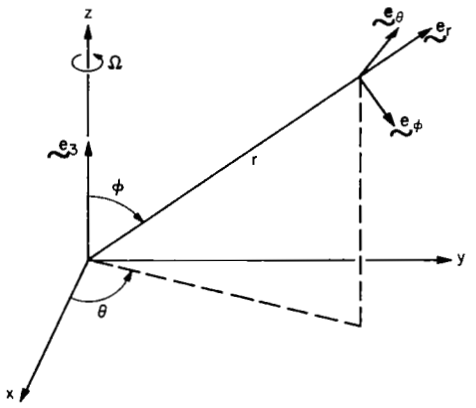

Figure 2.3.– Spherical coordinates for rotational symmetry.

polar angle ϕ is measured (fig. 2.3). The assumption of rotational symmetry implies the flow is invariant in the azimuthal coordinate θ, although there may be a velocity component $v_\theta = v_\theta(r,\phi,t)$.

Let $\underset{\sim}{e}_r$, $\underset{\sim}{e}_\phi$, and $\underset{\sim}{e}_\theta$ be the unit vectors in the respective directions of increasing r, ϕ, θ. Let any plane through the axis (containing $\underset{\sim}{e}_r$ and $\underset{\sim}{e}_\phi$, as well as $\underset{\sim}{e}_3$) be called the $r\phi$ plane. Let $\underset{\sim}{V}^*$ be the projection of $\underset{\sim}{V}(r,\phi,t)$ at the point (r,ϕ,θ) onto the $r\phi$ plane, so that

$$\underset{\sim}{V} = \underset{\sim}{V}^*(r,\phi,t) + \underset{\sim}{e}_\theta v_\theta(r,\phi,t) \tag{2.41}$$

Note that

$$\underset{\sim}{\nabla} \cdot \underset{\sim}{V} = \underset{\sim}{\nabla} \cdot \underset{\sim}{V}^* = \frac{1}{r^2}\frac{\partial}{\partial r}[r^2 v_r(r,\phi,t)] + \frac{1}{r \sin\phi}\frac{\partial}{\partial \phi}[(\sin\phi) v_\phi(r,\phi,t)] = 0 \tag{2.42}$$

where v_r and v_ϕ are the respective velocity components in the r and ϕ directions, and do not depend on θ. Then, for use in (2.32), let

$$\psi_2 = \theta \quad \text{and} \quad \psi_1 = \psi(r,\phi,t) \tag{2.43a}$$

so that

$$\left.\begin{aligned} \underset{\sim}{\nabla}\psi_2 &= \left(\frac{1}{r \sin\phi}\right)\underset{\sim}{e}_\theta \\ \underset{\sim}{\Omega} \cdot \nabla\psi_2 &= 0 \\ \nabla\psi_1 &= \underset{\sim}{e}_r \frac{\partial\psi}{\partial r} + \underset{\sim}{e}_\phi \frac{1}{r}\frac{\partial\psi}{\partial\phi} \\ V^* = \nabla\psi_1 \times \nabla\psi_2 &= \underset{\sim}{e}_r\left(\frac{1}{r^2 \sin\phi}\frac{\partial\psi}{\partial\phi}\right) + \underset{\sim}{e}_\phi\left(\frac{-1}{r \sin\phi}\frac{\partial\psi}{\partial r}\right) \\ &= \underset{\sim}{e}_r v_r(r,\phi,t) + \underset{\sim}{e}_\phi v_\phi(r,\phi,t) \end{aligned}\right\} \tag{2.43b}$$

From (2.43b),

$$\left.\begin{aligned} v_r &= \frac{1}{r^2 \sin\phi}\frac{\partial\psi}{\partial\phi} \quad \text{and} \quad v_\phi = \frac{-1}{r \sin\phi}\frac{\partial\psi}{\partial r} \\ \text{and so} \quad \underset{\sim}{\nabla}\psi_1 &= \underset{\sim}{e}_r(-v_\phi r \sin\phi) + \underset{\sim}{e}_\phi(v_r r \sin\phi) \end{aligned}\right\} \tag{2.43c}$$

Noting that:

$$\underset{\sim}{e}_3 \cdot \underset{\sim}{e}_r = \cos\phi$$
$$\underset{\sim}{e}_3 \cdot \underset{\sim}{e}_\phi = \cos[(\pi/2) + \phi] = -\sin\phi$$

we have

$$\underset{\sim}{\Omega} \cdot \underset{\sim}{\nabla}\psi_1 = -\Omega(r \sin \phi)(v_\phi \cos \phi + v_r \sin \phi) \tag{2.43d}$$

Also with

$$\underset{\sim}{e}_3 \times \underset{\sim}{e}_\theta = -(\underset{\sim}{e}_r \sin \phi + \underset{\sim}{e}_\phi \cos \phi)$$

we have

$$\underset{\sim}{\Omega} \times (\underset{\sim}{V} - \underset{\sim}{V}^*) = -\Omega v_\theta(\underset{\sim}{e}_r \sin \phi + \underset{\sim}{e}_\phi \cos \phi) \tag{2.43e}$$

With equations (2.43b, d, and e), equation (2.32) gives then

$$2\underset{\sim}{\Omega} \times \underset{\sim}{V} = 2\Omega[-v_\theta(\sin \phi)\underset{\sim}{e}_r - v_\theta(\cos \phi)\underset{\sim}{e}_\phi + (v_r \sin \phi + v_\phi \cos \phi)\underset{\sim}{e}_\theta] \tag{2.44}$$

For flow with rotational symmetry, equation (2.44) for spherical coordinates is equivalent to equation (2.40) for cylindrical coordinates. Comments on case 3 also apply here.

Further comments on the proper forms of the equations to use for small δ can be made when the respective forms of the vorticity equation are derived for the various cases in the next section.

Vorticity Equation and Vorticity-Stream Function Relations

Computation of a flow field with use of vorticity as a primary variable is advantageous because (see Lighthill, ref. 17, pp. 57-60; and Greenspan, ref. 8, pp. 20-21):

1. The unknown pressure and all conservative body forces are eliminated from the problem;
2. Large, sudden changes in velocity or angular velocity of the surface produce large sudden changes in fluid velocity and large impulsive pressures, whereas the vorticity distribution varies smoothly. (Vorticity changes are not propagated at the speed of sound, as are velocity and pressure changes.)

The fluid vorticity $\underset{\sim}{\omega}$ is defined by

$$\underset{\sim}{\omega} \equiv \underset{\sim}{\nabla} \times \underset{\sim}{V} \tag{2.45}$$

To obtain the vorticity equation corresponding to each of the momentum-equation forms (2.28) and (2.35) use first the vector identity

$$\underset{\sim}{V} \cdot \underset{\sim}{\nabla}\underset{\sim}{V} \equiv \underset{\sim}{\nabla}[(1/2)V^2] - \underset{\sim}{V} \times (\underset{\sim}{\nabla} \times \underset{\sim}{V}) \tag{2.46}$$

in the left side of each of those equations, and then take the curl of each equation. With use of several identities and with $\underset{\sim}{g}$ given by (2.12), one obtains from (2.28):

$$\frac{\partial \underset{\sim}{\omega}}{\partial t} - \underset{\sim}{\nabla} \times (\underset{\sim}{V} \times \underset{\sim}{\omega}) - \nu \nabla^2 \underset{\sim}{\omega} = \underset{\sim}{\nabla} \times (-\dot{\underset{\sim}{\Omega}} \times \underset{\sim}{R} - 2\underset{\sim}{\Omega} \times \underset{\sim}{V} + g\delta) \tag{2.47a}$$

and from (2.35) for flow independent of z:

$$\frac{\partial \underset{\sim}{\omega}}{\partial t} - \underset{\sim}{\nabla} \times (\underset{\sim}{V} \times \underset{\sim}{\omega}) - \nu \nabla^2 \underset{\sim}{\omega} = \underset{\sim}{\nabla} \times (-\dot{\underset{\sim}{\Omega}} \times \underset{\sim}{R} + g\delta) \tag{2.47b}$$

These forms of the vorticity equation are reduced further as follows: With the vector identities

$$\nabla \times (\underset{\sim}{A} \times \underset{\sim}{B}) \equiv \underset{\sim}{B} \cdot \nabla \underset{\sim}{A} - \underset{\sim}{A} \cdot \nabla \underset{\sim}{B} + \underset{\sim}{A}(\underset{\sim}{\nabla} \cdot \underset{\sim}{B}) - \underset{\sim}{B}(\underset{\sim}{\nabla} \cdot \underset{\sim}{A}) \tag{2.48}$$

and

$$\underset{\sim}{\nabla} \cdot \underset{\sim}{\omega} = \underset{\sim}{\nabla} \cdot (\underset{\sim}{\nabla} \times \underset{\sim}{V}) \equiv 0 \tag{2.49}$$

and with use of the approximate mass-conservation equation (2.20), the left sides of equations (2.47) become

$$\frac{\partial \underset{\sim}{\omega}}{\partial t} + \underset{\sim}{V} \cdot \nabla \underset{\sim}{\omega} - \underset{\sim}{\omega} \cdot \nabla \underset{\sim}{V} - \nu \nabla^2 \underset{\sim}{\omega} = \frac{D\underset{\sim}{\omega}}{Dt} - \underset{\sim}{\omega} \cdot \nabla \underset{\sim}{V} - \nu \nabla^2 \underset{\sim}{\omega} \tag{2.50a}$$

(The significance of $\underset{\sim}{\omega} \cdot \nabla \underset{\sim}{V}$ is discussed by Batchelor, ref. 14, pp. 267-268.) It may be noted for later convenience that with use of the following vector identity for the dyadic $\underset{\sim}{A}\underset{\sim}{B}$,

$$\nabla \cdot (\underset{\sim}{A}\underset{\sim}{B}) \equiv \underset{\sim}{A} \cdot \nabla \underset{\sim}{B} + (\underset{\sim}{\nabla} \cdot \underset{\sim}{A})\underset{\sim}{B}$$

along with (2.48), one can also write the left sides of equations (2.47) in the "divergence form"

$$\frac{\partial \underset{\sim}{\omega}}{\partial t} + \underset{\sim}{\nabla} \cdot (\underset{\sim}{V}\underset{\sim}{\omega}) - \underset{\sim}{\nabla} \cdot (\underset{\sim}{\omega}\underset{\sim}{V}) - \nu \nabla^2 \underset{\sim}{\omega} \tag{2.50b}$$

where, for example, in Cartesian coordinates

$$\underset{\sim}{\nabla} \cdot (\underset{\sim}{V}\underset{\sim}{\omega}) = \frac{\partial}{\partial x}(u\underset{\sim}{\omega}) + \frac{\partial}{\partial y}(v\underset{\sim}{\omega}) + \frac{\partial}{\partial z}(w\underset{\sim}{\omega})$$

$$\underset{\sim}{\nabla} \cdot (\underset{\sim}{\omega}\underset{\sim}{V}) = \frac{\partial}{\partial x}(\omega_x \underset{\sim}{V}) + \frac{\partial}{\partial y}(\omega_y \underset{\sim}{V}) + \frac{\partial}{\partial z}(\omega_z \underset{\sim}{V})$$

The right side of (2.47a) is reduced further by using the identity

$$\underset{\sim}{\nabla} \times (g\delta) \equiv \delta(\underset{\sim}{\nabla} \times \underset{\sim}{g}) + (\underset{\sim}{\nabla}\delta) \times \underset{\sim}{g} \tag{2.51}$$

with equations (2.12), (2.26), and (2.27a) so that

$$\underset{\sim}{\nabla} \times [-\dot{\underset{\sim}{\Omega}} \times \underset{\sim}{R} - 2\underset{\sim}{\Omega} \times \underset{\sim}{V} + \underset{\sim}{g}\delta] = (1 + \delta)\underset{\sim}{\nabla} \times (-\dot{\underset{\sim}{\Omega}} \times \underset{\sim}{R} - 2\underset{\sim}{\Omega} \times \underset{\sim}{V}) + (\underset{\sim}{\nabla}\delta) \times \underset{\sim}{g} \tag{2.52}$$

If then the quantities $\underset{\sim}{\nabla} \times (\dot{\underset{\sim}{\Omega}} \times \underset{\sim}{R})$ and $\underset{\sim}{\nabla} \times (\underset{\sim}{\Omega} \times \underset{\sim}{V})$ are expanded according to (2.48), for the case under consideration (constant inertial axis of rotation) with

$$\left.\begin{aligned} \underset{\sim}{\Omega} \equiv \underset{\sim}{e}_3\Omega(t) \ , \quad \underset{\sim}{\nabla}\underset{\sim}{\Omega} \equiv 0 \ , \quad \underset{\sim}{\nabla} \cdot \underset{\sim}{\Omega} \equiv 0 \\ \dot{\underset{\sim}{\Omega}} \cdot \underset{\sim}{\nabla}\underset{\sim}{R} = 0 \ , \quad \underset{\sim}{\nabla} \cdot \underset{\sim}{R} = 2 \end{aligned}\right\} \tag{2.53}$$

equation (2.47a) with (2.50a) and (2.52) becomes

$$\frac{D\underset{\sim}{\omega}}{Dt} - \underset{\sim}{\omega} \cdot \underset{\sim}{\nabla}\underset{\sim}{V} - \nu\nabla^2\underset{\sim}{\omega} = (\underset{\sim}{\nabla}\delta) \times \underset{\sim}{g} + 2(1 + \delta)(\underset{\sim}{\Omega} \cdot \underset{\sim}{\nabla}\underset{\sim}{V} - \dot{\underset{\sim}{\Omega}}) \tag{2.54}$$

where

$$\underset{\sim}{\Omega} \cdot \underset{\sim}{\nabla}\underset{\sim}{V} = \Omega(\partial\underset{\sim}{V}/\partial z) \quad \text{and} \quad \dot{\underset{\sim}{\Omega}} = \underset{\sim}{e}_3\dot{\Omega}$$

We have now arrived at a point where, for consistency with the previous development for small δ, we can neglect δ in comparison to unity in the body-force term. Equation (2.54) is then approximated finally by

$$\left.\begin{aligned} \frac{D\underset{\sim}{\omega}}{Dt} - \underset{\sim}{\omega} \cdot \underset{\sim}{\nabla}\underset{\sim}{V} - \nu\nabla^2\underset{\sim}{\omega} &= (\underset{\sim}{\nabla}\delta) \times \underset{\sim}{g} + 2(\underset{\sim}{\Omega} \cdot \underset{\sim}{\nabla}\underset{\sim}{V} - \dot{\underset{\sim}{\Omega}}) \\ &= (\underset{\sim}{\nabla}\delta) \times \underset{\sim}{g} + 2(\Omega\partial\underset{\sim}{V}/\partial z - \underset{\sim}{e}_3\dot{\Omega}) \end{aligned}\right\} \tag{2.55}$$

In the case where the flow is *independent of* z, equation (2.55) is equivalent to equation (2.47b) reduced to

$$\frac{D\underset{\sim}{\omega}}{Dt} - \underset{\sim}{\omega} \cdot \underset{\sim}{\nabla}\underset{\sim}{V} - \nu\nabla^2\underset{\sim}{\omega} = (\underset{\sim}{\nabla}\delta) \times \underset{\sim}{g} - \underset{\sim}{e}_3(2\dot{\Omega}) \tag{2.56}$$

In the further specialization to *two-dimensional flow* ($w = 0$), the vorticity is

$$\underset{\sim}{\omega} = \underset{\sim}{e}_3\omega \tag{2.57}$$

so that (2.56) becomes the scalar equation

$$\frac{D\omega}{Dt} - \nu\nabla^2\omega = [\underset{\sim}{\nabla}\delta \times \underset{\sim}{g}]_z - 2\dot{\Omega} \tag{2.58a}$$

or, with the left side replaced by (2.50b), in two-dimensional Cartesian coordinates (x,y),

$$\frac{\partial \omega}{\partial t} + \frac{\partial}{\partial x}(u\omega) + \frac{\partial}{\partial y}(v\omega) - \nu\nabla^2\omega = g_2\frac{\partial \delta}{\partial x} - g_1\frac{\partial \delta}{\partial y} - 2\dot{\Omega} \tag{2.58b}$$

or in two-dimensional polar coordinates (r,θ),

$$\frac{\partial \omega}{\partial t} + \frac{1}{r}\left[\frac{\partial}{\partial r}(rv_r\omega) + \frac{\partial}{\partial \theta}(v_\theta\omega)\right] - \nu\nabla^2\omega = g_\theta\frac{\partial \delta}{\partial r} - g_r\left(\frac{1}{r}\frac{\partial \delta}{\partial \theta}\right) - 2\dot{\Omega} \tag{2.58c}$$

where g_1 and g_2 are the x and y components of $\underset{\sim}{g}$, and g_r and g_θ are the r and θ components of $\underset{\sim}{g}$ in (2.12).

It is noted from the vorticity equation (2.55) that:

1. In the limit as $\delta \to 0$, the nonsteady rotation term in the momentum equation (2.28) is exhibited only in the term $-2\dot{\underset{\sim}{\Omega}}$ in the vorticity equation, whereas the Coriolis term results only in the term $2\underset{\sim}{\Omega} \cdot \underset{\sim}{\nabla}\underset{\sim}{V}$ in the vorticity equation, and *both of these* are in general not negligible as $\delta \to 0$ in three-dimensional flow where $\partial \underset{\sim}{V}/\partial z \neq 0$.

2. In the limiting case of rigid-body rotation (relative velocity $\underset{\sim}{V} \to 0$ and $\delta \to 0$), equation (2.55) reduces correctly to

$$\frac{\partial \underset{\sim}{\omega}}{\partial t} = -2\dot{\underset{\sim}{\Omega}}$$

3. In the special case of steady rotation ($\dot{\underset{\sim}{\Omega}} = 0$ for all time), the only *driving* term in (2.55) or (2.56) is the buoyancy-force term $(\underset{\sim}{\nabla}\delta) \times \underset{\sim}{g}$.

4. In general, the driving factors in (2.55) are both the buoyancy term $(\underset{\sim}{\nabla}\delta) \times \underset{\sim}{g}$ and $-2\dot{\underset{\sim}{\Omega}}$, these being the only terms that are independent of, or contain terms independent of, the relative velocity $\underset{\sim}{V}$. Thus, if both $(\underset{\sim}{\nabla}\delta) \times \underset{\sim}{g} = 0$ and $\dot{\underset{\sim}{\Omega}} = 0$, we have $\underset{\sim}{V} \to 0$ so that a rigid-body rotation (condition of no convection) is approached. The Coriolis term $2\underset{\sim}{\Omega} \cdot \underset{\sim}{\nabla}\underset{\sim}{V}$ in the three-dimensional equation plays an essentially passive role; that is, it apparently acts simply to absorb (oppose) part of the effect of the driving terms (see Ostrach, ref. 7), since it contains $\underset{\sim}{V}$ and vanishes as the flow approaches a rigid-body rotation when both $(\underset{\sim}{\nabla}\delta) \times \underset{\sim}{g}$ and $\dot{\underset{\sim}{\Omega}}$ are zero.

In connection with the use of the vorticity equation (2.55) or (2.56) it is convenient to use the stream functions for the special cases noted in the previous section, and to relate the stream function to the appropriate vorticity component.

In case 2 above, with no flow changes in the z direction, $\underset{\sim}{\omega}$, defined by (2.45), becomes

$$\underset{\sim}{\omega} = \underset{\sim}{\nabla} \times [\underset{\sim}{e}_3 w(x,y,t)] + \underset{\sim}{\nabla} \times \{\underset{\sim}{\nabla} \times [\underset{\sim}{e}_3 \psi(x,y,t)]\} \tag{2.59}$$

From the vector identity

$$\underset{\sim}{\nabla} \times (\underset{\sim}{\nabla} \times \underset{\sim}{A}) \equiv \underset{\sim}{\nabla}(\underset{\sim}{\nabla} \cdot \underset{\sim}{A}) - \nabla^2\underset{\sim}{A} \tag{2.60}$$

one has

$$\underset{\sim}{\nabla} \times [\underset{\sim}{\nabla} \times (\underset{\sim}{e}_3\psi)] = -\underset{\sim}{e}_3\nabla^2\psi \tag{2.61}$$

so that in rectangular Cartesian coordinates,

$$\underset{\sim}{\omega} = \underset{\sim}{e}_1 \frac{\partial w}{\partial y} - \underset{\sim}{e}_2 \frac{\partial w}{\partial x} - \underset{\sim}{e}_3 \nabla^2 \psi \tag{2.62}$$

In the case of cylindrical coordinates (r,θ,z) with flow independent of z,

$$\underset{\sim}{\omega} = \underset{\sim}{e}_r \left(\frac{1}{r} \frac{\partial w}{\partial \theta} \right) - \underset{\sim}{e}_\theta \frac{\partial w}{\partial r} - \underset{\sim}{e}_3 \nabla^2 \psi \tag{2.63a}$$

where

$$\nabla^2 \psi = \frac{1}{r^2} \left[r \frac{\partial}{\partial r} \left(r \frac{\partial \psi}{\partial r} \right) + \frac{\partial^2 \psi}{\partial \theta^2} \right] \tag{2.63b}$$

For two-dimensional flow, with (2.57) for $w = 0$, (2.62) and (2.63) reduce to

$$\omega = -\nabla^2 \psi \tag{2.64}$$

In case 3 above, with rotational symmetry in cylindrical coordinates,

$$\underset{\sim}{V} = \underset{\sim}{e}_r v_r(r,z,t) + \underset{\sim}{e}_\theta v_\theta(r,z,t) + \underset{\sim}{e}_3 v_z(r,z,t) \tag{2.65}$$

$$\underset{\sim}{\omega} = \underset{\sim}{\nabla} \times \underset{\sim}{V} = \underset{\sim}{e}_r \omega_r + \underset{\sim}{e}_\theta \omega_\theta + \underset{\sim}{e}_3 \omega_z \tag{2.66a}$$

where

$$\omega_r = - \frac{\partial v_\theta}{\partial z} \tag{2.66b}$$

$$\omega_\theta = - \left(\frac{\partial v_z}{\partial r} - \frac{\partial v_r}{\partial z} \right) \tag{2.66c}$$

$$\omega_z = \frac{1}{r} \frac{\partial}{\partial r} (r v_\theta) \tag{2.66d}$$

With

$$v_r = - \frac{1}{r} \frac{\partial \psi}{\partial z} \quad \text{and} \quad v_z = \frac{1}{r} \frac{\partial \psi}{\partial r} \tag{2.67}$$

from (2.39b), equation (2.66c) becomes

$$\left.\begin{aligned} -r\omega_\theta &= r \frac{\partial}{\partial r} \left(\frac{1}{r} \frac{\partial \psi}{\partial r} \right) + \frac{\partial^2 \psi}{\partial z^2} \\ &= \frac{\partial^2 \psi}{\partial r^2} - \frac{1}{r} \frac{\partial \psi}{\partial r} + \frac{\partial^2 \psi}{\partial z^2} \end{aligned}\right\} \tag{2.68}$$

Note that in this case, ω_θ is *not* directly related to $\nabla^2 \psi$, since

$$\left.\begin{aligned}\nabla^2\psi &= \frac{1}{r}\frac{\partial}{\partial r}\left(r\,\frac{\partial\psi}{\partial r}\right) + \frac{\partial^2\psi}{\partial z^2} \\ &= \frac{\partial^2\psi}{\partial r^2} + \frac{1}{r}\frac{\partial\psi}{\partial r} + \frac{\partial^2\psi}{\partial z^2}\end{aligned}\right\} \tag{2.69}$$

Equation (2.68) would be useful in conjunction with solving (2.55) for this special case.

In case 4 above, with rotational symmetry in spherical coordinates

$$\underset{\sim}{V} = \underset{\sim}{e}_r v_r(r,\phi,t) + \underset{\sim}{e}_\phi v_\phi(r,\phi,t) + \underset{\sim}{e}_\theta v_\theta(r,\phi,t) \tag{2.70}$$

$$\underset{\sim}{\omega} = \underset{\sim}{e}_r \omega_r + \underset{\sim}{e}_\phi \omega_\phi + \underset{\sim}{e}_\theta \omega_\theta \tag{2.71a}$$

where

$$\omega_r = \frac{1}{r\sin\phi}\frac{\partial}{\partial\phi}\left[(\sin\phi)v_\theta\right] \tag{2.71b}$$

$$\omega_\phi = \frac{-1}{r}\frac{\partial}{\partial r}(rv_\theta) \tag{2.71c}$$

$$\omega_\theta = \frac{-1}{r}\left[\frac{\partial v_r}{\partial\phi} - \frac{\partial}{\partial r}(rv_\phi)\right] \tag{2.71d}$$

With

$$v_r = \frac{1}{r^2\sin\phi}\frac{\partial\psi}{\partial\phi} \quad \text{and} \quad v_\phi = \frac{-1}{r\sin\phi}\frac{\partial\psi}{\partial r} \tag{2.72}$$

from (2.43c), equation (2.71d) becomes

$$-r^3(\sin\phi)\omega_\theta = r^2\frac{\partial^2\psi}{\partial r^2} + (\sin\phi)\frac{\partial}{\partial\phi}\left[\frac{1}{\sin\phi}\frac{\partial\psi}{\partial\phi}\right] \tag{2.73}$$

Note again that ω_θ is *not* directly related to $\nabla^2\psi$, which is given by

$$r^2\nabla^2\psi = \frac{\partial}{\partial r}\left(r^2\frac{\partial\psi}{\partial r}\right) + \frac{1}{\sin\phi}\frac{\partial}{\partial\phi}\left[(\sin\phi)\frac{\partial\psi}{\partial\phi}\right] \tag{2.74}$$

Equation (2.73) would be useful in conjunction with solving (2.55) for this special case.

Energy Equation

The energy-conservation equation is considered in two forms, (2.3a) and (2.3b). With the caloric equations simplified to the forms of (2.17) with $\underset{\sim}{\nabla}\cdot\underset{\sim}{V}$ assumed to be zero (eq. (2.20)) in expressing the viscous stress tensor

$\underset{\sim}{\tau}$ in (2.6) for use in (2.7) so that

$$\Phi = [\underset{\sim}{\nabla}\underset{\sim}{V} + (\underset{\sim}{\nabla}\underset{\sim}{V})_t] : \underset{\sim}{\nabla}\underset{\sim}{V} \tag{2.75}$$

and with k in (2.8) assumed to be nearly constant as noted above, the energy equations (2.3) take the forms

$$\rho c_v \frac{DT}{Dt} + p\underset{\sim}{\nabla} \cdot \underset{\sim}{V} = k\nabla^2 T + \mu\Phi \tag{2.76a}$$

and

$$\rho c_p \frac{DT}{Dt} - \frac{Dp}{Dt} = k\nabla^2 T + \mu\Phi \tag{2.76b}$$

For the conditions under consideration in this problem, we have retained the term $p\underset{\sim}{\nabla} \cdot \underset{\sim}{V}$ in (2.76a) for reasons given below.

If there is any apparent conflict in the results from either of the two forms of the energy equation, one should use the form that is most consistent with (2.16), rather than with the more restrictive equation (2.20), which results from letting $\delta \to 0$. Obviously, for a liquid in which $c_p \approx c_v$ and $\rho \approx$ constant, there is no difference in the two equations (with Dp/Dt very small). But in the present problem, there is a significant difference between c_p and c_v, so we must consider the relative consistency of *either* neglecting $p\underset{\sim}{\nabla} \cdot \underset{\sim}{V}$ in (2.76a) *or* neglecting Dp/Dt in (2.76b).

Consider first equation (2.76a). One could use (2.76a) with (2.20) substituted if, in fact,

$$|p\underset{\sim}{\nabla} \cdot \underset{\sim}{V}| \ll |k\nabla^2 T|$$

To determine whether $p\underset{\sim}{\nabla} \cdot \underset{\sim}{V}$ is negligible, write (2.1) as

$$p\underset{\sim}{\nabla} \cdot \underset{\sim}{V} = -\frac{p}{\rho}\frac{D\rho}{Dt}$$

and use the approximation from equation (2.16) that

$$\frac{1}{\rho}\frac{D\rho}{Dt} = \frac{-\beta}{1 - \beta\,\Delta T}\frac{DT}{Dt} \approx -\beta\frac{DT}{Dt}$$

so that

$$p\underset{\sim}{\nabla} \cdot \underset{\sim}{V} \approx p\beta\frac{DT}{Dt} \tag{2.77}$$

Near the critical point of a fluid, for example oxygen with $T \approx 150°$ K and $\beta \approx 0.01/°K$, one finds, for example, from the van der Waals equation of state, that

$$\frac{p}{\rho} > (RT)_{\text{perfect gas}} = O(c_v T) \tag{2.78}$$

Therefore, from equations (2.77) and (2.78),

$$|p\nabla \cdot \underset{\sim}{V}| > \left|(\beta T)\rho R \frac{DT}{Dt}\right| \approx \left|\rho c_v \frac{DT}{Dt}\right|$$

or

$$|p\nabla \cdot \underset{\sim}{V}| \geq \left|\rho c_v \frac{DT}{Dt}\right| \tag{2.79}$$

The result (2.79) indicates that $p\nabla \cdot \underset{\sim}{V}$ would *not* be negligible in determining DT/Dt from (2.76a).

Consider then the use of equation (2.76b), with use of the approximate form of the equation of state (2.16), where β (eq. (2.14a)) is to be determined from a functional relationship such as

$$p = p(\rho, T) \tag{2.80}$$

Because of (2.80), we can write

$$\frac{Dp}{Dt} = \left(\frac{\partial p}{\partial \rho}\right)_T \frac{D\rho}{Dt} + \left(\frac{\partial p}{\partial T}\right)_\rho \frac{DT}{Dt} \tag{2.81}$$

With the approximation represented by equation (2.16)

$$\frac{D\rho}{Dt} = -\rho_o \beta \frac{DT}{Dt} \tag{2.82}$$

and from the definition of β in (2.14a),

$$\beta = \left[\frac{-1}{\rho}\left(\frac{\partial \rho}{\partial T}\right)_p\right]_o \approx -\frac{1}{\rho_o}\left(\frac{\partial \rho}{\partial T}\right)_p$$

equation (2.81) becomes

$$\frac{Dp}{Dt} \approx \left[\left(\frac{\partial p}{\partial \rho}\right)_T \left(\frac{\partial \rho}{\partial T}\right)_p + \left(\frac{\partial p}{\partial T}\right)_\rho\right] \frac{DT}{Dt} \tag{2.83a}$$

But for a state function such as (2.80), a fundamental identity from calculus states that the bracketed quantity in equation (2.83a) is identically zero. Therefore

$$\frac{Dp}{Dt} \approx 0 \tag{2.83b}$$

This result shows in a rational way that use of the approximate state relation (2.16) is most compatible with the approximate energy equation (2.76b) in the form (as $\delta \to 0$ in (2.18a)):

$$\frac{DT}{Dt} = \left(\frac{k}{\rho_o c_p}\right)\nabla^2 T + \left(\frac{\nu}{c_p}\right)\Phi \tag{2.84}$$

(See also ref. 10, pp. 126, 127.) With use of (2.20), the left side of (2.84) may also be written as

$$\frac{DT}{Dt} = \frac{\partial T}{\partial t} + \underset{\sim}{\nabla} \cdot (\underset{\sim}{V}T) \tag{2.85a}$$

where in the special case of two-dimensional flow,

$$\underset{\sim}{\nabla} \cdot (\underset{\sim}{V}T) = \frac{\partial}{\partial x}(uT) + \frac{\partial}{\partial y}(vT) \tag{2.85b}$$

$$= \frac{1}{r}\frac{\partial}{\partial r}(rv_r T) + \frac{1}{r}\frac{\partial}{\partial \theta}(v_\theta T) \tag{2.85c}$$

PROBLEM DEFINITION AND APPROXIMATE FLOW EQUATIONS FOR TWO-DIMENSIONAL SQUARE TANK

In this section, the theory developed above is summarized and specialized for computation of the convection caused by time-dependent rotation and density variations due to temperature variations in a two-dimensional square tank. The configuration is as shown in figure 2.4. The x,y coordinate system is fixed relative to the tank, with the origin at the corner as shown. The rotation is about a point a distance R_c from the tank center, and the radius vector from that point is denoted by $\underset{\sim}{R}$ (see fig. 2.1) with components in the x and y directions equal to

$$\left.\begin{aligned} R_1 &= x - \frac{1}{2}\ell \\ R_2 &= y - \frac{1}{2}\ell + R_c \end{aligned}\right\} \tag{2.86}$$

The time-dependent angular velocity Ω is positive when counterclockwise. In the x,y coordinates the effective body force per unit mass, given by equation (2.12), becomes

$$\underset{\sim}{g} = \underset{\sim}{e}_1 g_1 + \underset{\sim}{e}_2 g_2 \tag{2.87a}$$

where

$$g_1 = R_1\Omega^2 + 2\Omega v + R_2\dot{\Omega} - a_1 \tag{2.87b}$$

$$g_2 = R_2\Omega^2 - 2\Omega u - R_1\dot{\Omega} - a_2 \tag{2.87c}$$

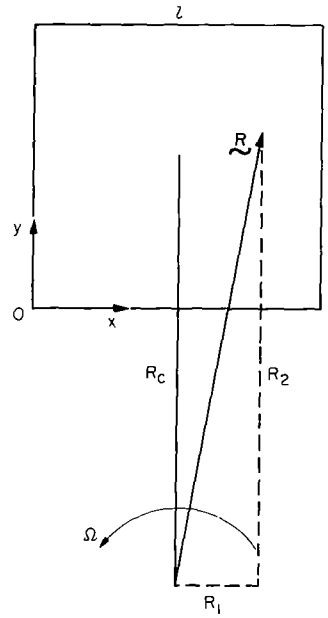

Figure 2.4.– Square tank configuration.

and where a_1 and a_2 are prescribed x and y components of $\underset{\sim}{a}$ (defined following equation (2.9)) and u and v are the x and y components of $\underset{\sim}{V}$ (eqs. (2.33)).

With δ given by equation (2.18b), the vorticity equation (2.58b) becomes

$$\frac{\partial \omega}{\partial t} + \frac{\partial}{\partial x}(u\omega) + \frac{\partial}{\partial y}(v\omega) = \nu\left(\frac{\partial^2 \omega}{\partial x^2} + \frac{\partial^2 \omega}{\partial y^2}\right) - g_2\beta \frac{\partial T}{\partial x} + g_1\beta \frac{\partial T}{\partial y} - 2\dot{\Omega} \tag{2.88}$$

The energy equation (2.84) with (2.85) becomes

$$\frac{\partial T}{\partial t} + \frac{\partial}{\partial x}(uT) + \frac{\partial}{\partial y}(vT) = \frac{k}{\rho_o c_p}\left(\frac{\partial^2 T}{\partial x^2} + \frac{\partial^2 T}{\partial y^2}\right) + \frac{\nu}{c_p}\Phi \tag{2.89a}$$

where the dissipation function, from (2.75) becomes

$$\Phi = 2\left[\left(\frac{\partial u}{\partial x}\right)^2 + \left(\frac{\partial v}{\partial y}\right)^2\right] + \left(\frac{\partial v}{\partial x} + \frac{\partial u}{\partial y}\right)^2 \tag{2.89b}$$

It is convenient to use the vorticity-stream function relation from equation (2.64):

$$\frac{\partial^2 \psi}{\partial x^2} + \frac{\partial^2 \psi}{\partial y^2} = -\omega \tag{2.90}$$

where from (2.33d),

$$u = \frac{\partial \psi}{\partial y}, \quad v = -\frac{\partial \psi}{\partial x} \tag{2.91}$$

Sufficient initial and boundary conditions are needed to specify the problem completely. Initially (t = 0), a temperature distribution is specified and the velocities u and v are everywhere zero (rigid-body rotation). At all times,

$$\left.\begin{array}{l} \text{on } x = 0, \; x = \ell \\ \qquad\quad y = 0, \; y = \ell \end{array}\right\} \; u = v = 0 \quad \text{or} \quad \frac{\partial \psi}{\partial y} = \frac{\partial \psi}{\partial x} = 0 \tag{2.92}$$

The condition in (2.92) on the normal component of velocity (tangential derivative of ψ) can be replaced by $\psi = 0$ on the boundary for application to equation (2.90). The condition on the tangential component of velocity (normal derivative of ψ) can then be incorporated into a condition on ω at each boundary for equation (2.88). The temperature or its normal derivative may be specified on the boundary at all times for equation (2.89a).

The function $\Omega(t)$ must be prescribed as a condition of the problem. As one example, for sudden reversal of rotation (with $\Omega = -\Omega_o$ for $t < 0$), one may use an approximation of

$$\Omega(t) = -\Omega_o + 2\Omega_o S(t) \tag{2.93a}$$

where Ω_o is a constant and $S(t)$ is the unit step function,

$$\left.\begin{aligned} S(t) &= 0 , \quad t < 0 \\ &= 1 , \quad t \geq 0 \end{aligned}\right\} \tag{2.93b}$$

Then from (2.93a),

$$\dot{\Omega}(t) = 2\Omega_o \dot{S}(t) \tag{2.93c}$$

where $\dot{S}(t)$ is the Dirac delta function. The simplest numerical approximations to $S(t)$ and $\dot{S}(t)$ may be used; for example (with t_1 very small),

$$\left.\begin{aligned} S(t) &= 0 \quad \text{for} \quad t < 0 \\ &= t/t_1 \quad \text{for} \quad 0 \leq t < t_1 \\ &= 1 \quad \text{for} \quad t \geq t_1 \end{aligned}\right\} \tag{2.94a}$$

$$\left.\begin{aligned} \dot{S}(t) &= 0 \quad \text{for} \quad t < 0 \\ &= 1/t_1 \quad \text{for} \quad 0 \leq t < t_1 \\ &= 0 \quad \text{for} \quad t \geq t_1 \end{aligned}\right\} \tag{2.94b}$$

For convenience in further treatment, equations (2.86) through (2.94) may be put into dimensionless form using the following dimensionless variables and parameters (where L is an arbitrary length):

$$\left.\begin{aligned} \xi &= \frac{x}{L} , \quad \eta = \frac{y}{L} , \quad \tau = \frac{\nu t}{L^2} \\ \omega^* &= \frac{\omega L^2}{\nu} , \quad H = \frac{T - T_o}{T_R - T_o} , \quad \Psi = \frac{\psi}{\nu} \\ U &= \frac{uL}{\nu} , \quad V = \frac{vL}{\nu} \\ \Omega^*(\tau) &= \frac{2\Omega(t)}{\nu L^{-2}} , \quad \Omega_o^* = \frac{2\Omega_o}{\nu L^{-2}} \\ G_1 &= Gr(g_1/\Omega_o^2 L) , \quad G_2 = Gr(g_2/\Omega_o^2 L) \\ a_1^* &= a_1/\Omega_o^2 L , \quad a_2^* = a_2/\Omega_o^2 L \\ \Phi^* &= (L^4/\nu^2)\Phi \end{aligned}\right\} \tag{2.95a}$$

with

$$\left.\begin{aligned}
&\text{Reynolds number} \quad \mathrm{Re} = \frac{\Omega_o L^2}{\nu} \\
&\text{Prandtl number} \quad \mathrm{Pr} = \frac{\rho_o \nu c_p}{k} \\
&\text{Grashof number} \quad \mathrm{Gr} = \frac{(\Omega_o^2 L) L^3 \beta (T_R - T_o)}{\nu^2} \\
&\text{Eckert number} \quad \mathrm{Ec} = \frac{(\Omega_o L)^2}{c_p (T_R - T_o)}
\end{aligned}\right\} \qquad (2.95b)$$

Equations (2.86) through (2.94) become, in *dimensionless* form (dropping the asterisks from ω^*, Ω^*, Φ^*, a_1^*, and a_2^* from here on):

$$\frac{\partial \omega}{\partial \tau} + \frac{\partial}{\partial \xi}(U\omega) + \frac{\partial}{\partial \eta}(V\omega) = \frac{\partial^2 \omega}{\partial \xi^2} + \frac{\partial^2 \omega}{\partial \eta^2} - G_2 \frac{\partial H}{\partial \xi} + G_1 \frac{\partial H}{\partial \eta} - \frac{d\Omega}{d\tau} \qquad (2.96)$$

$$\frac{\partial H}{\partial \tau} + \frac{\partial}{\partial \xi}(UH) + \frac{\partial}{\partial \eta}(VH) = \frac{1}{\mathrm{Pr}}\left(\frac{\partial^2 H}{\partial \xi^2} + \frac{\partial^2 H}{\partial \eta^2}\right) + \frac{\mathrm{Ec}}{\mathrm{Re}^2}\Phi \qquad (2.97)$$

$$\frac{\partial^2 \Psi}{\partial \xi^2} + \frac{\partial^2 \Psi}{\partial \eta^2} = -\omega \qquad (2.98)$$

$$U = \frac{\partial \Psi}{\partial \eta}, \quad V = -\frac{\partial \Psi}{\partial \xi} \qquad (2.99)$$

where

$$G_1 = \frac{\mathrm{Gr}}{\mathrm{Re}^2}\left[\left(\xi - \frac{1}{2}\frac{\ell}{L}\right)\frac{1}{4}\Omega^2 + \Omega V + \left(\eta - \frac{1}{2}\frac{\ell}{L} + \frac{R_c}{L}\right)\frac{1}{2}\frac{d\Omega}{d\tau}\right] - \mathrm{Gr}\, a_1 \qquad (2.100a)$$

$$G_2 = \frac{\mathrm{Gr}}{\mathrm{Re}^2}\left[\left(\eta - \frac{1}{2}\frac{\ell}{L} + \frac{R_c}{L}\right)\frac{1}{4}\Omega^2 - \Omega U - \left(\xi - \frac{1}{2}\frac{\ell}{L}\right)\frac{1}{2}\frac{d\Omega}{d\tau}\right] - \mathrm{Gr}\, a_2 \qquad (2.100b)$$

$$\Phi = 2\left[\left(\frac{\partial U}{\partial \xi}\right)^2 + \left(\frac{\partial V}{\partial \eta}\right)^2\right] + \left(\frac{\partial V}{\partial \xi} + \frac{\partial U}{\partial \eta}\right)^2 \qquad (2.101)$$

with conditions

$$\left.\begin{aligned}
&\xi = 0 \quad \text{and} \quad \xi = \ell/L \\
&\eta = 0 \quad \text{and} \quad \eta = \ell/L
\end{aligned}\right\} \quad \frac{\partial \Psi}{\partial \xi} = \frac{\partial \Psi}{\partial \eta} = \Psi = 0 \qquad (2.102)$$

The value of H or its normal derivative may be specified on the boundary. The dimensionless function $\Omega(\tau)$ may be specified, for example, by equations (2.93) and (2.94) with t and t_1 replaced by τ and τ_1.

CONCLUDING REMARKS

A set of general approximate equations has been developed that represents the Navier-Stokes description of convection of a thermally stratified fluid in a container with arbitrary time-dependent rotation. The equations are valid for combined forced and natural convection with significant, but sufficiently small, density and temperature gradients. All relevant terms representing effects of rotation and changes in rotation are included.

The special case of convection in a two-dimensional square container was formulated for subsequent computations.

REFERENCES

1. Prandtl, L.: Essentials of Fluid Dynamics. Hafner Pub., New York, 1952.

2. Bird, R. B.; Stewart, W. E.; and Lightfoot, E. N.: Transport Phenomena. John Wiley & Sons, New York, 1960.

3. Schlichting, H.: Boundary Layer Theory. First ed., McGraw-Hill Book Co., 1955.

4. Robinson, A. R.: Oceanography. Ch. 17, Research Frontiers in Fluid Dynamics, R. J. Seeger and G. Temple, eds., Interscience Pub., New York, 1965, pp. 504-533.

5. Parker, E. N.: Fluid-Dynamical Problems Associated with Interplanetary Space. Ch. 20, Research Frontiers in Fluid Dynamics, R. J. Seeger and G. Temple, eds., Interscience Pub., New York, 1965, pp. 677-717.

6. Turner, J. S.: Buoyant Plumes and Thermals. Annual Review of Fluid Mechanics, W. R. Sears, ed., Vol. 1, 1969, Annual Reviews, Inc., Palo Alto, Calif., pp. 29-44.

7. Ostrach, Simon: Laminar Flows with Body Forces. Section F, Theory of Laminar Flows, F. K. Moore, ed., Vol. IV of High Speed Aerodynamics and Jet Propulsion, Princeton Univ. Press, 1964, pp. 528-718.

8. Greenspan, H. P.: The Theory of Rotating Fluids. Cambridge Univ. Press, 1968.

9. Homsy, G. M.; and Hudson, J. L.: Centrifugally Driven Thermal Convection in a Rotating Cylinder. J. Fluid Mech., Vol. 35, Pt. 1, 1969, pp. 33-52.

10. Whitham, G. B.: The Navier-Stokes Equations of Motion. Section III, Laminar Boundary Layers, L. Rosenhead, ed., Oxford, Clarendon Press, 1963, pp. 114-162.

11. Briley, W. R.; and Walls, H. A.: A Numerical Study of Time-Dependent Rotating Flow in a Cylindrical Container at Low and Moderate Reynolds Numbers. Proc. Second Intern. Conf. on Numerical Methods in Fluid Dynamics, Sept. 15-19, 1970, Univ. of Calif., Berkeley. Maurice Holt, ed., Springer-Verlag, Berlin, 1971.

12. Becker, Robert A.: Introduction to Theoretical Mechanics. McGraw-Hill Book Co., 1954.

13. Hildebrand, Francis B.: Advanced Calculus for Applications. Prentice-Hall, Englewood Cliffs, N. J., 1962.

14. Batchelor, G. K.: An Introduction to Fluid Dynamics. Cambridge Univ. Press, 1967.

15. Synge, J. L.: Hydrodynamic Stability. Semi-centennial Pub. Amer. Math. Soc., Vol. 2, 1938, pp. 227-269.

16. Rosenhead, L., ed.: Laminar Boundary Layers. Oxford, Clarendon Press, 1963.

17. Lighthill, M. J.: Introduction. Boundary Layer Theory. Section II, Laminar Boundary Layers, L. Rosenhead, ed., Oxford, Clarendon Press, 1963, pp. 46-113.

3. COMPUTATIONAL METHOD FOR CALCULATING CONVECTION IN A ROTATING TANK

Harvard Lomax and F. R. Bailey

SUMMARY

A time-dependent finite-difference method is presented for calculating the convection of vorticity and energy in a stratified, supercritical cryogenic fluid contained within a two-dimensional square tank rotating in a gravitationless field. The finite-difference approximations to the convective part of the governing small-density-variation form of the Navier-Stokes equations are based on an explicit predictor-corrector scheme of second-order accuracy in time and space. A discussion of the stability and accuracy of this method is included. The solution for the stream function that appears in the governing equation is determined by using a direct solution of Poisson's equation based on double cyclic reduction.

INTRODUCTION

In this chapter, a numerical finite-differencing scheme is described that can be used to compute the convection of vorticity and energy within a two-dimensional square tank rotating in a gravitationless field.

The purpose of the analysis is to determine whether local temperature stratifications in an insulated oxygen tank traveling in space at high pressure could be broken up, or stirred, by very low rates of rotation and by rotation reversals. Effects of both viscosity and heat conduction are included in the study of the time-dependent mixing. The mathematical model that describes the two-dimensional behavior of such an environment is given by the Navier-Stokes equations for small-density variations, one form of which is given in the next section. Many numerical calculations of these equations have been carried out but not with the physical conditions described above. These physical conditions guided the choice of the numerical procedure. In particular, a method was chosen that has very little numerical dissipation but is not highly accurate with regard to dispersion, since the amount but not the details of the mixing was considered to be of paramount importance.

PROCEDURE

The geometry of the problem is shown in figure 3.1. A two-dimensional fluid within a square is being rotated at a rate Ω about some point exterior to the boundaries of the square. Since we are presenting only the basic principles of the numerical process, the details of deriving the particular form of the Navier-Stokes equation given next are omitted. The governing equations derived in chapter 2 are

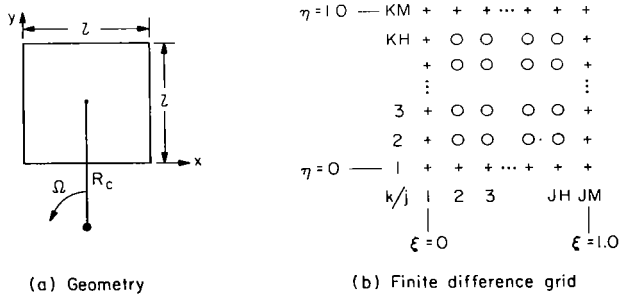

(a) Geometry (b) Finite difference grid

Figure 3.1.– Geometry and differencing grid for two-dimensional square tank.

$$\frac{\partial \omega}{\partial \tau} + \frac{\partial}{\partial \xi}(U\omega) + \frac{\partial}{\partial \eta}(V\omega) = \frac{\partial^2 \omega}{\partial \xi^2} + \frac{\partial^2 \omega}{\partial \eta^2} - G_2 \frac{\partial H}{\partial \xi} + G_1 \frac{\partial H}{\partial \eta} - \frac{d\Omega}{d\tau} \tag{3.1a}$$

$$\frac{\partial H}{\partial \tau} + \frac{\partial}{\partial \xi}(UH) + \frac{\partial}{\partial \eta}(VH) = \frac{1}{Pr}\left(\frac{\partial^2 H}{\partial \xi^2} + \frac{\partial^2 H}{\partial \eta^2}\right) \tag{3.1b}$$

$$\frac{\partial^2 \Psi}{\partial \xi^2} + \frac{\partial^2 \Psi}{\partial \eta^2} = -\omega \tag{3.1c}$$

$$U = \frac{\partial \Psi}{\partial \eta}, \quad V = -\frac{\partial \Psi}{\partial \xi} \tag{3.1d}$$

The independent variables τ and (ξ,η) are dimensionless forms representing time and Cartesian (x,y) space, respectively; ω, H, and Ψ are the dependent variables representing dimensionless forms of the vorticity, temperature, and stream function, respectively. The variables G_1 and G_2 represent the apparent body forces in the rotating system as defined in chapter 2 and Pr is the Prandtl number. Equations (3.1a), (3.1b), and (3.1c) are referred to as the vorticity, energy, and Poisson equations, respectively. Note that the vorticity and energy equations (later referred to as the transport equations) are written in conservative form.

The finite-difference computational domain is shown in figure 3.1(b). The crosses represent the boundary points corresponding to the walls of the container, and the open points refer to the interior points at which the dependent variables can change values. Any grid point at which a dependent variable can change in time is referred to here as a moving point for that dependent variable. This simplifies the description of the matrix formulations used in the analysis of the numerical methods. The value of any dependent variable, say ω, at a grid point is defined as

$$\omega^n_{j,k} = \omega(\xi_j, \eta_k, \tau_n)$$

where

$$\xi_j = (j-1)\Delta\xi \quad j = 1, 2, \ldots, JM$$

$$\eta_k = (k-1)\Delta\eta \quad k = 1, 2, \ldots, KM$$

$$\tau_n = n\,\Delta\tau \quad n = 0, 1, \ldots$$

Referring to figure 3.1(b), we see that this definition puts $\xi = 0$ along the left edge and $\eta = 0$ along the bottom of the grid, and restricts the number of moving points to $2 \le j \le JH$; $2 \le k \le KH$.

The transport equations and the equation for the stream function are quite different in character. Both the vorticity and energy equations are parabolic, time-dependent partial differential equations; whereas the Poisson equation for the stream function is elliptic and explicitly independent of time. This leads to the following generally accepted computational pattern. Given the values of all dependent variables over the mesh at the beginning of a time interval:

1. Advance the vorticity and energy one time increment (either implicitly or explicitly).

2. Using the newly evaluated vorticity, compute the stream function by solving the Poisson equation.

3. For increased accuracy, cycle step one and two in a conventional predictor-corrector process.

VORTICITY AND ENERGY EQUATIONS

Finite-Difference Scheme

The finite-difference approximations to the transport equations are based on the predictor-corrector scheme developed by MacCormack (ref. 1). The difference formulations are in conservative form and are accurate to second order in both space and time, having an error proportional to a third space derivative in dispersion and a fourth space derivative in dissipation (see ref. 2).

Predictor for the vorticity:

$$\tilde{\omega}_{j,k} = \omega^n_{j,k} - \frac{\Delta\tau}{\Delta\xi}\left[(U\omega)^n_{j+1,k} - (U\omega)^n_{j,k}\right] - \frac{\Delta\tau}{\Delta\eta}\left[(V\omega)^n_{j,k+1} - (V\omega)^n_{j,k}\right]$$

$$+ \frac{\Delta\tau}{(\Delta\xi)^2}\left(\omega^n_{j+1,k} - 2\omega^n_{j,k} + \omega^n_{j-1,k}\right) + \frac{\Delta\tau}{(\Delta\eta)^2}\left(\omega^n_{j,k+1} - 2\omega^n_{j,k} + \omega^n_{j,k-1}\right)$$

$$- \frac{G_2\,\Delta\tau}{2\,\Delta\xi}\left(H^n_{j+1,k} - H^n_{j-1,k}\right) + \frac{G_1\,\Delta\tau}{2\,\Delta\eta}\left(H^n_{j,k+1} - H^n_{j,k-1}\right) - \Delta\Omega \qquad (3.2a)$$

Predictor for the energy:

$$\tilde{H}_{j,k} = H^n_{j,k} - \frac{\Delta\tau}{\Delta\xi}\left[(UH)^n_{j+1,k} - (UH)^n_{j,k}\right] - \frac{\Delta\tau}{\Delta\eta}\left[(VH)^n_{j,k+1} - (VH)^n_{j,k}\right]$$

$$+ \frac{1}{Pr}\frac{\Delta\tau}{(\Delta\xi)^2}\left(H^n_{j+1,k} - 2H^n_{j,k} + H^n_{j-1,k}\right) + \frac{1}{Pr}\frac{\Delta\tau}{(\Delta\eta)^2}\left(H^n_{j,k+1} - 2H^n_{j,k} + H^n_{j,k-1}\right) \qquad (3.2b)$$

Corrector for the vorticity:

$$\omega^{n+1}_{j,k} = \frac{1}{2}\left\{\omega^n_{j,k} + \tilde{\omega}_{j,k} - \frac{\Delta\tau}{\Delta\xi}\left[(\tilde{U}\tilde{\omega})_{j,k} - (\tilde{U}\tilde{\omega})_{j-1,k}\right] - \frac{\Delta\tau}{\Delta\eta}\left[(\tilde{V}\tilde{\omega})_{j,k} - (\tilde{V}\tilde{\omega})_{j,k-1}\right]\right.$$

$$+ \frac{\Delta\tau}{(\Delta\xi)^2}\left[\tilde{\omega}_{j+1,k} - 2\tilde{\omega}_{j,k} + \tilde{\omega}_{j-1,k}\right] + \frac{\Delta\tau}{(\Delta\eta)^2}\left[\tilde{\omega}_{j,k+1} - 2\tilde{\omega}_{j,k} + \tilde{\omega}_{j,k-1}\right]$$

$$\left. - \frac{\tilde{G}_2\,\Delta\tau}{2\,\Delta\xi}\left(\tilde{H}_{j+1,k} - \tilde{H}_{j-1,k}\right) + \frac{\tilde{G}_1\,\Delta\tau}{2\,\Delta\eta}\left(\tilde{H}_{j,k+1} - \tilde{H}_{j,k-1}\right) - \Delta\Omega\right\} \qquad (3.2c)$$

Corrector for the energy:

$$H_{j,k}^{n+1} = \frac{1}{2}\left\{H_{j,k}^{n} + \tilde{H}_{j,k} - \frac{\Delta\tau}{\Delta\xi}\left[(\tilde{U}\tilde{H})_{j,k} - (\tilde{U}\tilde{H})_{j-1,k}\right] - \frac{\Delta\tau}{\Delta\eta}\left[(\tilde{V}\tilde{H})_{j,k} - (\tilde{V}\tilde{H})_{j,k-1}\right]\right.$$

$$\left. + \frac{\Delta\tau}{Pr(\Delta\xi)^2}\left(\tilde{H}_{j+1,k} - 2\tilde{H}_{j,k} + \tilde{H}_{j-1,k}\right) + \frac{\Delta\tau}{Pr(\Delta\eta)^2}\left(\tilde{H}_{j,k+1} - 2\tilde{H}_{j,k} + \tilde{H}_{j,k-1}\right)\right\} \tag{3.2d}$$

In these expressions the convective terms are differenced forward and backward in space for the predictor and corrector equations, respectively. In practice, however, this procedure is programmed to be cyclic so that all four possible combinations of forward-backward differencing are used in four successive time steps. In the intermediate step $\tilde{U}$ and $\tilde{V}$ are obtained via the solution of the Poisson equation for $\tilde{\Psi}$ from $\tilde{\omega}$. Similarly, in the final step U^{n+1} and V^{n+1} are obtained by the solution of the Poisson equation for Ψ^{n+1} from ω^{n+1}. Notice that the diffusion terms are central differenced in both the predictor and corrector. The term $\Delta\Omega$ in equations (3.2a) and (3.2c) is evaluated according to $\Delta\Omega = (d\Omega/d\tau)\Delta\tau$ where $d\Omega/d\tau$ is a specified time-dependent function.

Stability

The stability of a general set of nonlinear difference equations is usually estimated by studying the stability of an "equivalent" set of linear difference equations. We accept this philosophy and point out further that not only can the stability of the linear difference equations be established but their complete analytic solution can be determined in a straightforward manner.

Consider, for example, the simple one-dimensional diffusion equation

$$\frac{\partial\phi}{\partial\tau} = \mu\frac{\partial^2\phi}{\partial\xi^2} \tag{3.3}$$

A well-known difference version is

$$\phi_j^{n+1} = \phi_j^n + \mu\frac{\Delta\tau}{(\Delta\xi)^2}\left(\phi_{j+1}^n - 2\phi_j^n + \phi_{j-1}^n\right) \tag{3.4}$$

which can be expressed in vector, matrix notation by

$$\underset{\sim}{\phi}_{n+1} = \underset{\sim}{B}\underset{\sim}{\phi}_n + \underset{\sim}{f} \tag{3.5a}$$

or

$$(\underset{\sim}{E}\underset{\sim}{I} - \underset{\sim}{B})\underset{\sim}{\phi}_n = \underset{\sim}{f} \tag{3.5b}$$

where E is the displacement operator, and $\underset{\sim}{f}$ contains the boundary conditions. Note that when there is no space index, the time index is written as a subscript rather than a superscript. This is done in this section to clarify exponentiation. If $\underset{\sim}{f}$ is a vector of constants[1] the solution of equation (3.5) can be written ($\underset{\sim}{I}$ being the unitary matrix)

$$\underset{\sim}{\phi}_n = \sum_j \underset{\sim}{c}_j(\lambda_j)^n + [\underset{\sim}{I} - \underset{\sim}{B}]^{-1}\underset{\sim}{f} \tag{3.6}$$

The $\underset{\sim}{c}_j$ are constants determined by the initial conditions, and λ_j are the values of the scalar E, which are the assumed distinct roots of the characteristic polynomial equation

$$P(E) \equiv \det(E\underset{\sim}{I} - \underset{\sim}{B}) = 0 \tag{3.7}$$

The matrix $\underset{\sim}{B}$ and the vector $\underset{\sim}{f}$ in equation (3.5) depend on the choice of differencing scheme and the boundary conditions. If they represent equation (3.4) with boundary conditions given at the two ends $\xi = 0$ and $\xi = 1$, they become

$$\left.\begin{aligned} \underset{\sim}{B} &= \underset{\sim}{T}(\beta,\ 1 - 2\beta,\ \beta) \\ \underset{\sim}{f} &= (\beta\phi_1,\ 0,\ \ldots,\ 0,\ \beta\phi_{JM})^T \end{aligned}\right\} \tag{3.8}$$

where $\beta \equiv \mu\Delta\tau/\Delta\xi^2$ and $\underset{\sim}{T}$ is a square tridiagonal matrix defined by

$$\underset{\sim}{T}(d_{-1},d_0,d_1) \equiv \begin{bmatrix} d_0 & d_1 & 0 & \ldots & 0 & 0 \\ d_{-1} & d_0 & d_1 & & 0 & 0 \\ 0 & d_{-1} & d_0 & & 0 & 0 \\ \cdot & & & & & \\ \cdot & & & & \ldots & \\ \cdot & & & & & \\ 0 & 0 & 0 & & d_0 & d_1 \\ 0 & 0 & 0 & \ldots & d_{-1} & d_0 \end{bmatrix} \tag{3.9}$$

The eigenvalues of $\underset{\sim}{T}(d_{-1},d_0,d_1)$ are

$$\lambda_j = d_0 + 2\sqrt{d_1 d_{-1}}\cos\frac{j\pi}{M+1}, \quad j = 1, \ldots, M \tag{3.10}$$

where M is the number of moving points. Notice that if $\underset{\sim}{B}$ is independent of E, the roots of $\det(E\underset{\sim}{I} - \underset{\sim}{B}) = 0$ coincide with the eigenvalues of $\underset{\sim}{B}$. Using

---

[1]That is, if the boundary conditions are independent of τ. When such is not the case the particular solution is more complicated, but can be found (see refs. 3 and 4).

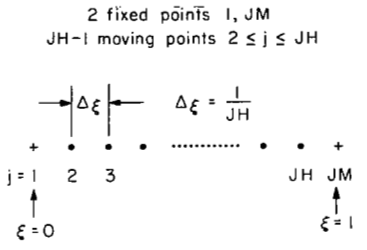

Sketch (a)

the normalized mesh spacing shown in sketch (a), we can find the eigenvalues of $\underset{\sim}{B}$ in equation (3.8); and using equation (3.6), we can write the analytic solution to equation (3.4) as

$$\underset{\sim}{\phi}_n = \sum_{j=1}^{JH-1} \underset{\sim}{c}_j [1 - 2\beta + 2\beta \cos(j\pi/JH)]^n + [\underset{\sim}{I} - \underset{\sim}{B}]^{-1} \underset{\sim}{f} \tag{3.11a}$$

under the imposed boundary conditions. Equation (3.11a) has the alternative expression

$$\underset{\sim}{\phi}_n = \sum_{j=1}^{JH-1} \underset{\sim}{c}_j \left(1 - \frac{4\mu\,\Delta\tau}{\Delta\xi^2} \sin^2 \frac{j\pi\,\Delta\xi}{2}\right)^n + [\underset{\sim}{I} - \underset{\sim}{B}]^{-1} \underset{\sim}{f} \tag{3.11b}$$

Clearly, as n increases the solution of a set of linear difference equations can grow unboundedly if the absolute value of any λ_j in equation (3.6) is greater than one. Two remarks should now be considered. First, it is possible in an *analytic* construction to set to zero all the elements in the vector $\underset{\sim}{c}_j$ multiplying a given λ_j. The magnitude of such λ_j could be greater than one and a bounded solution would result as $n \to \infty$. This behavior is basically related to a saddlepoint problem (ref. 5). Second, it is possible that all of the $|\lambda_j|$ are less than one but they have a structure such that a computed solution will appear to be growing in an unbounded manner as the first several time steps are calculated. This behavior is discussed in reference 6, p. 152. Nevertheless, equations such as equation (3.11) are the exact solutions of the linear difference approximations and they tell us precisely (except for round-off error) what a computer would calculate after any number of time steps.

The stability of difference equations is generally not (for an exception see ref. 7, p. 222) viewed in the above light. More often an amplification factor is developed along lines similar to those introduced by Von Neumann, as discussed in reference 8. Thus the term

$$\phi(\tau,\xi,\eta) = \bar{\phi}(\tau) e^{ik_\xi \xi} e^{ik_\eta \eta} \tag{3.12}$$

is introduced into the difference equation and the ratio $\lambda = \bar{\phi}(\tau + \Delta\tau)/\bar{\phi}(\tau)$ is determined. This ratio is referred to as the amplification factor and the values k_ξ and k_η are called the wave numbers. The condition for stability is, of course, that $|\lambda| \leq 1$. Applying this technique to equation (3.4), one finds

$$\left.\begin{aligned} \lambda &= 1 + \beta(e^{ik_\xi \Delta\xi} - 2 + e^{-ik_\xi \Delta\xi}) \\ \text{or} \\ \lambda &= 1 - 2\beta + 2\beta \cos k_\xi \Delta\xi \end{aligned}\right\} \tag{3.13}$$

This appears to be the same as the term inside the parenthesis in equation (3.11a), but it is not because the arguments of the cosine terms are different. We can make the two approaches identical, however, if we reexamine the discussion under equation (3.7).

The solution given by equation (3.11) depended on the nature of the matrix $\underset{\sim}{B}$, which in turn depended on the boundary conditions. Suppose, instead of fixing the conditions at $\xi = 0$ and $\xi = 1$, we require that the solution be periodic. In such a case equation (3.8) would become

$$\left.\begin{aligned} \underset{\sim}{B} &= \underset{\sim}{T}_p(\beta,\ 1 - 2\beta,\ \beta) \\ \underset{\sim}{f} &= (0,\ 0,\ \ldots,\ 0,\ 0)^T \end{aligned}\right\} \tag{3.14}$$

where $\underset{\sim}{T}_p$ is a square "periodic-tridiagonal" matrix defined by

$$\underset{\sim}{T}_p(d_{-1}, d_0, d_1) = \begin{bmatrix} d_0 & d_1 & 0 & 0 & d_{-1} \\ d_{-1} & d_0 & d_1 & 0 & 0 \\ 0 & d_{-1} & d_0 & 0 & 0 \\ & & & & \\ 0 & 0 & 0 & d_0 & d_1 \\ d_1 & 0 & 0 & d_{-1} & d_0 \end{bmatrix} \tag{3.15}$$

the eigenvalues of which are

$$\lambda_j = d_0 + (d_{-1} + d_1)\cos\frac{2\pi(j-1)}{M} + i(d_{-1} - d_1)\sin\frac{2\pi(j-1)}{M} \qquad j = 1,\ 2,\ \ldots,\ M \tag{3.16}$$

Using equations (3.14) and (3.16), we see that the exact analytic solution to equation (3.4) is

$$\underset{\sim}{\phi}_n = \sum_{j=1}^{JH-1} \underset{\sim}{c}_j \left[1 - 2\beta + 2\beta\cos\left(\frac{2\pi(j-1)}{JH-1}\right)\right]^n \tag{3.17a}$$

when the boundary conditions are periodic. This has the alternative form

$$\underset{\sim}{\phi}_n = \sum_{j=1}^{JH-1} \underset{\sim}{c}_j \left[1 - \frac{4\mu\,\Delta\tau}{\Delta\xi^2}\sin^2(\pi(j-1)\Delta\xi)\right]^n \tag{3.17b}$$

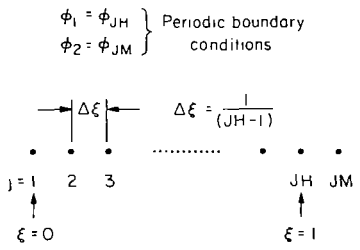

Sketch (b)

where $\Delta\xi = 1/(JH-1)$ for a periodic mesh (see sketch (b)). The term in the brackets in equation (3.17) corresponds to equation (3.13).

The analytic solutions to linear difference equations with periodic boundary conditions are especially easy to find because the eigenvalues in their $\underset{\sim}{B}$ matrix can be readily determined. In fact, the simplest way to find these eigenvalues is

often by the separation of variables technique employed in the discussion of equation (3.12). Consider, for example, the model equation that couples convection and diffusion

$$\frac{\partial \phi}{\partial \tau} = -c \frac{\partial \phi}{\partial \xi} + \mu \frac{\partial^2 \phi}{\partial \xi^2} \tag{3.18}$$

The finite-difference approximation equivalent to the one used on equation (3.1) to form equation (3.2) gives

$$\tilde{\phi}_j = \phi_j^n - \alpha(\phi_{j+1}^n - \phi_j^n) + \beta(\phi_{j+1}^n - 2\phi_j^n + \phi_{j-1}^n) \tag{3.19a}$$

$$\phi_j^{n+1} = \frac{1}{2}\left[\phi_j^n + \tilde{\phi}_j - \alpha(\tilde{\phi}_j - \tilde{\phi}_{j-1}) + \beta(\tilde{\phi}_{j+1} - 2\tilde{\phi}_j + \tilde{\phi}_{j-1})\right] \tag{3.19b}$$

where $\alpha \equiv c\,\Delta\tau/\Delta\xi$, often referred to as the Courant number. Substituting the predictor equation (3.19a) into the corrector equation (3.19b) gives

$$\begin{aligned}\phi_j^{n+1} = \phi_j^n &- \frac{1}{2}\alpha(\phi_{j+1}^n - \phi_{j-1}^n) + \left(\frac{\alpha^2}{2} + \beta\right)(\phi_{j+1}^n - 2\phi_j^n + \phi_{j-1}^n) \\ &- \frac{\alpha\beta}{2}(\phi_{j+2}^n - 2\phi_{j+1}^n + 2\phi_{j-1}^n - \phi_{j-2}^n) \\ &+ \frac{\beta^2}{2}(\phi_{j+2}^n - 4\phi_{j+1}^n + 6\phi_j^n - 4\phi_{j-1}^n + \phi_{j-2}^n)\end{aligned} \tag{3.20}$$

The $\underset{\sim}{B}$ matrix for this difference equation with periodic boundary conditions is the "periodic-pentadiagonal" matrix

$$\underset{\sim}{P}_p(d_{-2}, d_{-1}, d_0, d_1, d_2) \equiv \begin{bmatrix} d_0 & d_1 & d_2 & 0 & 0 & \cdots & 0 & d_{-2} & d_{-1} \\ d_{-1} & d_0 & d_1 & d_2 & 0 & & 0 & 0 & d_{-2} \\ d_{-2} & d_{-1} & d_0 & d_1 & d_2 & & 0 & 0 & 0 \\ \vdots & & & & & & & & \\ 0 & 0 & 0 & & & & d_0 & d_1 & d_2 \\ d_2 & 0 & 0 & & & & d_{-1} & d_0 & d_1 \\ d_1 & d_2 & 0 & & & & d_{-2} & d_{-1} & d_0 \end{bmatrix} \tag{3.21a}$$

where

$$\left.\begin{aligned} d_{-2} &= \alpha\beta/2 + \beta^2/2 \\ d_{-1} &= \alpha/2 + \alpha^2/2 + \beta - \alpha\beta - 2\beta^2 \\ d_0 &= 1 - \alpha^2 - 2\beta + 3\beta^2 \\ d_1 &= -\alpha/2 + \alpha^2/2 + \beta + \alpha\beta - 2\beta^2 \\ d_2 &= -\alpha\beta/2 + \beta^2/2 \end{aligned}\right\} \qquad (3.21b)$$

and its exact analytic solution is

$$\phi_n = \sum_{j=1}^{JH-1} c_j (\lambda_j)^n \qquad (3.22a)$$

where

$$\lambda_j = 1 + (\alpha^2 + 2\beta)\left\{\cos\left[\frac{2\pi(j-1)}{JH-1}\right] - 1\right\} + 2\beta^2\left\{\cos\left[\frac{2\pi(j-1)}{JH-1}\right] - 1\right\}^2$$
$$-i\left\{(\alpha - 2\alpha\beta)\sin\left[\frac{2\pi(j-1)}{JH-1}\right] + \alpha\beta \sin\left[\frac{4\pi(j-1)}{JH-1}\right]\right\}, \quad j = 1, \ldots, JH-1 \qquad (3.22b)$$

these being the eigenvalues of equation (3.21a) with elements defined by equation (3.21b). Although these eigenvalues are complex, each complex λ_j has a conjugate so the summation (3.22a) results in real numbers.

It can be shown that $|\lambda_j|$ has extrema at $j = 1$ and at $j = 1 + (JH-1)/2$. Notice that $|\lambda_1| = 1$ for all α and β. Designate the value of λ_j at $j = 1 + (JH-1)/2$ by λ_c, and one can write

$$|\lambda_c| = |1 - 2\alpha^2 + 4\beta(2\beta - 1)| \qquad (3.23)$$

The stability boundary is formed by finding the values of α and β for which $|\lambda_c| \leq 1$. This boundary is formed by two lines: one, where $\lambda_c \leq 1$, which results in

$$2\beta(2\beta - 1) - \alpha^2 \leq 0 \qquad (3.24)$$

and the other, where $\lambda_c \geq -1$, which results in

$$\alpha^2 + 2\beta(1 - 2\beta) \leq 1 \qquad (3.25)$$

The α,β combinations that produce stability for equation (3.19) with periodic boundary conditions are shown in figure 3.2. The rectangle for which $0 \leq |\alpha| \leq \sqrt{3}/2$ and $0 \leq \beta \leq 1/2$ represents the practical stability boundary. Note that $\beta = \mu\,\Delta\tau/\Delta\xi^2$ is taken to be positive since only positive diffusion,

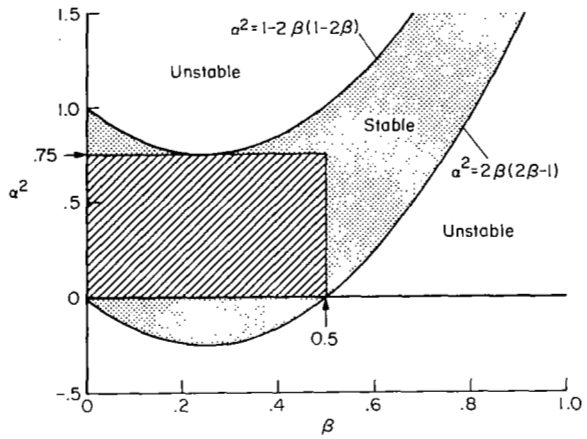

Figure 3.2.– Stability boundaries for equations (3.19) with periodic boundary conditions.

viscosity, or thermal conductivity coefficients are considered. On the other hand $\alpha = c\,\Delta\tau/\Delta\xi$ can be positive or negative depending on the direction of the wave velocity. Note that the effect of coupling diffusion to convection is to lower the maximum generally allowable value of the Courant number from 1 to 0.866. It follows from the above that the stability of the method represented by equation (3.19) when applied to periodic boundary conditions requires that Δt be chosen so that

$$\Delta\tau \leq \text{both } \frac{\Delta\xi^2}{2\mu} \text{ and } \frac{\sqrt{3}}{2}\frac{\Delta\xi}{|c|} \tag{3.26}$$

In the more important two-dimensional case the concepts described above remain the same but the algebra becomes more involved. The partial differential equation coupling diffusion and convection for two-dimensional flow is

$$\frac{\partial\phi}{\partial\tau} = -U\frac{\partial\phi}{\partial\xi} - V\frac{\partial\phi}{\partial\eta} + \mu\left(\frac{\partial^2\phi}{\partial\xi^2} + \frac{\partial^2\phi}{\partial\eta^2}\right) \tag{3.27}$$

where U, V, and μ are constants if the equation is to be linear. If the predictor-corrector sequence, defined for one-dimensional flow by equation (3.2), is applied to equation (3.27), and periodic boundary conditions are imposed, detailed calculations show that the stability boundaries for $|\lambda_c|$ are the same as those given by equations (3.24) and (3.25) except that

$$\left.\begin{aligned} \alpha &= |U|\frac{\Delta\tau}{\Delta\xi} + |V|\frac{\Delta\tau}{\Delta\eta} \\ \beta &= \mu\,\Delta\tau\left[\frac{1}{\Delta\xi^2} + \frac{1}{\Delta\eta^2}\right] \end{aligned}\right\} \tag{3.28}$$

This means that the difference equations with periodic boundary conditions are stable if

$$\Delta\tau \leq \text{both } \frac{1}{2\mu}\left(\frac{\Delta\xi^2\,\Delta\eta^2}{\Delta\xi^2 + \Delta\eta^2}\right) \text{ and } \frac{\sqrt{3}}{2}\left(\frac{\Delta\xi\,\Delta\eta}{|U|\Delta\eta + |V|\Delta\xi}\right) \tag{3.29}$$

In the application to physical problems the effectiveness of the predictor-corrector method, described by equation (3.19) for the linear and equation (3.2) for the nonlinear cases, respectively, depends on the relative magnitudes of the diffusion coefficients (i.e., the viscosity and thermal conductivity) and some representative or average value of the velocities. If there is a high degree of diffusion (μ large) then the first term in equation (3.29) would be the smallest and the time step size would be forced, by reasons of stability, to be unnecessarily small for a given accuracy. In such cases an

implicit differencing of the diffusion terms is suggested (refs. 9, 10). If, on the other hand, the diffusion is low relative to the magnitude of the (average) velocity, the physical requirements associated with the domain of dependence limit the size of the time step, and the explicit method described is entirely adequate.

In the particular case regarding the convective mixing of oxygen at high pressure and low temperature, both the viscosity and the thermal conductivity are so low (ch. 6) that the explicit method is entirely satisfactory from the viewpoint of stability.

Accuracy

The accuracy of the differencing scheme given by equation (3.19) can be estimated in several ways. By accuracy we mean, of course, how well it represents the basic partial differential equation (3.18). We choose here to discuss this accuracy by deriving the "modified partial differential" equation, that is, the differential equation actually represented by the difference equation (see ref. 2) and comparing this to the basic partial differential equation. One can derive the modified partial differential equation for equation (3.19) by expanding each term in a Taylor series about the point represented by (n,j). Time derivatives of higher than first order are eliminated by repetitive use of equation (3.20) itself. The result of such a procedure gives

$$\phi_\tau = -c\phi_\xi + \mu\phi_{\xi\xi} - \frac{c}{6}[(\Delta\xi)^2 - c^2(\Delta\tau)^2]\phi_{\xi\xi\xi} - \left\{\frac{c^2\,\Delta\tau}{8}[(\Delta\xi)^2 - c^2(\Delta\tau)^2] - \frac{\mu}{12}[(\Delta\xi)^2 - 6c^2(\Delta\tau)^2]\right\}\phi_{\xi\xi\xi\xi} + \ldots \quad (3.30)$$

The coefficient of the third derivative represents, to the lowest order, the dispersion or phase error, and the coefficient of the fourth derivative represents, again to the lowest order, the dissipation or diffusion error.

Note that the error in dispersion is due only to the finite differencing of the convection term (given by the coefficient of c in eq. (3.18)) and is of order $(\Delta\xi)^2$, $(\Delta\tau)^2$. The error in dissipation or diffusion is caused by the finite differencing of both the convection and diffusion terms, orders being $(\Delta\tau)(\Delta\xi)^2$, $(\Delta\tau)^3$, and $(\Delta\xi)^2$, $(\Delta\tau)^2$, respectively. When the magnitudes of the viscosity and thermal conductivity coefficients are small, as they are in our intended physical application, the principal error is in dispersion and is proportional to $(c/6)[(\Delta\xi)^2 - c^2(\Delta\tau)^2]$. In the practical problem, c represents a local velocity and the magnitude of the velocity varies throughout the tank. One can show that the term $(c/6)[(\Delta\xi)^2 - c^2(\Delta\tau)^2]$ is zero when $c\,\Delta\tau/\Delta\xi$ is either zero or one, and a maximum in that interval when $c\,\Delta\tau/\Delta\xi = 1/\sqrt{3}$. Since $|c\,\Delta\tau/\Delta\xi|_{max} \leq 1$ for stability, the maximum error in dispersion given by the lowest order error term in the modified partial differential equation (3.30) is $-(c\,\Delta\xi^2/9)\phi_{\xi\xi\xi}$ if numerical stability is the only bound on the time step size.

To get less dispersive error with the differencing scheme given in equation (3.19) one must choose a time step such that $c\,\Delta\tau/\Delta\xi < 1/\sqrt{3}$.

POISSON EQUATION

The finite-difference approximation to the Poisson equation (3.1c) for the stream function may be written with second-order accuracy by the well-known five-point formula as

$$\frac{\Psi_{j,k-1} - 2\Psi_{j,k} + \Psi_{j,k+1}}{(\Delta\eta)^2} + \frac{\Psi_{j-1,k} - 2\Psi_{j,k} + \Psi_{j+1,k}}{(\Delta\xi)^2} = -\omega_{j,k} \qquad (3.31)$$

$$j = 2, \ldots, JM-1, \quad k = 2, \ldots, KM-1$$

Given a $(JM-2) \times (KM-2)$ internal distribution of vorticity and $2(JM + KM - 2)$ boundary values for the stream function as shown in figure 3.1(b), we wish to find the $(JM-2) \times (KM-2)$ interior values of Ψ that satisfy equation (3.31). We can find such a solution by iterative techniques such as SOR and ADI (ref. 11), but since the equation is linear we can also solve it by direct inversion of a set of linear, simultaneous algebraic equations. These so-called direct methods require far less computing time than the iterative ones when used to find solutions to equation (3.31). The particular one used here was developed by Buneman (ref. 12) and is referred to as the double cyclic reduction method. It is an extension of the odd/even reduction scheme (refs. 13, 14).

Odd/Even Reduction of a Tridiagonal Matrix

Consider the tridiagonal set of algebraic equations

$$\begin{bmatrix} a & -1 & 0 & 0 & 0 & 0 & 0 \\ -1 & a & -1 & 0 & 0 & 0 & 0 \\ 0 & -1 & a & -1 & 0 & 0 & 0 \\ 0 & 0 & -1 & a & -1 & 0 & 0 \\ 0 & 0 & 0 & -1 & a & -1 & 0 \\ 0 & 0 & 0 & 0 & -1 & a & -1 \\ 0 & 0 & 0 & 0 & 0 & -1 & a \end{bmatrix} \begin{bmatrix} u_2 \\ u_3 \\ u_4 \\ u_5 \\ u_6 \\ u_7 \\ u_8 \end{bmatrix} = \begin{bmatrix} f_2 \\ f_3 \\ f_4 \\ f_5 \\ f_6 \\ f_7 \\ f_8 \end{bmatrix} \qquad (3.32)$$

Multiplying the odd rows by a and adding the adjacent rows to it gives

$$\begin{bmatrix} a^2-2 & -1 & 0 \\ -1 & a^2-2 & -1 \\ 0 & -1 & a^2-2 \end{bmatrix} \begin{bmatrix} u_3 \\ u_5 \\ u_7 \end{bmatrix} = \begin{bmatrix} af_3 + f_2 + f_4 \\ af_5 + f_4 + f_6 \\ af_7 + f_6 + f_8 \end{bmatrix} \qquad (3.33)$$

which is obviously recursive if the number of rows equals 2^L-1 where L is an integer. If we set

$$a^{(1)} = a\ , \quad a^{(\ell+1)} = [a^{(\ell)}]^2 - 2 \tag{3.34a}$$

$$f_n^{(1)} = f_n\ , \quad f_n^{(\ell+1)} = a^{(\ell)} f_n^{(\ell)} + f_{n-2^{\ell-1}}^{(\ell)} + f_{n+2^{\ell-1}}^{(\ell)} \tag{3.34b}$$

and let M represent the midpoint in the u vector ($M = 1 + 2^{L-1}$), we have after $L-1$ recursions

$$a^{(L)} u_M = f_M^{(L)} \tag{3.35}$$

This is solved for u_M and a backward recursion gives the completed solution.

One of the advantages of this scheme is the efficient use of core storage. Only one array is needed in the calculation, it is initially filled with the elements of $\underset{\sim}{f}$, which are then overwritten and replaced by the values of $\underset{\sim}{u}$ in the solution. Table 3.1 shows how an array[2] of 17 is overwritten by the forward recursion, at the end of which every other value of $\underset{\sim}{f}$ has been overwritten. Table 3.2 shows the backward recursion. The final value of u_9 is computed by equation (3.35), then u_5 and u_{13} are found, and so on, until all the u from 2 to 16 are evaluated and have replaced the original $f_2, \ldots, f_{16}$.

The same concept can be applied to find the direct solution of the two-dimensional equation (3.31). When equation (3.31) is multiplied by $(\Delta\xi)^2$ and written in matrix form, we obtain

$$\begin{bmatrix} \underset{\sim}{A} & -\underset{\sim}{I} & & & \\ -\underset{\sim}{I} & \underset{\sim}{A} & -\underset{\sim}{I} & & \\ & -\underset{\sim}{I} & \underset{\sim}{A} & -\underset{\sim}{I} & \\ & & -\underset{\sim}{I} & \underset{\sim}{A} & -\underset{\sim}{I} \\ & & & -\underset{\sim}{I} & \underset{\sim}{A} \end{bmatrix} \begin{bmatrix} \underset{\sim}{\Psi}_2 \\ \underset{\sim}{\Psi}_3 \\ \\ \\ \underset{\sim}{\Psi}_{JM-1} \end{bmatrix} = \begin{bmatrix} \underset{\sim}{f}_2 \\ \underset{\sim}{f}_3 \\ \\ \\ \underset{\sim}{f}_{JM-1} \end{bmatrix} \tag{3.36}$$

where $\underset{\sim}{A}$ is a $(KM-2) \times (KM-2)$ tridiagonal matrix with $-2[1 + (\Delta\xi/\Delta\eta)^2]$ on the diagonal and $(\Delta\xi/\Delta\eta)^2$ on each side; $\underset{\sim}{I}$ is the $(KM-2) \times (KM-2)$ identity matrix; $\underset{\sim}{\Psi}_j$ is the vector of stream functions in the jth column of the grid; and $\underset{\sim}{f}_j$ is the jth column of vorticities and boundary values. Note that JM must be $2^{L_1}+1$ and KM must be $2^{L_2}+1$ where L_1 and L_2 are integers.

[2] $L = 4$ giving $2^4 - 1 = 15$ moving points, but a word at each end is reserved and set to zero to simplify the backward recursion; see table 3.2.

TABLE 3.1.- FORWARD RECURSION IN ODD/EVEN REDUCTION. COLUMN ON LEFT IS ORIGINALLY STORED, THEN SUCCESSIVELY USED AND OVERWRITTEN BY COLUMNS 2, 3, AND 4

f_1			
f_2			
$f_3 \leftarrow a^{(1)} f_3+f_2+f_4$			
f_4			
$f_5 \leftarrow a^{(1)} f_5+f_4+f_6$	$f_5 \leftarrow a^{(2)} f_5+f_3+f_7$		
f_6			
$f_7 \leftarrow a^{(1)} f_7+f_6+f_8$			
f_8			
$f_9 \leftarrow a^{(1)} f_9+f_8+f_{10}$	$f_9 \leftarrow a^{(2)} f_9+f_7+f_{11}$	$f_9 \leftarrow a^{(3)} f_9+f_5+f_{13}$	
f_{10}			
$f_{11} \leftarrow a^{(1)} f_{11}+f_{10}+f_{12}$			
f_{12}			
$f_{13} \leftarrow a^{(1)} f_{13}+f_{12}+f_{14}$	$f_{13} \leftarrow a^{(2)} f_{13}+f_{11}+f_{15}$		
f_{14}			
$f_{15} \leftarrow a^{(1)} f_{15}+f_{14}+f_{16}$			
f_{16}			
f_{17}			

TABLE 3.2.- BACKWARD RECURSION IN ODD/EVEN REDUCTION. COLUMN ON LEFT IS ORIGINALLY STORED, THEN OVERWRITTEN BY COLUMNS 2, 3, 4, AND 5

$f_1 \leftarrow 0.0$				
f_2				$\leftarrow (f_2+f_1+f_3)/a^{(1)}$
f_3			$\leftarrow (f_3+f_1+f_5)/a^{(2)}$	
f_4				$\leftarrow (f_4+f_3+f_5)/a^{(1)}$
f_5		$\leftarrow (f_5+f_1+f_9)/a^{(3)}$		
f_6				$\leftarrow (f_6+f_5+f_7)/a^{(1)}$
f_7			$\leftarrow (f_7+f_5+f_9)/a^{(2)}$	
f_8				$\leftarrow (f_8+f_7+f_9)/a^{(1)}$
$f_9 \leftarrow f_9/a^{(4)}$				
f_{10}				$\leftarrow (f_{10}+f_9+f_{11})/a^{(1)}$
f_{11}			$\leftarrow (f_{11}+f_9+f_{13})/a^{(2)}$	
f_{12}				$\leftarrow (f_{12}+f_{11}+f_{13})/a^{(1)}$
f_{13}		$\leftarrow (f_{13}+f_9+f_{17}/a^{(3)}$		
f_{14}				$\leftarrow (f_{14}+f_{13}+f_{15})/a^{(1)}$
f_{15}			$\leftarrow (f_{15}+f_{13}+f_{17})/a^{(2)}$	
f_{16}				$\leftarrow (f_{16}+f_{15}+f_{17})/a^{(1)}$
$f_{17} \leftarrow 0.0$				

The process of odd/even reduction described for a simple matrix such as that given by equation (3.32) can now be applied to a block matrix such as that given by equation (3.36). The concept is simplified if we refer at once to tables 3.1 and 3.2 and recall that matrix and algebraic arithmetic are identical in addition and differ in multiplication only on commutivity. Consider, first, table 3.1. Note that all operations are formed by simple additions and multiplications of the data existing in the single $\underset{\sim}{f}$ array at any given stage in the calculations. The same is true in the two-dimensional case, except that the operations are on the column vectors f. For example, for the two-dimensional case, in table 3.1 the first entry of the second column would be replaced by $\underset{\sim}{A}^{(1)}\underset{\sim}{f}_3 + \underset{\sim}{f}_2 + \underset{\sim}{f}_4$, which is a tridiagonal multiplication into a vector and two vector additions.

The two-dimensional equivalent of equation (3.34a) is formed by the matrix definitions

$$\underset{\sim}{A}^{(1)} = \underset{\sim}{A} , \quad \underset{\sim}{A}^{(\ell+1)} = \underset{\sim}{A}^{(\ell)}\underset{\sim}{A}^{(\ell)} - 2\underset{\sim}{I} \tag{3.37}$$

The essential part of this relationship is that $\underset{\sim}{A}^{(\ell+1)}$ can always be reduced to a product of tridiagonal matrices. Thus

$$\left.\begin{aligned}
&\underset{\sim}{A}^{(1)} = \underset{\sim}{A} \\
&\underset{\sim}{A}^{(2)} = (\underset{\sim}{A} - \sqrt{2}\,\underset{\sim}{I})(\underset{\sim}{A} + \sqrt{2}\,\underset{\sim}{I}) \\
&\underset{\sim}{A}^{(3)} = (\underset{\sim}{A} - \sqrt{2 - \sqrt{2}}\,\underset{\sim}{I})(\underset{\sim}{A} - \sqrt{2 + \sqrt{2}}\,\underset{\sim}{I})(\underset{\sim}{A} + \sqrt{2 - \sqrt{2}}\,\underset{\sim}{I})(\underset{\sim}{A} + \sqrt{2 + \sqrt{2}}\,\underset{\sim}{I}) \\
&\vdots \\
&\underset{\sim}{A}^{(\ell)} = (\underset{\sim}{A} - \lambda_1\underset{\sim}{I})(\underset{\sim}{A} - \lambda_2\underset{\sim}{I}) \cdots (\underset{\sim}{A} - \lambda_k\underset{\sim}{I}) \\
&\quad k = 2^{\ell-1} \\
&\quad \lambda_j = 2\cos\frac{(2j-1)\pi}{2k} , \quad j = 1, 2, \ldots, k
\end{aligned}\right\} \tag{3.38}$$

In general, $\underset{\sim}{A}^{(\ell)}$ is the product of $2^{\ell-1}$ tridiagonal matrices that have constant entries along the two off diagonals and differ only by the constant λ_j along the diagonal. If we write a subroutine that will perform such a simple operation, we can apply it twice in succession to form each of $\underset{\sim}{A}^{(2)}\underset{\sim}{f}_5$, $\underset{\sim}{A}^{(2)}\underset{\sim}{f}_9$, and $\underset{\sim}{A}^{(2)}\underset{\sim}{f}_{13}$, and four times to form $\underset{\sim}{A}^{(3)}\underset{\sim}{f}_9$ in the two-dimensional equivalent of table 3.1.

The remarkable property of the process being described comes in the two-dimensional equivalent of the procedure outlined in table 3.2. The matrix equivalent of an algebraic division is a product using the matrix inverse. This would greatly complicate the extension of the backward recursion if the factorization shown in equation (3.38) did not exist. Since such a factorization does exist, however, the actual computation of $\underset{\sim}{u}_M$ in the two-dimensional

equivalent to equation (3.35)

$$\underset{\sim}{A}^{(L)}\underset{\sim}{u}_M = \underset{\sim}{f}_M^{(L)} \tag{3.39}$$

is found by performing 2^{L-1} tridiagonal inversions (each identical to the scalar manipulations shown in tables 3.1 and 3.2 on the data in $\underset{\sim}{f}_M$. For example, the two-dimensional equivalent of $(f_3+f_1+f_5)/a^{(2)}$ in table 3.2 is

$$(\underset{\sim}{A} - \sqrt{2}\ \underset{\sim}{I})^{-1}(\underset{\sim}{A} + \sqrt{2}\ \underset{\sim}{I})^{-1}(\underset{\sim}{f}_3 + \underset{\sim}{f}_1 + \underset{\sim}{f}_5) \tag{3.40}$$

and is computed by two successive calls to a tridiagonal inversion subroutine, each call having a different constant for the diagonal entry but both with a fixed constant for the two off-diagonal entries.

This describes the *concept* of one- and two-dimensional odd/even reduction of the Poisson equation. In *application* to the two-dimensional case (eq. (3.31)) the matrix products formed by the forward recursion can lead to very large floating point numbers. A clever way to avoid this numerical complication has been devised by Buneman and a FORTRAN program that computes the Poisson equation for Dirichlet boundary conditions using Buneman's version of odd/even reduction is listed in reference 12.

BOUNDARY CONDITIONS

The boundary condition for the energy equation (3.1b) is satisfied by specifying either the temperature or the heat flux at the wall. The boundary condition for the Poisson equation (3.1c) is satisfied by setting $\Psi = 0$ along the edges. This corresponds to the condition of no mass flow through any portion of the wall. The boundary condition for the vorticity equation (3.1b) is somewhat more subtle and is described below.

For a viscous fluid, the additional condition of no slip at the walls is met if the normal stream-function derivative (or tangential velocity) vanishes at the walls. This boundary condition is satisfied in the vorticity equation (3.1a) in the following way. First, notice from equation (3.1c) that along a horizontal wall

$$\omega = -\Psi_{\eta\eta} \tag{3.41a}$$

and along a vertical wall

$$\omega = -\Psi_{\xi\xi} \tag{3.41b}$$

since Ψ itself is zero along the walls. Next consider a Taylor's series expansion for the stream function at a point on the wall. Using it to find the value of Ψ at an interior point next to the wall, one finds (taking the bottom wall as an example)

$$\Psi_{j,2} = \Psi_{j,1} + \left(\frac{\partial\Psi}{\partial\eta}\right)_{j,1}\Delta\eta + \frac{1}{2}\left(\frac{\partial^2\Psi}{\partial\eta^2}\right)_{j,1}(\Delta\eta)^2 + O(\Delta\eta)^3 \tag{3.42}$$

Again $\Psi_{j,1}$ must be zero since it is the value of Ψ at the wall, and now we can apply the no-slip condition by also setting the tangential velocity at the wall $(\partial\Psi/\partial\eta)_{j,1}$ equal to zero. This reduces to a boundary condition for ω; namely, at the wall ω is given by

$$\omega_{j,1} = \frac{-2\Psi_{j,2}}{(\Delta\eta)^2} \tag{3.43}$$

where $\Psi_{j,2}$ has been calculated in a previous predictor or corrector sequence. Similar formulas are also derived for the other walls. Formulas of higher order may be obtained by expanding about deeper interior points; for example, the second-order approximation for points (j,1) is found by simultaneously solving the expansions

$$A\Psi_{j,2} = A\left[\Psi_{j,1} + \left(\frac{\partial\Psi}{\partial\eta}\right)_{j,1}(\Delta\eta) + \frac{1}{2}\left(\frac{\partial^2\Psi}{\partial\eta^2}\right)_{j,1}(\Delta\eta)^2 + \frac{1}{6}\left(\frac{\partial^3\Psi}{\partial\eta^3}\right)_{j,1}(\Delta\eta)^3 + O(\Delta\eta)^4\right] \tag{3.44a}$$

$$B\Psi_{j,3} = B\left[\Psi_{j,1} + 2\left(\frac{\partial\Psi}{\partial\eta}\right)_{j,1}(\Delta\eta) + 2\left(\frac{\partial^2\Psi}{\partial\eta^2}\right)_{j,1}(\Delta\eta)^2 + \frac{4}{3}\left(\frac{\partial^3\Psi}{\partial\eta^3}\right)_{j,1}(\Delta\eta)^3 + O(\Delta\eta)^4\right] \tag{3.44b}$$

to obtain

$$\omega_{j,1} = -\left(\frac{8\Psi_{j,2} - \Psi_{j,3}}{2(\Delta\eta)^2}\right) \tag{3.45}$$

Singularities exist in the analytic solutions for the flow at the corners of the box, and it is possible for a corner to lie outside the radius of convergence of a Taylor series expansion about one of the neighboring points. In fact, the calculations did show instabilities near the corner points when the higher order equations were used, and it is believed they developed for the reason just described. As a result, the lower order equations, typified by equation (3.43), were used for the boundary condition on the vorticity throughout the calculations. The sacrifice in accuracy is not considered important for the nature of the mixing problem involved.

COMPUTATIONAL PROCEDURE

To begin the convection calculations, the initial velocities are set to zero and the temperature distribution specified. The subsequent computational

procedure is described by the following steps:

1. Calculate the predicted vorticity and temperature distributions from equations (3.2a) and (3.2b).
2. Calculate the corresponding stream function by Buneman's double cyclic reduction method.
3. Apply the wall boundary conditions for the vorticity from equation (3.43).
4. Calculate the corrected vorticity and temperature distributions from equations (3.2c) and (3.2d).
5. Calculate the corresponding stream function as in step 2.
6. Apply the wall boundary condition as in step 3.

The calculations for one time step are now complete. The procedure continues until the desired number of time steps are complete.

CONCLUDING REMARKS

A finite-difference predictor-corrector scheme has been described for calculating convection in a rotating tank. The assumption is made that the stability bounds and the order of accuracy of a set of nonlinear difference equations can be estimated by studying an "equivalent" set of linear model equations. Such being the case, it is pointed out that not only can the stability of the linear difference equations representing convection be established, but the complete analytic solution of them can be written for the n(th) time step without ever going to a computer. Furthermore, such an analytic solution to a set of linear difference equations with periodic boundary conditions predicts stability boundaries identical to those obtained from an amplification factor analysis. The accuracy study for these convective equations is based on a study of the modified partial differential equations, and it shows that the approximations are characterized by second-order errors in both dispersion and dissipation.

Finally, a fast, efficient, and direct numerical solution to Poisson's equation is described. It is based on double cyclic reduction techniques introduced by Buzbee, Golub, and Nielson in reference 13.

REFERENCES

1. MacCormack, R. W.: The Effect of Viscosity in Hypervelocity Impact Cratering. AIAA Paper 69-354, 1969.

2. Lomax, Harvard; Kutler, Paul; and Fuller, F. B.: The Numerical Solution of Partial Differential Equations Governing Convection. AGARDograph No. 146, 1970.

3. Boole, George: Calculus of Finite Differences. Fourth ed., J. F. Moulton, ed., Chelsea Pub. Co., New York, 1958.

4. Milne-Thomson, Louis Melville: The Calculus of Finite Differences. Macmillan, 1933.

5. Lomax, Harvard: Stable Implicit and Explicit Numerical Methods for Integrating Quasi-Linear Differential Equations with Parasitic-Stiff and Parasitic-Saddle Eigenvalues. NASA TN D-4703, 1968.

6. Richtmeyer, R. D.; and Morton, K. W.: Difference Methods for Initial-Value Problems. Second ed., Interscience Pub., Inc., 1967.

7. Fox, L.: Numerical Solution of Ordinary and Partial Differential Equations. Pergamon Press, 1962.

8. O'Brien, G. G.; Hyman, M. A.; and Kaplan, S.: A Study of the Numerical Solutions of Partial Differential Equations. J. Math. Phys., Vol. 29, 1951, pp. 223-251.

9. Aziz, K.; and Hellums, J. D.: Numerical Solution of the Three-Dimensional Equations of Motion for Laminar Natural Convection. Phys. Fluids, Vol. 10, 1967, pp. 314-324.

10. Wilkes, J. O.; and Churchill, S. W.: The Finite-Difference Computation of Natural Convection in a Rectangular Enclosure. Amer. Inst. Chem. Engr. J., Vol. 12, 1966, pp. 161-166.

11. Forsythe, G. E.; and Wasow, W. R.: Finite-Difference Methods for Partial Differential Equations. John Wiley & Sons, Inc., 1960.

12. Buneman, O.: A Compact Non-Iterative Poisson Solver. Rep. SU-IPR-294, Institute for Plasma Research, Stanford Univ., Stanford, Calif., 1969.

13. Buzbee, B. L.; Golub, G. H.; and Nielson, C. W.: The Method of Odd-Even Reduction and Factorization with Application to Poisson's Equation. Rep. LA-4141, Los Alamos Scientific Lab., Los Alamos, New Mexico, 1969.

14. Hockney, R. W.: The Potential Calculation and Some Applications. Vol. 9, Methods in Computational Physics, B. Alder, S. Fernback, and M. Rotenberg, eds., Academic Press, 1970, pp. 135-211.

4. CALCULATION OF THERMODYNAMIC PROPERTIES OF OXYGEN NEAR THE CRITICAL POINT

Walter A. Reinhardt

SUMMARY

Methods are developed for the versatile and efficient evaluation of the thermodynamic properties of cryogenic oxygen. The semiempirical equations of state of Stewart are used in this discussion. An arbitrary choice of independent thermodynamic variables within a limited set is allowed. Comments on procedures that lead to an expansion of the variable set are given. A method for the efficient rapid evaluation of integrals representing volume averages of spatially varying thermodynamic quantities is described. A number of graphs are given that show state relations plotted in different ways to demonstrate the methods used. In addition to being instructive, these curves serve as a valuable ready reference on cryogenic oxygen properties.

INTRODUCTION

The principal objective of this work is to formulate the thermodynamic properties of cryogenic oxygen to permit their efficient evaluation by electronic computers. The resulting computer programs are used in conjunction with other codes in the simulation study of the behavior of gases stored in tanks of maneuvering space vehicles. Comments on the complementary numerical codes along with discussions on the complete problem and background surveys related to this report are given in chapter 1 of this report. It is worthwhile to orient the reader, however, on the material presented in this article by briefly reviewing a few pertinent considerations that necessitated the availability of accurate thermodynamic properties that can be rapidly computed.

In the case of the Apollo spacecraft, the onboard cryogenic storage system provides gaseous hydrogen and oxygen (oxygen is of particular interest in this study) used in the electrical power system and environmental control system of the command and service module. Fluids are stored in the system at temperatures and pressures slightly greater than critical where the density is so large that the fluid is not distinguishable as being either liquid or gas. Cryogenic storage allows spacecraft minimum volume and weight requirements to be met and ensures single-phase delivery of the fluids (ref. 1). To maintain a constant pressure within the tanks, as required by the electrical power and environmental control systems as oxygen is drawn from the system, heat is added by means of contained electrical heaters. The added heat can remain in the neighborhood of the heaters, however, in the absence of conductive or convective mixing; there then result large thermal gradients ("thermal stratification") within the stored fluids. Because oxygen has a very low thermal conductivity, conduction currents are negligible. Also, convective mixing processes do not take place in the absence of any spacecraft accelerations in the otherwise gravity-free environment. If particularly severe thermal stratification occurs, a spacecraft maneuver (such as a midcourse correction on a flight to the moon, for example) could lead to mixing that would then result in a large abrupt pressure decrease or "pressure collapse" (ch. 1 and ref. 2) with attendant possibility of catastrophic equipment failure. Prior to Apollo 14, fans were included within the storage tanks to ensure that the fluid was mixed and

uniform temperatures maintained. The subject study of this report is that of investigating the use of vehicle maneuvers (in particular, rotations) as a means toward the maintenance of uniform temperatures and pressures. The nominal operating pressure requirements of the cryogenic gas storage system are 900 ±35 psia (62 ±2.4 atm) or, stated in a slightly different manner, that the pressures must not deviate by more than about 4 percent from the mean stated value. This suggests that accurate relations are required for gas properties if reliance is to be placed on interpretations gained from numerical computations. The semiempirical thermodynamic properties published for cryogenic oxygen by Stewart (ref. 3) and by Weber (ref. 4) satisfy the accuracy requirements.

One complication that occurs in the analytical description of fluid properties near the critical point is that the properties require two independent variables with both variables showing strong nonlinear behavior. In this respect, the relatively simple descriptions such as provided by van der Waals' or Beattie-Bridgeman's equations of state (see, e.g., ref. 5 or 6) are not at all satisfactory. In fact, the required state equations can be quite complicated, as shown in both Stewart's and Weber's papers (refs. 3 and 4). An additional problem that occurs with such relations is that should a different choice of independent variables be required, considerable computer time can be expended in the application of conventional inversion methods.

In the discussion that follows, particular emphasis is placed on formulating the thermodynamic properties of cryogenic oxygen in such a manner that flexible and time-wise efficient evaluations are possible. By flexible it is meant that an arbitrary choice of independent variables is allowed. A minimization of redundant arithmetic operations leads to an efficient computer program.

It was found that a "modified virial" representation of Stewart's equations leads to the least computational redundancy. Finding zeros by means of successive linear interpolations (ref. 7) provides the means for obtaining rapid function inversions. The thermal equation of state and the caloric equation of state are plotted in several different ways to demonstrate the flexibility of the procedures described.

A method is also described that is particularly valuable for the rapid evaluation of volume integrals of thermodynamic spatially varying quantities (e.g., temperature) where the integrals represent volume averages. An important concept of this method is that accuracy can be traded to obtain computing speed. Thus, by sacrificing the numerical accuracy beyond that specified by the semiempirical formula, one obtains significant savings in computational time. The method is particularly well suited for certain classes of numerical simulation studies, since evaluation time is nearly independent of the number of spatial mesh points.

The author wishes to acknowledge several helpful conversations with Prof. Richard B. Stewart, Mechanical Engineering Department, University of Idaho, Moscow, Idaho, and with Dr. Loyd A. Weber, Cryogenics Division, National Bureau of Standards Laboratory, Boulder, Colorado.

THERMODYNAMIC QUANTITIES

There are several accurate representations for the thermal equation of state for cryogenic oxygen. In one case (ref. 4), accurate experimental results in tabular form are published that encompass a broad range of values of pressure and temperature ($54.6° \leq T \leq 300°$ K; $1 \leq p \leq 330$ atm). A value of a state variable, say pressure, can be made available on an electronic computer by the use of a table-lookup and interpolation procedure once the other pair of variables, density and temperature, are specified. In the second case (ref. 3), the state variable is represented by a complicated analytical function of two independent variables. Specification of values for the two independent variables and evaluation of the function are then necessary to obtain a value for the state variable.

A purpose of this work is to design a flexible procedure for obtaining thermodynamic state variables – that is, a procedure that allows the rapid determination of an arbitrary variable given any pair of other variables. To expedite this task, it was decided to minimize the coding problems encountered by representing the state equation as a complicated analytical relation. As a result of interpolation problems, table-lookup procedures that depend on two independent variables often are inapplicable to general usage. For example, when derivatives of thermodynamic quantities are required, numerical differentiation of table quantities can result in an unacceptable lack of smoothness. Although one can develop procedures to overcome these difficulties, they are avoided by the use of the analytical relation.

In the discussion that follows the analytical representation given by Stewart in reference 3 is used. It will also be shown that by modifying Stewart's original formulation to one similar to the virial state equation (see, e.g., ref. 6) one can significantly reduce computer evaluation time.

One should note that although Stewart's formulation was used, much of the content of this chapter is of a general nature and therefore applies independently of this particular choice.

Quantities Defined Explicitly

This section concerns the various thermodynamic quantities that are defined explicitly in terms of representations containing the independent variables. Particular emphasis is given to formulations of the state equations where redundant arithmetic operations are held to a minimum; hence, evaluation time is also minimal.

The particular state relations to be discussed are the analytical formulation of the thermal equation of state $p = p_a(T,\rho)$, the equivalent "physical" representation $p = p_p(T,\rho)$, and the caloric equation of state $e = U(T,\rho)$.

Thermal equation of state (analytical representation)—The equation of state that results from Stewart's work is given by

$$p = p_a(T,\rho)$$

$$= RT\rho$$

$$+\left(n_1T + n_2 + \frac{n_3}{T^2} + \frac{n_4}{T^4} + \frac{n_5}{T^6}\right)\rho^2$$

$$+\left(n_6T^2 + n_7T + n_8 + \frac{n_9}{T} + \frac{n_{10}}{T^2}\right)\rho^3$$

$$+(n_{11}T + n_{12})\rho^4$$

$$+\left(n_{13} + \frac{n_{14}}{T}\right)\rho^5$$

$$+\left(\frac{n_{15}}{T^2} + \frac{n_{16}}{T^3} + \frac{n_{17}}{T^4}\right)\rho^3 \exp(n_{25}\rho^2)$$

$$+\left(\frac{n_{18}}{T^2} + \frac{n_{19}}{T^3} + \frac{n_{20}}{T^4}\right)\rho^5 \exp(n_{25}\rho^2)$$

$$+\left(\frac{n_{21}}{T^2} + \frac{n_{22}}{T^3} + \frac{n_{23}}{T^4}\right)\rho^7 \exp(n_{25}\rho^2)$$

$$+n_{24} \exp[n_{27}(T-T_c)^2]\rho^{n_{28}+1} v \exp(n_{26}v^2) \qquad (4.1a)$$

where

$$v = \rho^{n_{28}} - \rho_c^{n_{28}} \qquad (4.1b)$$

In equations (4.1) p, T, and ρ are the variables representing pressure, temperature, and density, respectively. The symbol $p_a(T,\rho)$ denotes the right-hand side of the equation; the subscript c signifies critical point value. The quantity R is the universal gas constant. Values for the coefficients in the above equation, n_1 through n_{28}, are listed in the first column of table 4.1. Constants as well as some convenient conversion factors are listed in table 4.2. In reference 3, the coefficients n_i were determined by the use of a least-squares procedure applied to experimental data provided largely by Dr. L. A. Weber of the National Bureau of Standards Laboratory, Boulder, Colorado. The measurements have since been improved by Weber (ref. 4). Differences between the latest measurements and the quantities computed by the use of equation (4.1a) are not significant (of order 0.1 percent) except in the neighborhood of the critical point where the density deviates by about 2 percent. The error for pressures and temperatures is less in this region.

Several choices for the n_i given in equations (4.1) are listed in table 4.1; they differ only in units. In the first two columns of the table, quantities n_i are given both with and without a bar; the n_i with bar are the

TABLE 4.1.- COEFFICIENTS FOR STEWART'S THERMAL EQUATION OF STATE (REF. 3) IN DIFFERENT UNITS

i	$\overline{n_i}$ (p,atm; ρ,g-mole/liter; T,°K)	n_i (ρ,g-mole/cc; T,°K)	$[n_i]$	n_i^* (dimensionless)
1	3.38759078D-03	4.12851466D 01	ρ^{-1}	5.50454716D-01
2	-1.31606223D 00	-1.60390749D 04	T/ρ	-1.38172091D 00
3	-7.38828523D 03	-9.00422923D 07	T^3/ρ	-3.23827743D-01
4	1.92049067D 07	2.34053474D 11	T^5/ρ	3.51405940D-02
5	-2.90260005D 10	-3.53744819D 14	T^7/ρ	-2.21722921D-03
6	-5.70101162D-08	-6.94792010D-01	$(T\rho^2)^{-1}$	-1.91160034D-02
7	7.96822375D-05	9.71101019D 02	ρ^{-2}	1.72631459D-01
8	6.07022502D-03	7.39788677D 04	T/ρ^2	8.49721211D-02
9	-2.71019658D 00	-3.30296280D 07	$(T/\rho)^2$	-2.45123930D-01
10	-3.59419602D 01	-4.38030799D 08	$(T/\rho)^3$	-2.10038991D-02
11	1.02209557D-06	1.24564530D 04	ρ^{-3}	2.95241697D-02
12	1.90454505D-04	2.32110154D 06	T/ρ^3	3.55459957D-02
13	1.21708394D-05	1.48328096D 08	T/ρ^4	3.02864054D-02
14	2.44255945D-03	2.97678886D 10	$(T/\rho^2)^2$	3.92722326D-02
15	1.73655508D 02	2.11636930D 09	T^3/ρ^2	1.01481465D-01
16	3.01752841D 05	3.67751334D 12	$(T^2/\rho)^2$	1.13936476D 00
17	-3.49528517D 07	-4.25976365D 14	T^5/ρ^2	-8.52721624D-01
18	8.86724004D-01	1.08066567D 13	T^3/ρ^4	9.21175040D-02
19	-2.67817667D 02	-3.26393959D 15	$(T/\rho)^4$	-1.79765426D-01
20	1.05670904D 05	1.28782933D 18	T^5/ρ^4	4.58284972D-01
21	5.63771075D-03	6.87077425D 16	$(T/\rho^2)^3$	1.04114692D-01
22	-1.12012813D 00	-1.36511926D 19	T^4/ρ^6	-1.33656530D-01
23	1.46829491D 02	1.78943605D 21	T^5/ρ^6	1.13200675D-01
24	9.98868924D-04	3.05781529D 03	$T/\rho^{2n_{28}}$	8.32903264D-03
25	-5.60000000D-03	-5.60000000D 03	ρ^{-2}	-9.95505258D-01
26	-1.57000000D-01	-3.94366040D 04	$\rho^{-2n_{28}}$	-1.66253033D 01
27	-3.50000000D-01	-3.50000000D-01	T^2	-1.46114912D-05
28	9.00000000D-01	9.00000000D-01	1	9.00000000D-01

Note: The last four digits beginning with D are representations for the exponent; for example, 9.00000000D-01 can also be written 9×10^{-1}.

TABLE 4.2.- CONSTANTS AND CONVERSION FACTORS

R (Universal Gas Constant) = 0.0820535 liter-atm/g-mole °K

Critical point values for molecular oxygen (ref. 3):

p_c = 50.14 atm
T_c = 154.77° K
ρ_c = 13.333 g-mole/liter
e_c = 742.2 J/g-mole

Conversion factors:

1 g-mole O_2 = 31.9988 g (C^{12} = 12.000 scale)
1 liter-atm = 101.3278 J (abs.) = 24.2179 cal = 0.0960417 Btu
1 atm = 1.01325×10^5 N/m^2 = 1.01325×10^6 dyne/cm^2 = 14.696006 lb(wt)/sq in.

values listed by Stewart in his thesis (ref. 3), and those without a bar are to be used with the equations to be introduced here. These quantities (except n_{25} through n_{28}) differ by a factor that is the universal gas constant. Stewart's units for pressure, density, and temperature were atmospheres, g-mole/liter, and degree Kelvin, respectively (in Weber's paper, ref. 4, the corresponding choice is MN/m^2, g-mole/cm^3, and degree Kelvin). The coefficients without a bar have units (n_i) simply expressed as the ratio of powers of density and temperature (in Stewart's units) as indicated by the symbols ρ and T listed on the right of the unbarred quantities in table 4.1. The conversion factors required for transformation of these constants are listed in table 4.2. In the last column of table 4.1 the coefficients, denoted as n_i^*, are made dimensionless by appropriate ratios of the critical point values T_c and ρ_c. The dimensionless thermal equation of state that results can be useful also for the approximate evaluation of state properties of other nonpolar molecules (such as N_2, A, Xe, H_2) by introducing the "principle of corresponding states" (ref. 6, p. 235).

The analytical formulation, equation (4.1), is fairly complicated and is not in the most efficient format for frequent evaluation by an electronic computer. More useful is the modified virial formulation[1] given by

$$\frac{p}{\rho RT} = Z = 1 + \sum_{i=1}^{8} A_i^{(1)}(T) g_i^{(1)}(\rho) \tag{4.2}$$

Most conventional state relations can be cast in this form (see, e.g., ch. 3 and 4, ref. 6, and ref. 8). Although it can be argued that equation (4.2) represents only a trivial reformulation of equation (4.1), it will become evident that worthwhile advantages are realized by capitalizing on certain features of the modified virial formulation. The quantities $A_i^{(1)}(T)$ and $g_i^{(1)}(\rho)$ are defined in the first columns of tables 4.3 and 4.4. The virial coefficients, the coefficients resulting from a power series expansion in density of the compressibility factor Z defined above, are readily found (ref. 6, p. 131, eq. (3.0-1)) and are given by the following linear combinations of the $A_i^{(1)}$ quantities.

$$\left.\begin{aligned} B(T) &= A_1^{(1)} \\ C(T) &= A_2^{(1)} + A_5^{(1)} \\ D(T) &= A_3^{(1)} \\ E(T) &= A_4^{(1)} + A_6^{(1)} \\ &\cdots \end{aligned}\right\} \tag{4.3}$$

[1]Hust and Gosman (ref. 9, p. 231) have discussed the criterion required of a real-fluid thermal equation of state to ensure nonsingular state behavior as the ideal-gas limit of very low densities is reached. The thermal state equations that can be placed in the modified virial form always satisfy their stated criterion provided that the functions $g_i^{(n)}(\rho)$ are bounded as the density becomes infinitesimally small.

TABLE 4.3.- TEMPERATURE-DEPENDENT COEFFICIENTS REQUIRED FOR STEWART'S REPRESENTATIONS

i	$A_i^{(1)}(T)$	$A_i^{(2)}(T) = TA_i^{(1)'}(T)$
1	$(n_1) + \left(\frac{n_2}{T}\right) + \left(\frac{n_3}{T^3}\right) + \left(\frac{n_4}{T^5}\right) + \left(\frac{n_5}{T^7}\right)$	$-\left[\left(\frac{n_2}{T}\right) + 3\left(\frac{n_3}{T^3}\right) + 5\left(\frac{n_4}{T^5}\right) + 7\left(\frac{n_5}{T^7}\right)\right]$
2	$(n_6T) + (n_7) + \left(\frac{n_8}{T}\right) + \left(\frac{n_9}{T^2}\right) + \left(\frac{n_{10}}{T^3}\right)$	$-\left[-(n_6T) + \left(\frac{n_8}{T}\right) + 2\left(\frac{n_9}{T^2}\right) + 3\left(\frac{n_{10}}{T^3}\right)\right]$
3	$(n_{11}) + \left(\frac{n_{12}}{T}\right)$	$-\left(\frac{n_{12}}{T}\right)$
4	$\left(\frac{n_{13}}{T}\right) + \left(\frac{n_{14}}{T^2}\right)$	$-\left[\left(\frac{n_{13}}{T}\right) + 2\left(\frac{n_{14}}{T^2}\right)\right]$
5	$\left(\frac{n_{15}}{T^3}\right) + \left(\frac{n_{16}}{T^4}\right) + \left(\frac{n_{17}}{T^5}\right)$	$-\left[3\left(\frac{n_{15}}{T^3}\right) + 4\left(\frac{n_{16}}{T^4}\right) + 5\left(\frac{n_{17}}{T^5}\right)\right]$
6	$\left(\frac{n_{18}}{T^3}\right) + \left(\frac{n_{19}}{T^4}\right) + \left(\frac{n_{20}}{T^5}\right)$	$-\left[3\left(\frac{n_{18}}{T^3}\right) + 4\left(\frac{n_{19}}{T^4}\right) + 5\left(\frac{n_{20}}{T^5}\right)\right]$
7	$\left(\frac{n_{21}}{T^3}\right) + \left(\frac{n_{22}}{T^4}\right) + \left(\frac{n_{23}}{T^5}\right)$	$-\left[3\left(\frac{n_{21}}{T^3}\right) + 4\left(\frac{n_{22}}{T^4}\right) + 5\left(\frac{n_{23}}{T^5}\right)\right]$
8	$\left\{\left(\frac{n_{24}}{T}\right)\exp[n_{27}(T-T_c)^2]\right\}$	$\left\{\left(\frac{n_{24}}{T}\right)\exp[n_{27}(T-T_c)^2]\right\}\left[2n_{27}(T-T_c) - \frac{1}{T}\right]T$

TABLE 4.4.- DENSITY-DEPENDENT COEFFICIENTS REQUIRED FOR STEWART'S REPRESENTATIONS

i	$g_i^{(1)}(\rho)$	$g_i^{(2)}(\rho) = \int^{\rho} \frac{g_i^{(1)}(\rho)}{\rho}\, d\rho$ (indefinite integral)
1	ρ	ρ
2	ρ^2	$\rho^2/2$
3	ρ^3	$\rho^3/3$
4	ρ^4	$\rho^4/4$
5	$\rho^2 e^u$	$e^u/2n_{25}$
6	$\rho^4 e^u$	$e^u u/2n_{25}^2$
7	$\rho^6 e^u$	$e^u u(u-2)/2n_{25}^3$
8	$\rho^{n_{28}} v e^{n_{26}v^2}$	$\exp(n_{26}v^2)/2n_{26}n_{28}$

Note: $u = \rho^2 n_{25}$; $v = \rho^{n_{28}} - \rho_c^{n_{28}}$.

When the state equation is expressed in the modified virial form, approximations are readily introduced that can lead to simplifications (e.g., for sufficiently small densities, say $\rho < \sqrt{|10^{-5}/n_{25}|}$, only the lowest order virial term need be considered).

A more important aspect of the formulation is that the variable dependence is separated. That is, the temperature-dependent quantities are evaluated separately from those that are density dependent. Use of this feature saves considerable computational time. For example, in the case where pressure and temperature are given and the density (implicitly defined) is to be found, as discussed in a later section, the required computer time is greatly abbreviated if the temperature quantities are evaluated only once. Further, since the coefficients $A_i^{(1)}(T)$ are polynomials in temperature, it turns out that by separately evaluating and storing the individual terms (in parenthesis in table 4.3), one can use the same quantities during the subsequent evaluation of other thermodynamic quantities. For a given density and temperature, once the thermal equation of state is evaluated relatively little additional computer time is required to evaluate the other thermodynamic properties obtained by differentiation or integration of the thermal equation of state (internal energy, enthalpy, specific heat, and entropy). The significance of these comments will be particularly evident in the discussion that follows.

Thermal equation of state (physical representation)—The relation $p_a(T,\rho)$ as defined in the previous section is multivalued in terms of the density variable ρ (fig. 4.1(a)). Such multiplicity, of course, is not physically realistic. It is therefore convenient to define a new function $p = p_p(T,\rho)$ that is single valued, although discontinuous, and is a physical representation. We define this function as

$$p_p(T,\rho) = p_a(T,\rho) \begin{cases} T \geq T_c \text{ and } 0 \leq \rho \leq 0.042 \\ T < T_c \text{ and } \rho \leq \rho_{SV}(T) \\ \qquad \text{or} \\ \qquad\quad \rho \geq \rho_{SL}(T) \end{cases}$$

$$= p_v(T) \qquad T < T_c \text{ and } \rho_{SV}(T) \leq \rho \leq \rho_{SL}(T) \tag{4.4}$$

where $p_v(T)$ is the vapor pressure equation later defined by equation (4.9), $\rho_{SV}(T)$ is the density corresponding to the saturated vapor boundary, and $\rho_{SL}(T)$ is the density corresponding to the saturated liquid boundary. The procedure that leads to the evaluation of these quantities is discussed in a later section. Note that although $p_p(T,\rho)$ is identical to $p_a(T,\rho)$ *almost* everywhere, it is not convenient to code both these quantities as the same subprogram. The reason lies in the fact that $p_a(T,\rho)$ is required in the evaluation of the implicitly defined boundary quantities ρ_{SV} and ρ_{SL} contained in $p_p(T,\rho)$.

Caloric equation of state—Once the thermal equation of state and an expression for low-density specific heat are given, an equation for the internal energy can be derived that is valid for all temperatures above critical and

for temperatures below critical provided that the computed pressures do not exceed the vapor pressure $p_v(T)$ (or the specified density is always less than the saturated-vapor density $\rho_{SV}(T)$). Introduction of the Clausius-Clapeyron equation allows one to generalize the energy equation to include also the low-temperature, high-density (i.e., high pressure $p \geq p_v(T)$) cryogenic region. The derivation procedure will not be discussed here (see, e.g., Hust and Gosman, ref. 9). The emphasis here is on the presentation of optimal formulations of the thermodynamic quantities that lead to their efficient computer evaluation.

The caloric equation for internal energy (see, e.g., ref. 9) with terms to account for energy changes in the two-phase region is given by

$$e = U(T,\rho)$$

$$= U(T_o,0) + U^o(T) - U^o(T_o) + U(T,\rho) - U(T,0) \;, \quad T \geq T_c \tag{4.5a}$$

$$= U(T_o,0) + U^o(T) - U^o(T_o) + U(T,\rho)[S(\rho_{SV}-\rho) + S(\rho-\rho_{SL})]$$

$$-U(T,0) + S(\rho-\rho_{SV})\Big\{U(T,\rho_{SV}) - U(T,\rho_{SL})S(\rho-\rho_{SL})$$

$$+ \frac{\rho_{SL}-\rho_{SV}}{\rho_{SV}\rho_{SL}}\left[\frac{\rho_{SL}}{\rho}\left(\frac{\rho-\rho_{SV}}{\rho_{SL}-\rho_{SV}}\right) S(\rho_{SL}-\rho) + S(\rho-\rho_{SL})\right]\left[p_v(T) - T\frac{dp_v(T)}{dT}\right]\Big\}, \quad T < T_c \tag{4.5b}$$

where the constant $U(T_o,0) = H^o_{T_o} - RT_o = 1133.655$ J/g-mole ($H^o_{T_o} = 1590.929$ J/g-mole and $T_o = 55°$ K) is the low-density or ideal gas reference energy for oxygen. The quantity $S(x)$ is the symmetrical Heaviside unit step function, which is unity or zero depending on whether the argument x is greater or less than zero, respectively, and has value 1/2 when the argument is zero. The energy quantity $U(T,\rho)$ is obtained by evaluation of the indefinite isothermal integral

$$U(T,\rho) = \int^{\rho} \left[p - T\left(\frac{\partial p}{\partial T}\right)_{\rho}\right]_T \frac{d\rho}{\rho^2} \tag{4.6}$$

The ideal gas (or low density) constant-volume specific heat and its indefinite integral $U^o(T)$ (needed in eq. (4.5)) are given by

$$\frac{c_v^o(T)}{R} = \sum_{\ell=1}^{8}\left(\frac{c_\ell}{R}T^{\ell-4}\right) + \left(\frac{c_8}{R}\right)\exp\left(\frac{c_9}{T}\right)\left[\frac{(c_9/T)}{\exp(c_9/T)-1}\right]^2 \tag{4.7}$$

$$\frac{U^o(T)}{RT} = \frac{1}{T}\int^T \frac{c_v^o(T)}{R}\,dT$$

$$= \sum_{\ell=1,\neq 3}^{8}\frac{1}{\ell-3}\left(\frac{c_\ell T^{\ell-4}}{R}\right) + \left(\frac{c_3}{RT}\right)\ell n\, T + \frac{c_8}{R}\left[\frac{(c_9/T)}{\exp(c_9/T)-1}\right] \tag{4.8}$$

The coefficients C_ℓ/R are listed for oxygen in the first column of table 4.5. Note also that the third term of the second equation has been removed from the summation sign.

Equation (4.5) also requires the vapor pressure equation and its derivative as given by

$$\ln p_v(T) = a_o + \sum_{\ell=1}^{7} (a_\ell T)^\ell \tag{4.9}$$

$$\frac{dp_v(T)}{dT} = \frac{p_v(T)}{T} \sum_{\ell=1}^{7} \ell(a_\ell T)^\ell \tag{4.10}$$

The coefficients a_ℓ are listed in the second column of table 4.5.

TABLE 4.5.- DIMENSIONLESS COEFFICIENTS FOR THE LOW-DENSITY SPECIFIC HEAT RELATIONS (EQS. (4.7) AND (4.8)) AND FOR THE VAPOR PRESSURE RELATIONS (EQS. (4.9) AND (4.10)) FOR OXYGEN

ℓ	C_ℓ/R	a_ℓ
1	-1.86442361D 02	-6.25967185D 01
2	2.07840241D 01	2.47450429D 00
3	-3.42642911D-01	-4.68973315D-02
4	3.50297163D 00	5.48202337D-04
5	2.05866482D-07	-4.09349868D-06
6	-1.11035799D-08	1.91471914D-08
7	2.08612876D-11	-5.13113688D-11
8	1.01894691D 00	6.02656934D-14
9	2.23918105D 03	

(Coefficients from ref. 3)

The final quantities are the temperature-dependent saturation densities $\rho_{SV}(T)$ and $\rho_{SL}(T)$ described earlier.

The caloric equations (4.5) are actually more general than the representation given by Hust and Gosman (ref. 9, eq. (43)). Here the equation is generalized to account for the changes in internal energy in the two-phase region due to the work done as isothermal changes in volume occur (i.e., the region $T < T_c$ and $\rho_{SV} \le \rho \le \rho_{SL}$). The factor

$$\left[\frac{\rho_{SL}}{\rho}\left(\frac{\rho - \rho_{SV}}{\rho_{SL} - \rho_{SV}}\right) S(\rho_{SL} - \rho) + S(\rho - \rho_{SL})\right]$$

was introduced to take account of these effects. Because of the coefficient step function $S(\rho - \rho_{SV})$, the curley bracket expression makes no contribution

to the internal energy for densities less than the value on the vapor boundary $\rho_{SV}(T)$. For densities larger than that of the saturated vapor the bracket factor increases in value as the ratio of specific volume differences given by

$$\frac{\Delta v(\rho,\rho_{SV})}{\Delta v(\rho_{SL},\rho_{SV})} = \frac{1/\rho_{SV} - 1/\rho}{1/\rho_{SV} - 1/\rho_{SL}} = \frac{\rho_{SL}(\rho-\rho_{SV})}{\rho(\rho_{SL}-\rho_{SV})} \tag{4.11}$$

Equation (4.11) increases varying linearly with volume until the saturated-liquid boundary is reached. The bracket expression has the value unity for all values of density in the liquid region $\rho \geq \rho_{SL}$. The coefficient of the term $U(T,\rho)$ in equation (4.5b) is nonzero only outside the two-phase region. Aside from the differences in notation, the caloric equation gives the same results as that given by Hust and Gosman everywhere outside the two-phase region.

The Heaviside symmetrical unit step function was introduced to minimize the number of regions to be considered by separate energy equations. When the energy equations are coded for electronic computer evaluation, however, the unit step function is most conveniently represented by use of logical statements in such a manner that the respective coefficient quantities are evaluated only when the step function is not zero (i.e., has positive arguments).

The quantity in the caloric equation that depends explicitly on the thermal equation of state is $U(T,\rho)$ as defined by equation (4.6). It is worthwhile to obtain an expression for this quantity that depends only on the coefficients contained within the modified virial equation of state. We first write the expression for the thermodynamic derivative $(\partial p/\partial T)_\rho$. We find

$$\left(\frac{\partial p}{\partial T}\right)_\rho = \rho R\left[T\left(\frac{\partial z}{\partial T}\right)_\rho + Z\right] \tag{4.12}$$

where

$$T\left(\frac{\partial z}{\partial T}\right)_\rho = \sum_{i=1}^{8} [TA_i^{(1)'}(T)]g_i^{(1)}(\rho) \tag{4.13a}$$

$$= \sum_{i=1}^{8} A_i^{(2)}(T)g_i^{(1)}(\rho) \tag{4.13b}$$

The coefficients $TA_i^{(1)'}(T)$ contained in equation (4.13a) (prime denotes differentiation) are listed in the second column of table 4.3. Note that these coefficients contain terms that differ by integer factors from the terms contained in the thermal equation of state listed in the first column (except the eighth coefficient). Hence, little additional computer time need be expended provided the caloric and thermal equations of state are both evaluated together. A similar comment applies to the evaluation of the vapor pressure equation and its associated derivative, as well as the low-density specific heat and its associated indefinite integral. The indefinite integral, equation (4.6), can now be evaluated, with the result

$$U(T,\rho) = -RT \sum_{i=1}^{8} A_i^{(2)}(T) g_i^{(2)}(\rho) \tag{4.14}$$

where

$$g_i^{(2)}(\rho) = \int^{\rho} g_i^{(1)}(\rho) \frac{d\rho}{\rho} \tag{4.15}$$

The quantities $g_i^{(2)}(\rho)$ are defined in the second column of table 4.4. Note that both coefficients $A_i^{(2)}$ and $g_i^{(2)}$ have been defined such that their respective products are also dimensionless. This turns out to be particularly advantageous when units conversion is required.

Quantities Defined Implicitly

Often a choice of independent variables other than density and temperature (e.g., pressure and temperature or energy and density) would be more advantageous. Since the state equations are sufficiently complicated to preclude the existence of explicit relations with the desired variable dependence, one has to resort to numerical evaluation. A procedure is described here for "inverting" the thermal equation of state to obtain, in effect, the state relation $\rho = \rho(p,T)$. Extension of the procedure to obtain analogous equations with still different variable dependence is straightforward and is not discussed here.

Density is obtained as a function of pressure and temperature by solving for the zeros of the equation

$$f(\rho;T) = p - p_a(T,\rho) \tag{4.16}$$

This equation is readily solved for all values of pressure and temperature, except that an additional complication results in the case where temperatures below critical are specified. The "successive linear interpolation procedure" described in reference 7 was found satisfactory for finding the roots of equation (4.16), particularly since it requires only that the lower and upper bounds of the roots be specified. The procedure converges quite rapidly; in general, fewer than eight separate evaluations of $f(\rho)$, or "iterations," are required to obtain a value of the root. For specified temperatures greater than critical the root of equation (4.16) lies in the interval $0 \leq \rho \leq 0.042$ g-mole-cm^3. The constants that represent the interval boundaries were found by searching the tables given by Stewart (ref. 3) to find the maximum and minimum values of the density.

In the case that temperatures below critical are specified, $f(\rho)$ has zero value for three distinct values of density. The root-finding procedure then requires isolation of the three branches of the multivalued function $p_a(T,\rho)$ for $T < T_c$. Figure 4.1(a) shows the multivalued character of pressure plotted as a function of density. The various curves pictured are isotherms. The entire region above the critical isotherm is the region where the density

bounds have already been specified. Note that a specie is characterized as being in the gas phase when stored at pressures and densities that lie on isotherms above the critical isotherm. The region below the critical isotherm and to the left of the line labeled $\rho_B(p)$ in figure 4.1(a) isolates what we shall call the vapor region or branch. In this region, the pressure is also less than the vapor pressure $p_V(T)$. We define $\rho_B(p)$ by

$$\rho_B(p) = \rho_1 \left(\frac{p}{p_1}\right)^a \tag{4.17}$$

where

$$a = \ell n(\rho_c/\rho_1)/\ell n(p_c/p_1)$$

$$p_1 = 1 \text{ atm}$$

$$\rho_1 = 3\times10^{-4} \text{ g-mole/cm}^3$$

This relation is readily found by observing that it represents a straight line on a log-log graph between the pair of points having coordinates (p_1,ρ_1) and (p_c,ρ_c). The line $\rho_B(p)$, although somewhat arbitrarily defined, is a simple representation that can be rapidly evaluated numerically.

The two-phase branch is bounded on the left by the line $\rho_B(p)$ and on the right by the three vertical segments $\rho = \rho_c$, $150° \le T \le T_c$; $\rho = 0.02$, $120° \le T \le 150°$; and $\rho = 0.03$, $T < 120°$ K. In this region, pressures computed from the equation $p_a(T,\rho)$ do not agree with experimental data; hence, this region is ignored in the iteration procedure. In fact, the pressure depends only on temperature in the two-phase region and therefore is independent of density. Finally, the liquid branch is isolated by observing that it is bounded by the three-segment curve, the critical isotherm and the already specified largest density value $\rho_{max} = 0.042$ g-mole/cm^3. In this region, the pressure is characterized as having values that exceed the vapor pressure $p_V(T)$.

The root-finding procedure converges most rapidly for bounds that most closely surround the value of the root. The values given above are somewhat arbitrary, and one can, perhaps, introduce even better bounds. Those specified above, however, were found satisfactory. If, as recommended earlier, the $A_i^{(1)}(T)$ quantities (eq. (4.2)) are reevaluated only when the temperatures are different (a similar comment applies for the $g_i^{(1)}(\rho)$ relations), then, although about six to eight iterations are required to find $\rho(p,T)$, the actual computer time expended is only a factor of two or three greater than the longest evaluation time required to find $p_a(T,\rho)$ (i.e., the time required when *both* ρ and T have values that are different when compared to a previous evaluation).

For the reader's convenience the diagram below shows a logical sequence of operations that leads directly to the categorization of a specified combination of the variables p and T into a particular branch. The rounded blocks labeled f(ρ) (eq. (4.16)) denote the root-finding procedure described in reference 7 with appropriate bounds as specified.

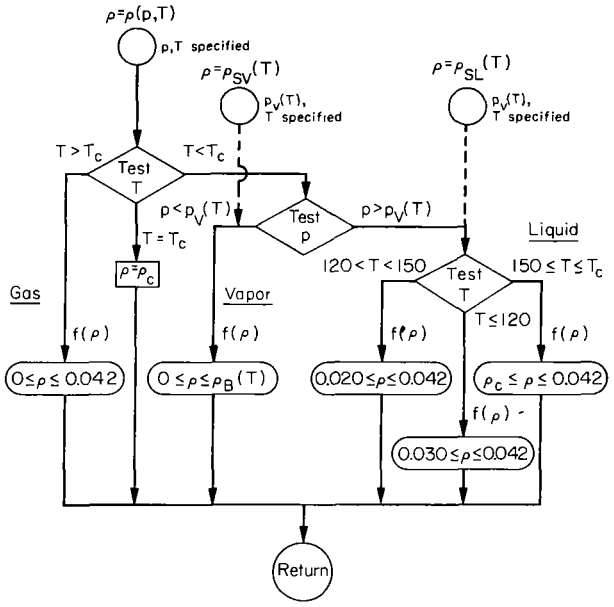

Flow chart that shows the sequence of operations required to evaluate density $\rho(pT)$ as well as the saturation densities $\rho_{SV}(T)$ and $\rho_{SL}(T)$.

By slightly altering the procedure just described one can also obtain the saturation densities $\rho_{SV}(T)$ and $\rho_{SL}(T)$. As commented earlier, these quantities are the exact boundaries of the two-phase region. Specifically, these quantities are the outer two of the three roots that satisfy $f(\rho) = 0$, $T < T_c$ where the specified pressure is that computed from the vapor-pressure equation $p = p_V(T)$. We have been concerned with the removal of the multivalued character of $p_a(T,\rho)$ so that $\rho(p,T)$ can be evaluated unambiguously. It turns out that special allowance must be made for the computation of the saturation densities. This is indicated on the flow chart by two special entry locations (the small circles denoted separately as $\rho_{SV}(T)$ and $\rho_{SL}(T)$) at which point $p = p_V(T)$ and T are specified. By this procedure, the saturation densities can be accurately computed for all temperatures less than about 150° K. For temperatures larger than this value but less than T_c the saturation-density curves (fig. 4.1(b)) vary little with changes in density; therefore accurate numerical evaluation is difficult. For the temperatures $150 \leq T \leq T_c$, these quantities are specified explicitly, a procedure that was also found necessary by Weber (ref. 4). The present procedure deviates from that of Weber in that to maintain internal consistency, special tables, with relatively few numbers of elements, were generated by smoothing the $\rho_{SV}(T)$ and $\rho_{SL}(T)$ appropriately obtained from solutions of equation (4.16) (the uppermost value of density in both tables is precisely the critical value ρ_c). A table-lookup procedure with linear interpolation was then used to find such values of the saturation densities.

Quantities Based on Spatially Dependent Variables

When a system is not in thermodynamic equilibrium (see, e.g., ref. 10, p. 60) much insight on its properties can be gained by the calculation of certain thermodynamic averages, such as density and energy. The final state can often be predicted if some property of the system (say, energy) is conserved while relaxation to equilibrium occurs. In this section we introduce a method

whereby one can rapidly predict the final state of a stratified fluid should the fluid be subjected to some mechanism that results in complete and adiabatic mixing. Since the procedure requires that evaluations be done numerically, variables (and summations) defined at discrete points rather than continuous variables (and integrations) will be considered. Also, since considerable amounts of computer time can be expended in the evaluation of the thermodynamic relations over a field of many points, particular emphasis is laid on the development of a procedure that minimizes redundant arithmetic operations and is therefore relatively efficient.

The problem described above can be briefly outlined as follows. One first finds the quantities

$$\rho(x,y) = \rho[p, T(x,y)] \tag{4.18}$$

$$e(x,y) = U[T(x,y), \rho(x,y)] \tag{4.19}$$

by the use of procedures described earlier. The notation shows results on the left-hand side of the equation that are found from the function evaluations designated on the right-hand side. The pressure p and the temperature $T(x,y)$ are considered known. The total mass M and the total energy E are found next by evaluating the integrals

$$M = \int_{v_T} \rho \, dv = \bar{\rho} v_T \tag{4.20}$$

$$E = \int_{v_T} \rho e \, dv = \overline{\rho e} v_T \tag{4.21}$$

over the entire tank volume. Introduction of the volume averages $\bar{\rho}$ and $\overline{\rho e}$ for the mass and energy densities as defined above (v_T is the total tank volume) then allows one to find

$$T_{col} = T(\overline{\rho e}/\bar{\rho}, \bar{\rho}) \tag{4.22}$$

$$p_{col} = p_p(T_{col}, \bar{\rho}) \tag{4.23}$$

The temperature is found by inverting the caloric equation of state (4.19). The results denoted by the symbols T_{col} and p_{col} are the temperature and pressure to which the system would "collapse" and that uniquely characterize the uniform final state of the oxygen contained within the tank. During a space flight, $\bar{\rho}$ remains constant unless fluid is drawn from the tank. If severe thermal stratification occurs, mixing (by vehicle maneuvers, for example) can bring about large abrupt pressure decreases (see fig. 4.1(c) and discussion) that could conceivably lead to spacecraft equipment failures. These concepts are not new, however, and are discussed elsewhere (ref. 2 and ch. 6).

The evaluation of equations (4.18) and (4.19) is particularly time consuming. The matrix

$$T_{jk} = T(j\ \Delta x,\ k\ \Delta y) \tag{4.24}$$

where

$$\left.\begin{aligned} x &= j\ \Delta x\ , \quad 1 \le j \le JM \\ y &= k\ \Delta y\ , \quad 1 \le k \le KM \end{aligned}\right\} \tag{4.25}$$

can contain many elements. Furthermore, it can occur that the temperature field describes situations where many volume elements are at temperatures different from that of the uniform surrounding gas. Once the density and energy, equations (4.18) and (4.19), are evaluated, we could efficiently evaluate the integrals, equations (4.20) and (4.21), if like temperatures were grouped together. However, we must consider that the T_{jk} are randomly mixed and like temperatures are not ordered in any systematic manner. It also appears wasteful to recalculate values for, say, density and energy when differences result that are not numerically significant (e.g., less than 0.1 percent). In the interest of minimizing the number of separate evaluations of thermodynamic functions a procedure is to be described whereby, in essence, one first counts the number of times that a particular temperature appears in the array T_{jk}. In this manner a "temperature distribution function" is then constructed that applies strictly to an equally spaced Cartesian coordinate system. In non-Cartesian systems, however, additional complexity results. The analytical foundation for the temperature distribution function is established in the discussion that follows.

We first define a dimensionless temperature

$$\tau = A_o(T - T_{min}) \tag{4.25a}$$

or, in the case that the spatial dependence is discrete,

$$\tau_{jk} = A_o(T_{jk} - T_{min}) \tag{4.25b}$$

where A_o and T_{min} are both constants; the value of A_o is arbitrary and T_{min} is the very lowest bound of all possible temperature values T (or T_{jk}). A temperature distribution function $F(\tau)$ is now defined such that $F(\tau)d\tau$ is proportional to the volume of a gas with dimensionless temperature between τ and $\tau + d\tau$. Then

$$F(\tau) = C \int_{v_T} \delta(\tilde{\tau} - \tau)d\tilde{v} \tag{4.26}$$

where C is an arbitrary constant set equal to unity; the constant can be used to normalize the distribution function in such a manner that its integral over all possible temperatures is unity. The function $\delta(\tilde{\tau} - \tau)$ is the Dirac δ function defined such that

$$\int_{\tau_1}^{\tau_2} \delta(\tilde{\tau} - \tau)d\tau$$

equals unity provided $\tau_1 \le \tilde{\tau} \le \tau_2$ and equals zero if $\tilde{\tau}$ is not within the integration interval.

If the volume elements are discretized, we have

$$F(\tau)d\tau = \sum_{j,k=1}^{JM,KM} [S(\tau - \tau_{jk}) - S(\tau - \tau_{jk} + d\tau)]W_{jk} \tag{4.27a}$$

$$= \sum_{j,k=1}^{JM,KM} \delta(\tau - \tau_{jk})d\tau W_{jk} \tag{4.27b}$$

where S denotes the symmetrical Heaviside step function described earlier; $W_{jk} = \Delta v_{jk} N_t / V_T$ is a "weighting" function; Δv_{jk} is the gas volume associated with the discrete volume element of the cell labeled j,k; N_t corresponds to the total number of volume centered computational grid points; and V_T already defined, is the tank volume. It follows that when C = 1, $\sum_{j,k} W_{jk} = N_t$. To further clarify the meaning of the weighting function W_{jk}, if all Δv_{jk} were equal (such that we have an equally spaced Cartesian system), the W_{jk} would then all be unity; that is, $V_T/\Delta v_{jk} = N_T$.

We now seek a discretized version of $F(\tau)$. A simple possibility is to define a function

$$\tilde{F}_N = \int_{N-\frac{1}{2}}^{N+\frac{1}{2}} F(\tau)d\tau = \sum_{j,k=1}^{JM,KM} \left[S\left(\tau_{jk} - N + \frac{1}{2}\right) - S\left(\tau_{jk} - N - \frac{1}{2}\right) \right] W_{jk} \tag{4.28}$$

Then $\tilde{F}_N$ is the weighted number of computational grid points with dimensionless temperature between N - 1/2 and N + 1/2. The mean dimensionless temperature τ within this interval is N (an integer). How one can evaluate $\tilde{F}_N$ rapidly with a computer is explained later. Other thermodynamic variables such as the associated dimensional temperature T_N, density ρ_N, and energy e_N can be evaluated according to the relations

$$T_N = T_{min} + \frac{N}{A_o} \tag{4.29a}$$

$$\rho_N = \rho(p, T_N) \tag{4.29b}$$

$$e_N = U(T_N, \rho_N) \tag{4.29c}$$

It will be shown that fewer evaluations of these quantities over the entire grid occur than if a procedure is followed whereby the T_{jk} are used directly.

Consistent with our definition for the distribution function, equation (4.26), it can be shown that, in general, the volume average of a thermodynamic quantity, say $g(\tau)$, is given by

$$\bar{g} = \frac{1}{N_t} \int_0^\infty F(\tau) g(\tau) d\tau \tag{4.30}$$

We separate the integration interval into a sum of subintervals that cover the range of possible temperature values

$$\bar{g} = \frac{1}{N_T} \sum_{N=1}^{N_{max}} \int_{N-\frac{1}{2}}^{N+\frac{1}{2}} g(\tau) F(\tau) d\tau \tag{4.31a}$$

where

$$N_{max} = A_o (T_{max} - T_{min}) \tag{4.31b}$$

To zeroth order, equation (4.31a) is approximated by

$$\bar{g} \approx \frac{1}{N_t} \sum_{N=1}^{N_{max}} g_N \tilde{F}_N \tag{4.32}$$

The accuracy of the average computed by this equation can be improved by increasing the value of the arbitrary constant A_o, but at the expense of increasing the number of temperatures T_N at which the therodynamic functions are computed.

A more efficient procedure is to use a higher order method as follows. The function $g(\tau)$ can be expanded in a Taylor series

$$g(\tau) = \sum_{m=o}^{\infty} \frac{g^{(m)}(N)}{m!} (\tau - N)^m \tag{4.33}$$

Substitution of the series into the exact equation (4.31a) yields

$$\bar{g} = \frac{1}{N_t} \sum_{N=1}^{N_{max}} \sum_{m=o}^{\infty} \frac{g^{(m)}(N)}{m!} \tilde{F}_{Nm} \tag{4.34a}$$

where

$$\tilde{F}_{Nm} = \int_{N-\frac{1}{2}}^{N+\frac{1}{2}} F(\tau)(\tau - N)^m d\tau \tag{4.34b}$$

Substitution of equation (4.27b) into equation (4.34b) leads to

$$\tilde{F}_{Nm} = \sum_{j,k} \left[S\left(\tau_{jk} - N + \frac{1}{2}\right) - S\left(\tau_{jk} - N - \frac{1}{2}\right) \right] (\tau_{jk} - N)^m W_{jk} \qquad (4.35)$$

With equations (4.34a) and (4.35), it is possible, in principle, to compute $\bar{g}$ to any order of accuracy, although if one carries too many terms the original purpose for introducing the procedure - increased computational efficiency - is defeated. With $m = 0$, we see that equations (4.34) and (4.35) become identical to equation (4.28). One can readily evaluate an equivalent set of relations that are valid to first order. One first introduces a simple difference relation for the derivative $g^{(1)}(N)$ and then with the definition

$$F_N = \int_{N-1}^{N+1} F(\tau)(1 - |\tau - N|)d\tau \qquad (4.36a)$$

it can then be shown that the average

$$\bar{g} = \sum_{N=1}^{N_{max}} F_N g_N \qquad (4.36b)$$

is correct to order $(\tau - N)$ in the expansion (4.33) for $g(\tau)$.

The temperature distribution functions are particularly simple to find with an electronic computer especially when integer subscript notation is used. To illustrate this point, let F(N) be the variable in FORTRAN language that represents the zeroth-order representation for the distribution function, equation (4.28). The one-dimensional array F(N) must be of sufficiently large dimension to contain all of its possible elements; it must contain at least NMAX elements, where NMAX is given by equation (4.31b). We next set all of the elements of F(N) equal to zero since those locations in computer memory will be used to accumulate the sums denoted on the right-hand side of equation (4.28). We then process each element in the array T(J,K) that represents the variable T_{jk}. We do this by first evaluating N = A_o[T(J,K) - TMIN] (note that we are using the automatic truncation feature of FORTRAN language whereby the integer on the left-hand side of the equation represents the largest integer value less than or equal to the floating-point result of the expression given on the right-hand side of the equation). We define TMIN as the FORTRAN equivalent of T_{min}. The weighting factor W(J,K) associated with the spatial point j,k is then added to what is contained in F(N) by the use of the FORTRAN statement F(N) = F(N) + W(J,K). This procedure, briefly outlined, is easily generalized such that one can find the associated distribution function, equation (4.36) or the higher order forms, equation (4.35). Several example plots of temperature distributions are given in chapter 6. The procedure for finding the averages, equation (4.32), or, in the case of the higher order representations, equation (4.34a), is straightforward and simple to program on an electronic computer. It need only be said that one will also obtain additional savings in computer time if the thermodynamic quantities, say ρ_N, e_N, that

correspond to the temperatures T_N are not computed when the associated distribution function quantities $F(N)$ have zero value.

EXAMPLE EVALUATIONS OF THE THERMODYNAMIC FUNCTIONS

The explicit representations $p = p_a(T,\rho)$, $p = p_p(T,\rho)$, and $e = U(T,\rho)$ have been defined. By the procedure discussed, one can invert the above relations so that, in effect, the above list is readily expandable to also include representations of the type $\rho = \rho(p,T)$, $\rho = \rho(e,T)$, $T = T(p,\rho)$, and $T = T(e,\rho)$. Our number of equations is now sufficiently complete that a value of any one variable of the set p, ρ, T, and e can be found once values are specified for any other two variables of the set. In principle, by introducing additional thermodynamic functions (such as enthalpy and entropy, for example) the list can be expanded further.

In this section a series of plots are given that illustrate the flexibility of the procedures discussed. These plots are arranged so that the curves within each graph represent cuts along curves on both the p-ρ-T (figs. 4.1, 4.2, and 4.3) and the internal energy surfaces (figs. 4.4, 4.5, and 4.6). The figures are further arranged according to the particular variables displayed along the ordinate and the abscissa. Pressure is plotted versus density in figure 4.1. Other figures show pressure versus temperature (fig. 4.2), density versus temperature (fig. 4.3), and energy versus density (fig. 4.4), temperature (fig. 4.5), and pressure (fig. 4.6). Each figure shows curves for constant temperature (isotherms), constant pressure (isobars), constant density (isochores), or constant energy (isoenergetics), as appropriate. Such plots may be instructive as well as useful as a ready reference.

Recall, however, that the basic equations used are semiempirical and therefore the results plotted have quantitative value only within the regions where the constants were fitted by the least-squares procedure with experimental data by Stewart. Thus, the extreme values that are displayed (in particular, for the largest values of temperature and density) may not be precisely accurate. The less accurate ranges of the curves are often easily identified by the inflections or by the discontinuities in curvature occurring at the very ends of the curves. In the case that more accurate values are required than can be read from the curves, the reader is referred to the tables given in reference 3 or 4, or the equations given in this chapter.

Figure 4.1(a) shows a number of isotherms on a log-log plot of pressure versus density that illustrate the analytical behavior of Stewart's equation of state $p_a(T,\rho)$ ((4.1), or, as modified, eq. (4.2)). The lowest isotherm corresponds to a temperature of 100° K. The higher curves are for higher temperatures that increase by increments of 10° K and by 20° K for temperatures above 200° K, except the curve drawn for the critical isotherm $T = T_c$, between the isotherms 150° and 160° K. Small crosses are drawn on the isotherms below the critical to show where the phase boundaries intersect. Knowledge of the exact behavior of these isotherms as computed from Stewart's equation can be quite helpful. Since the smooth multivalued character of the equation is displayed,

one can readily isolate appropriate branches in the manner indicated by the straight-line segments so that an inverse of the function can be obtained, as discussed in the previous section. Although the state equation contains transcendental terms of a complicated nature (see, e.g., eq. (4.1)) their plotted results have the same overall characteristics of an equation that is a cubic in density for the range of parameters shown. As such, the equation is not greatly different from the van der Waals equation (ref. 6) except, of course, for the magnitude of the computed values. One observes that the critical isotherm contains an inflection at the critical point (which can be identified as the point where the line segments converge) as indeed it must. An inflection also appears at the critical point in the density-temperature plane shown by figure 4.3.

Figures 4.1(b), 4.2(a), and 4.3(a) illustrate the behavior of the "physical" representation of the thermal equation of state (4.4). Note that pressure is independent of density in the two-phase region as it should be. The manner in which the two-phase region degenerates to the vapor pressure curve can be understood by comparing figures 4.1(b) and 4.2(a) (also, cf. fig. 4.3(a) with fig. 2 in Weber's paper, ref. 4). Difficulty will be encountered if one tests the computed pressure $p = p_a(T,\rho)$ against the vapor pressure $p_V(T)$ as a possibly simpler scheme than that described with regard to equation (4.4) for separation of the vapor from the liquid regions (the rule quoted in elementary texts on thermodynamics, such as ref. 5, is that for $T < T_c$ one has vapor for $p < p_V(T)$ and liquid for $p > p_V(T)$). The test fails in the comparison of $p_a(T,\rho)$ with $p_V(T)$ since the pressure computed from the analytical representation has widely varying values in the two-phase region. One must use the computed saturation densities (see flow chart) to correctly separate regions.

Figures 4.1(c), 4.2(b), and 4.3(b) show the behavior of isoenergetic curves on the respective coordinate planes p-ρ, p-T, and ρ-T. In comparing figures 4.1(b) and 4.1(c) at the lower densities, note that as the temperature increases, the effect of density on energy becomes less (the isoenergetic and isothermal lines become colinear implying $e \to e(T) = \text{constant}$). We recall from elementary principles (see, e.g., ref. 5 or 6) that in the low-density gaseous region the energy depends only on temperature $e = e(T)$. This feature can also be observed in some of the other figures; see, for example, figures 4.3(b), 4.4(a), and, in particular, 4.5(a) where we see that energy remains approximately constant for the isochores less than 1 g-mole/cm^3. Thus an appropriate limiting behavior is correctly displayed.

One other feature of importance displayed in figure 4.1(c) is that in the cryogenic region where pressure and density both have large values, adiabatic mixing of a thermally stratified fluid contained with a closed container (here one follows a constant energy curve, say, the curve labeled -2000 J/g-mole) would have only a small effect on the value of density, but could lead to rather severe pressure reductions.[2]

[2]By use of thermodynamic arguments it can be shown that during mixing the pressure reduces rather than increases (ref. 2).

Figures 4.4, 4.5, and 4.6 illustrate the effect of isotherms, isobars, and isochores drawn on an energy surface. Note that discontinuities in energy occur along isotherms in the energy-pressure plane (or along isobars in the energy-temperature plane); for example, see figures 4.5(b) and 4.6(b). The magnitude of the energy jump is a measure of the heat of vaporization associated with the respective values of temperature and pressure noted. Analogous discontinuities are not observed in the case of energy versus density (fig. 4.4) since the effect of work done in compressing the vapor to obtain a liquid was accounted for in the caloric equation. One can use the abrupt changes observed in slope values to mark the phase-change boundaries. In the case of figure 4.5(a), the slope of the isochores $(\partial U/\partial T)_\rho$ is identified as the constant-volume specific heat. Plots of specific heat are given in reference 3 (pp. 47 and 48).

REFERENCES

1. Chandler, W. A.: Cryogenic Storage for Space Electrical Power. Astronaut. Aerosp. Eng., Vol. 1, 1963, pp. 97-101.

2. Kamat, D. V.; and Abraham, W. H.: Pressure Collapse in Oxygen Storage Under Zero-g. J. Spacecraft, Vol. 5, 1968, p. 184.

3. Stewart, R. B.: The Thermodynamic Properties of Oxygen. Ph.D. Thesis, Dept. Mech. Eng., Univ. Iowa, 1966.

4. Weber, L. A.: P-V-T, Thermodynamic and Related Properties of Oxygen from the Triple Point to 300 K at Pressures to 33 MN/m^2. J. Res. NBS - A, Phys. and Chem., Vol. 74A, 1970, p. 93.

5. Zemansky, N. W.: Heat and Thermodynamics. McGraw-Hill Book Co., 1957.

6. Hirschfelder, J. O.; Curtiss, C. F.; and Bird, R. B.: Molecular Theory of Gases and Liquids. John Wiley & Sons, Inc., 1954.

7. Dekker, T. J.: Constructive Aspects of the Fundamental Theorem of Algebra, B. Dejon and P. Henrici, eds., John Wiley & Sons, Inc., 1969, p. 37.

8. Otto, Jos.: Thermische Zustandsgrössen der Gase bei mittleren und kleinen Drucken. Handbuch der Experimentalphysik, W. Wien, ed., Vol. 8, Pt. 2, Akademische Verlagsgesellschaft, Leipzig, 1929, pp. 79-228.

9. Hust, J. G.; and Gosman, A. L.: Functions for the Calculation of Entropy, Enthalpy, and Internal Energy for Real Fluids Using Equations of State and Specific Heats. Advances Cryogenic Eng., Vol. 9, 1964, p. 227.

10. Vincenti, W. G.; and Kruger, C. H., Jr.: Introduction to Physical Gas Dynamics. John Wiley & Sons, Inc., 1965.

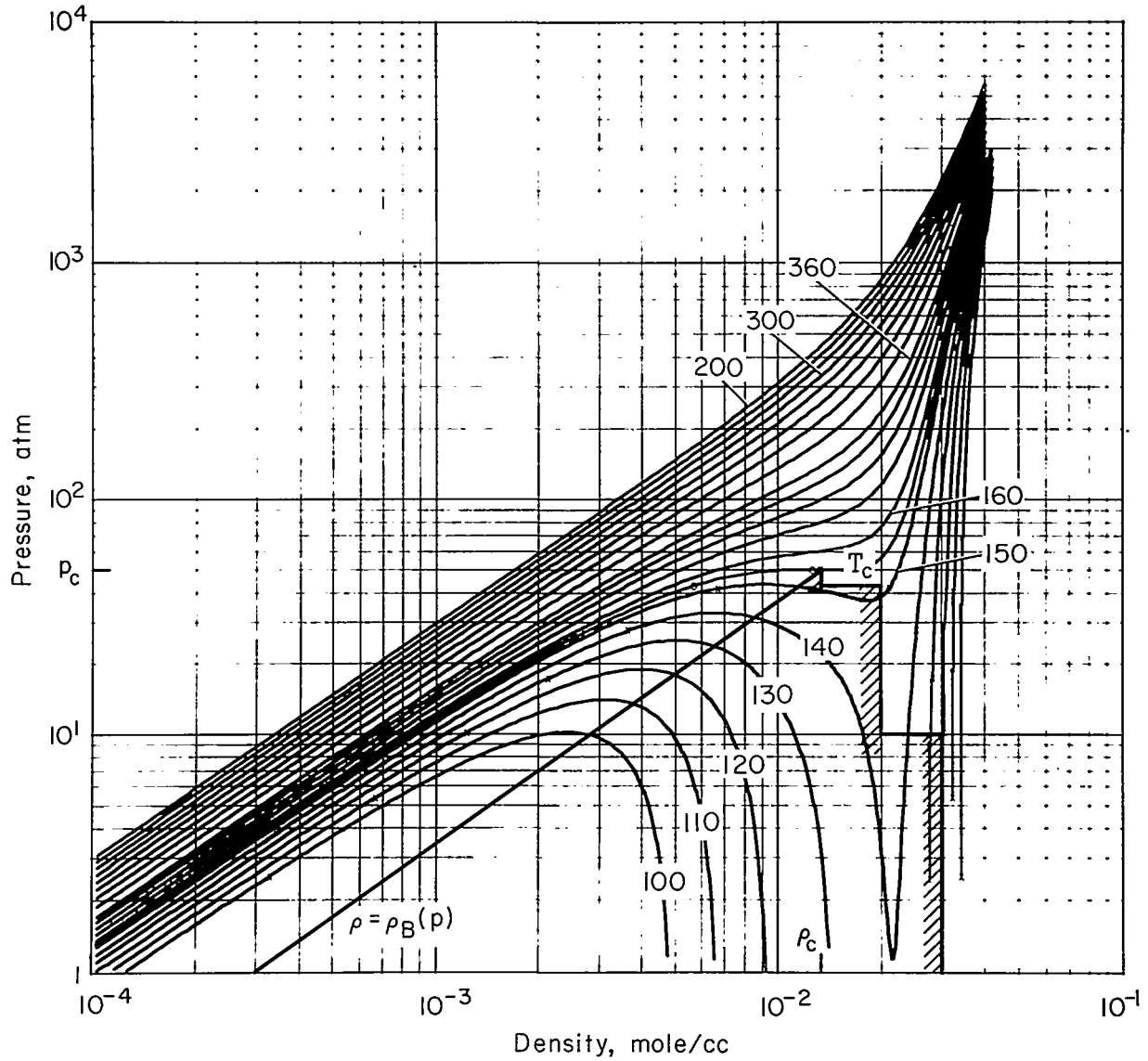

(a) Isotherms computed on the basis of the analytical representation $p_a(T,\rho)$, equation (4.1) or (4.2).

Figure 4.1.— Pressure versus density.

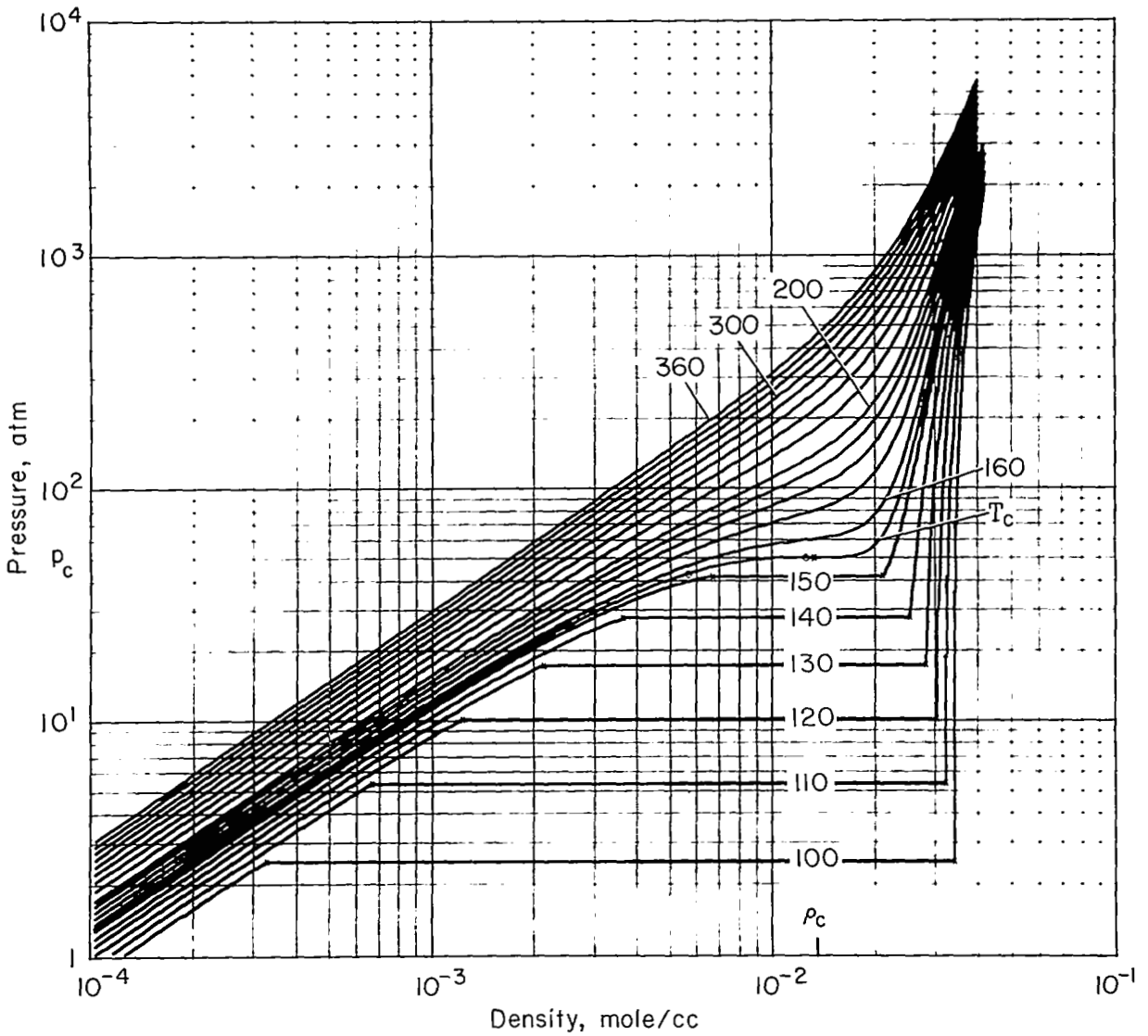

(b) Isotherms computed on the basis of the physical representation $p_p(T,\rho)$, equation (4.4).

Figure 4.1.– Continued.

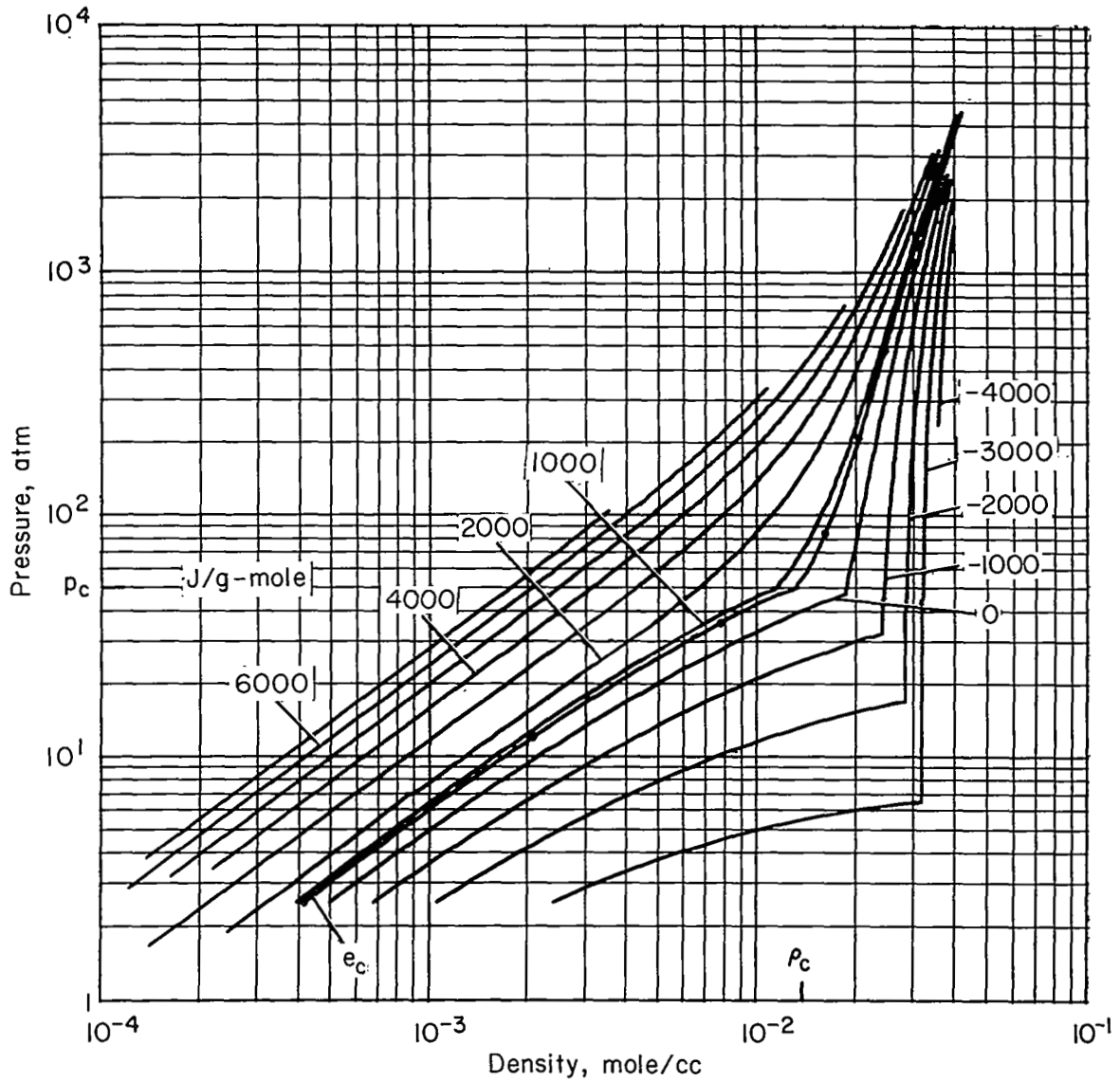

(c) Isoenergetics computed from $p(e,\rho)$ obtained by inverting equations (4.5).

Figure 4.1.– Concluded.

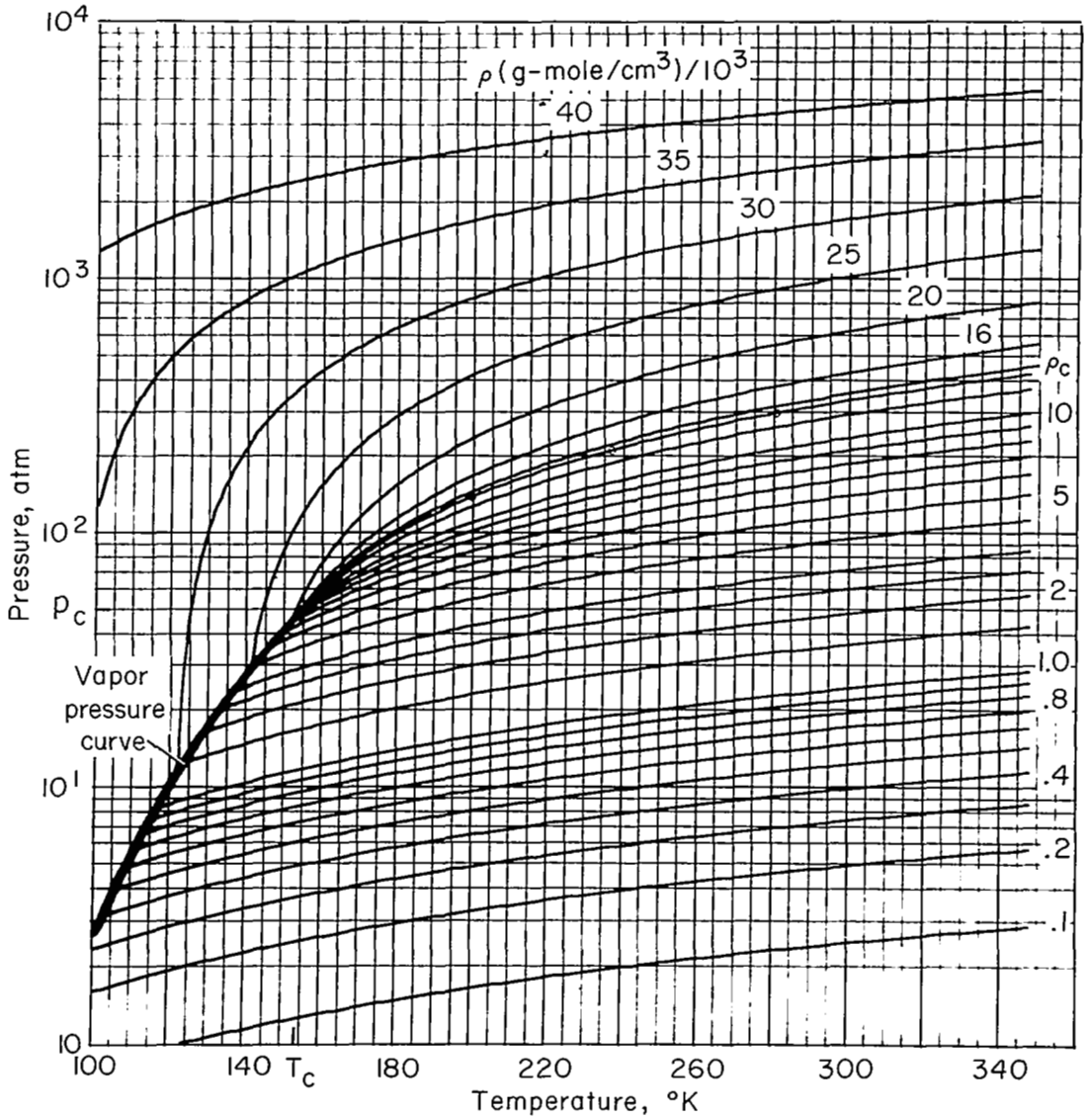

(a) Isochores.

Figure 4.2.– Pressure versus temperature.

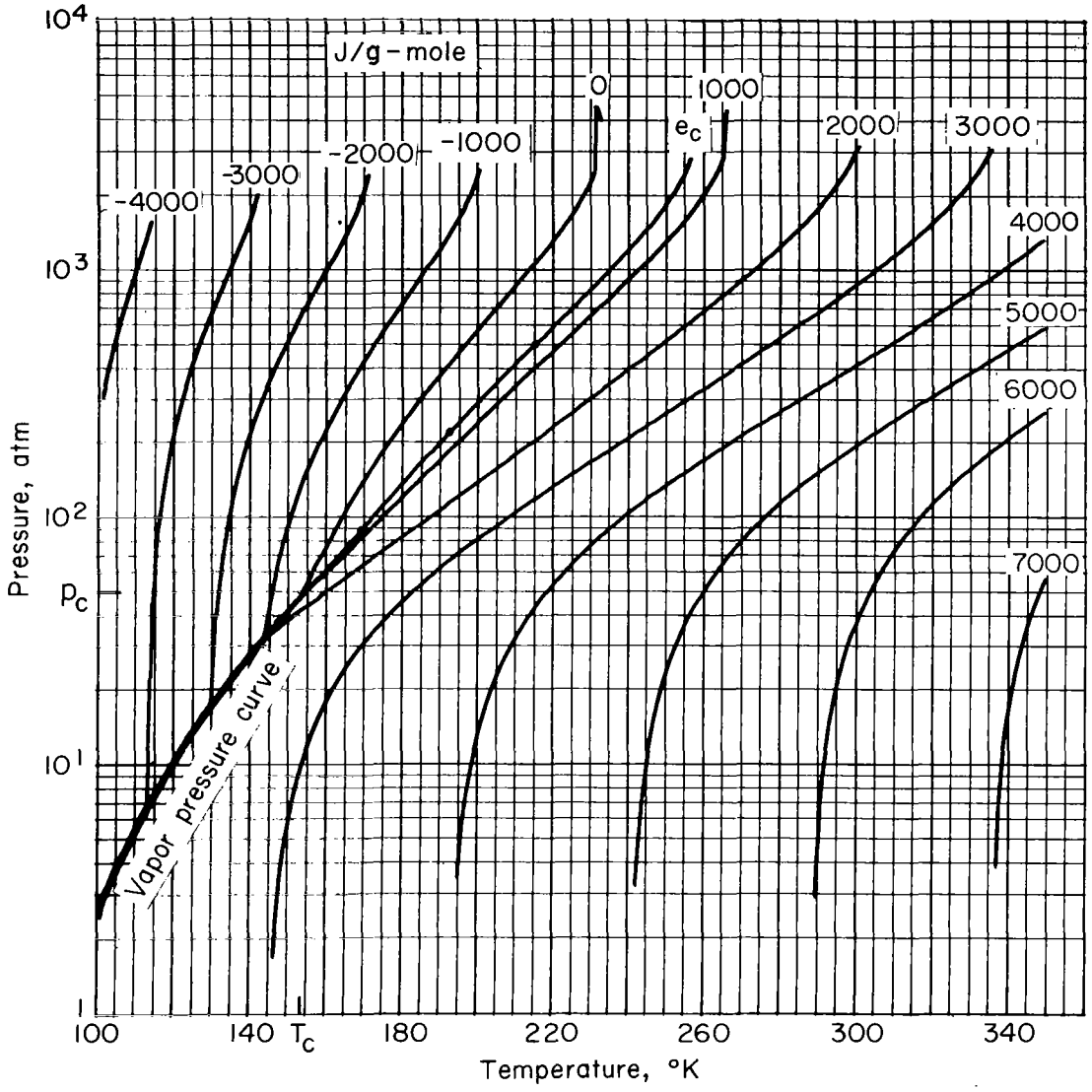

(b) Isoenergetics.

Figure 4.2.– Concluded.

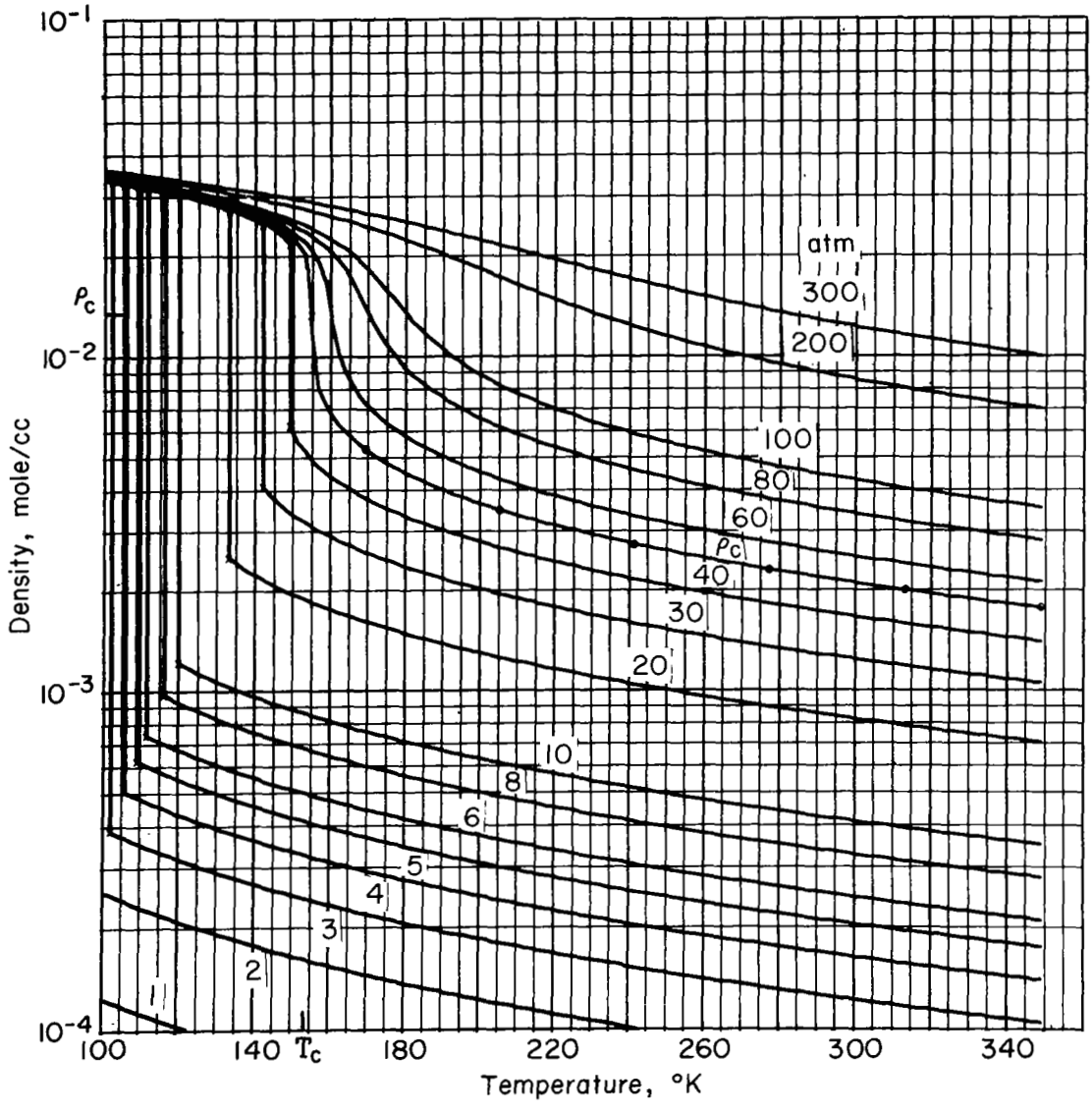

(a) Isobars.

Figure 4.3.– Density versus temperature.

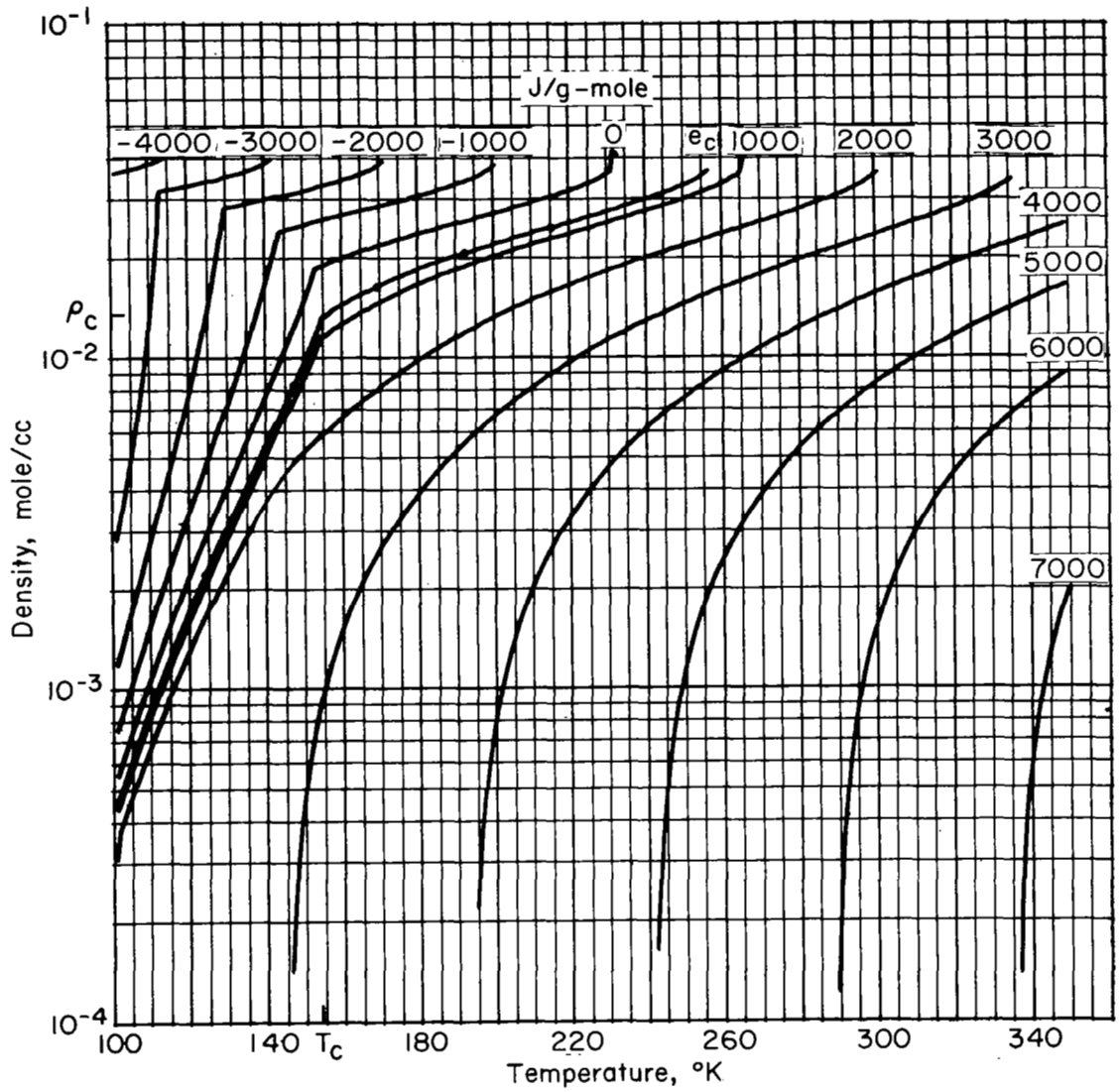

(b) Isoenergetics.

Figure 4.3.– Concluded.

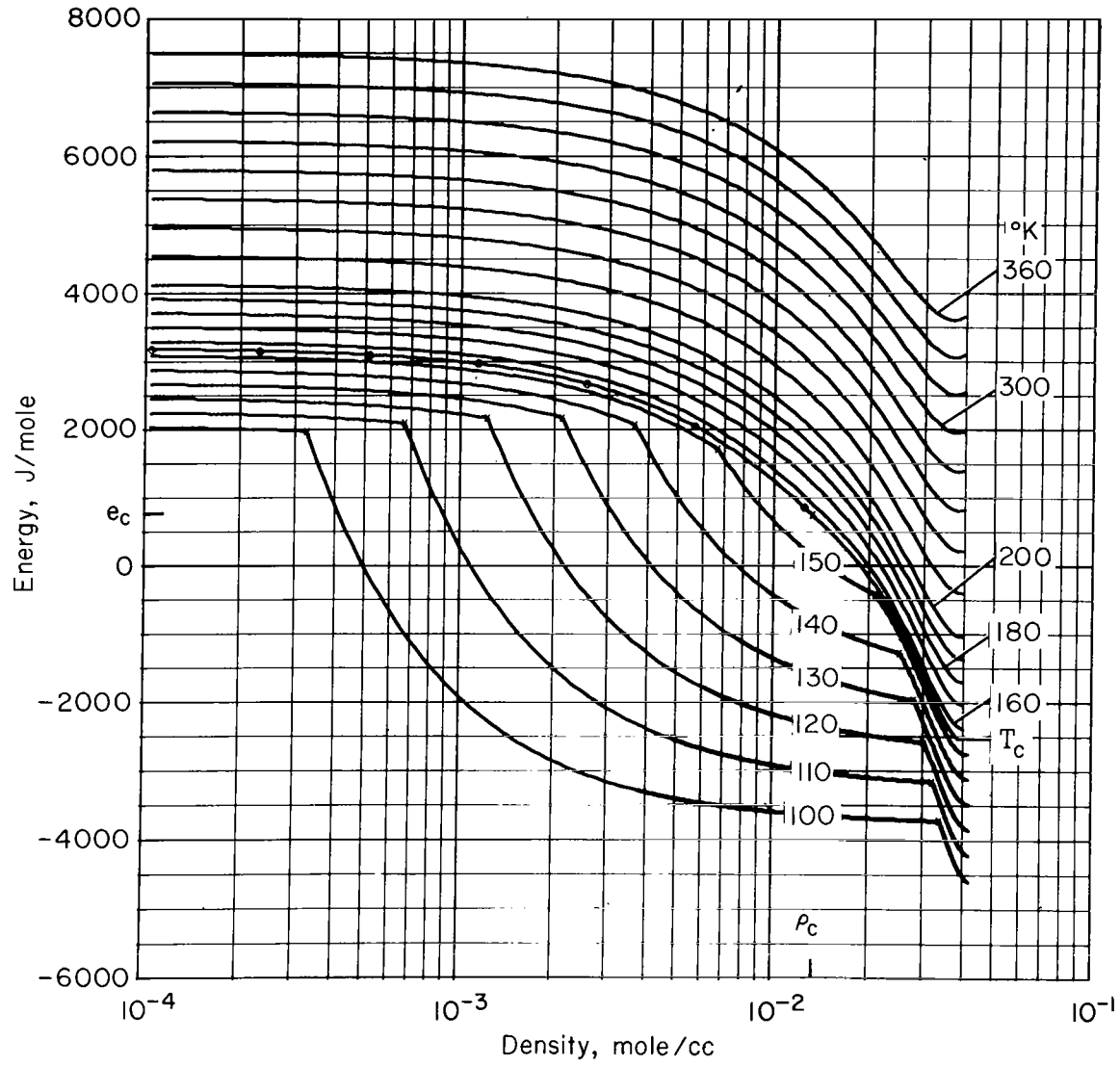

(a) Isotherms.

Figure 4.4.– Internal energy versus density.

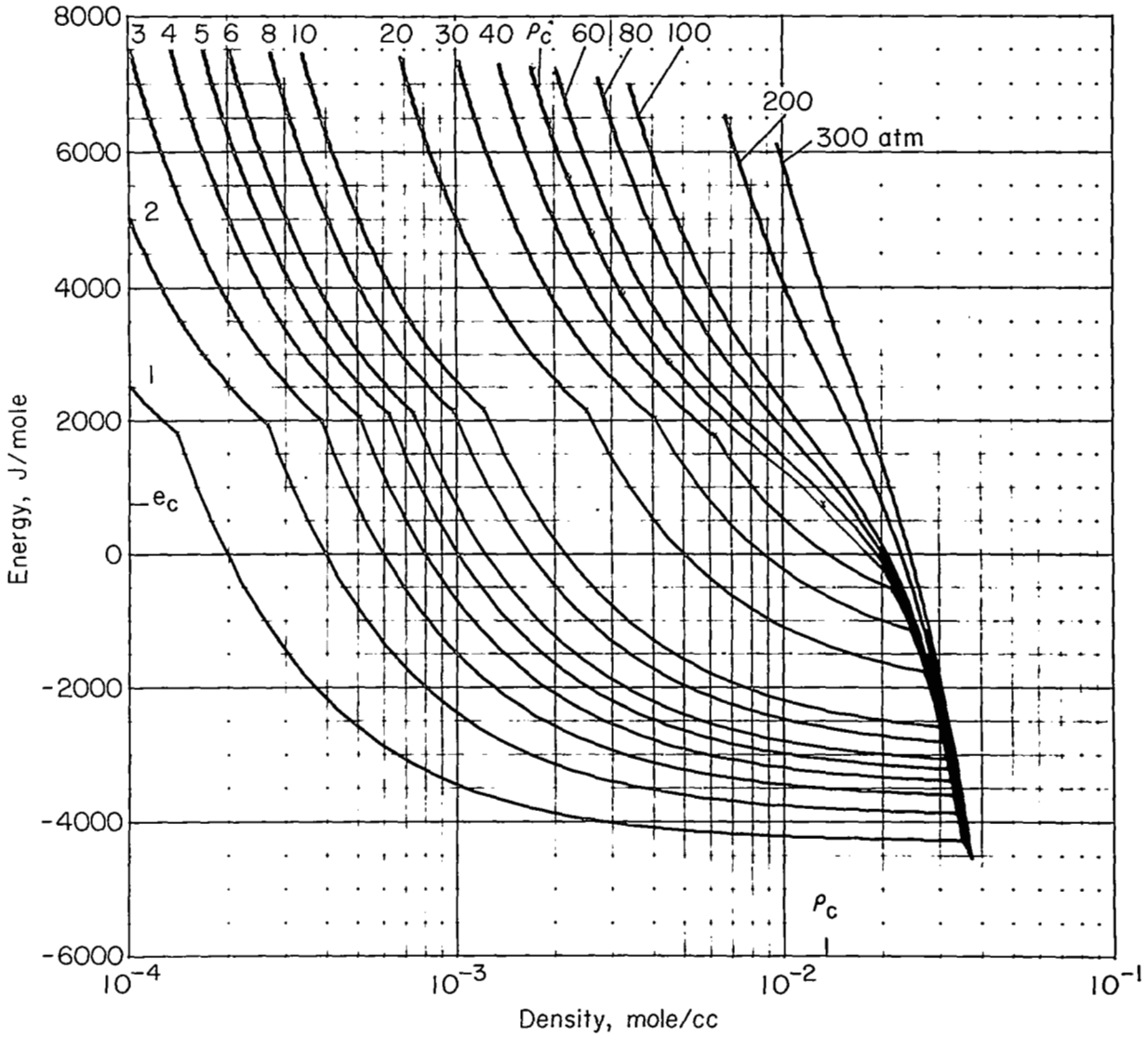

(b) Isobars.

Figure 4.4.– Concluded.

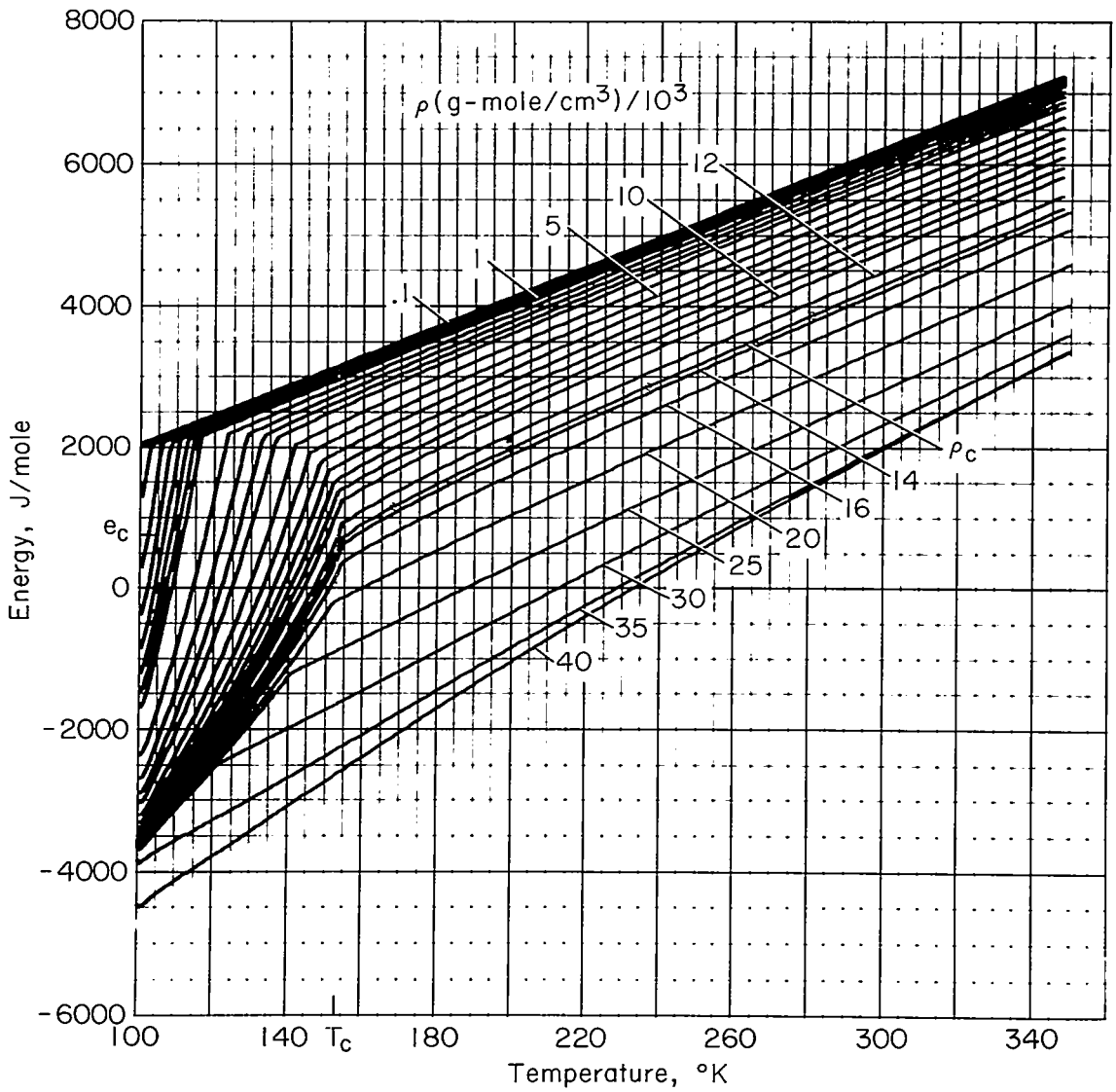

(a) Isochores.

Figure 4.5.– Internal energy versus temperature.

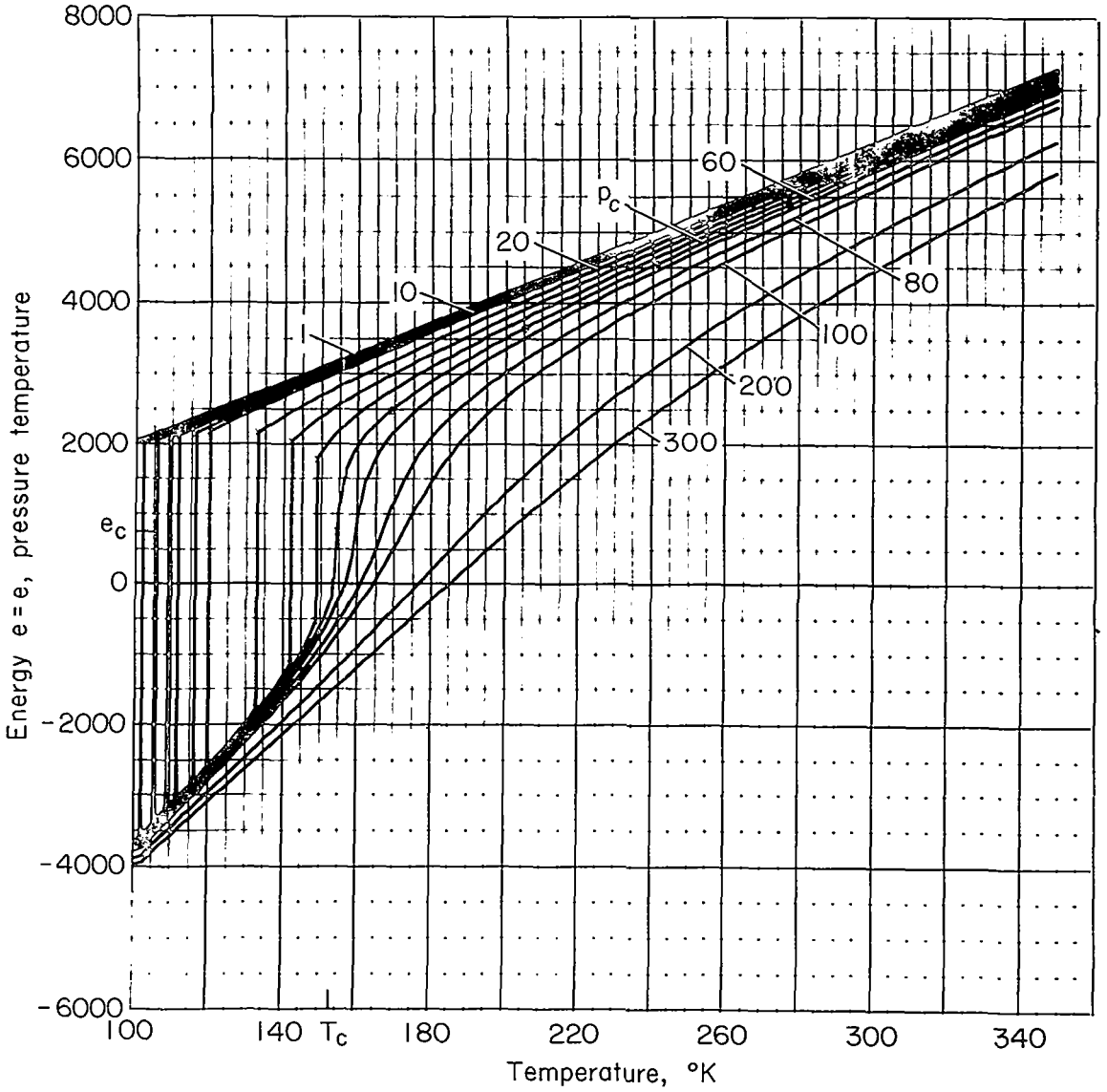

(b) Isobars.

Figure 4.5.– Concluded.

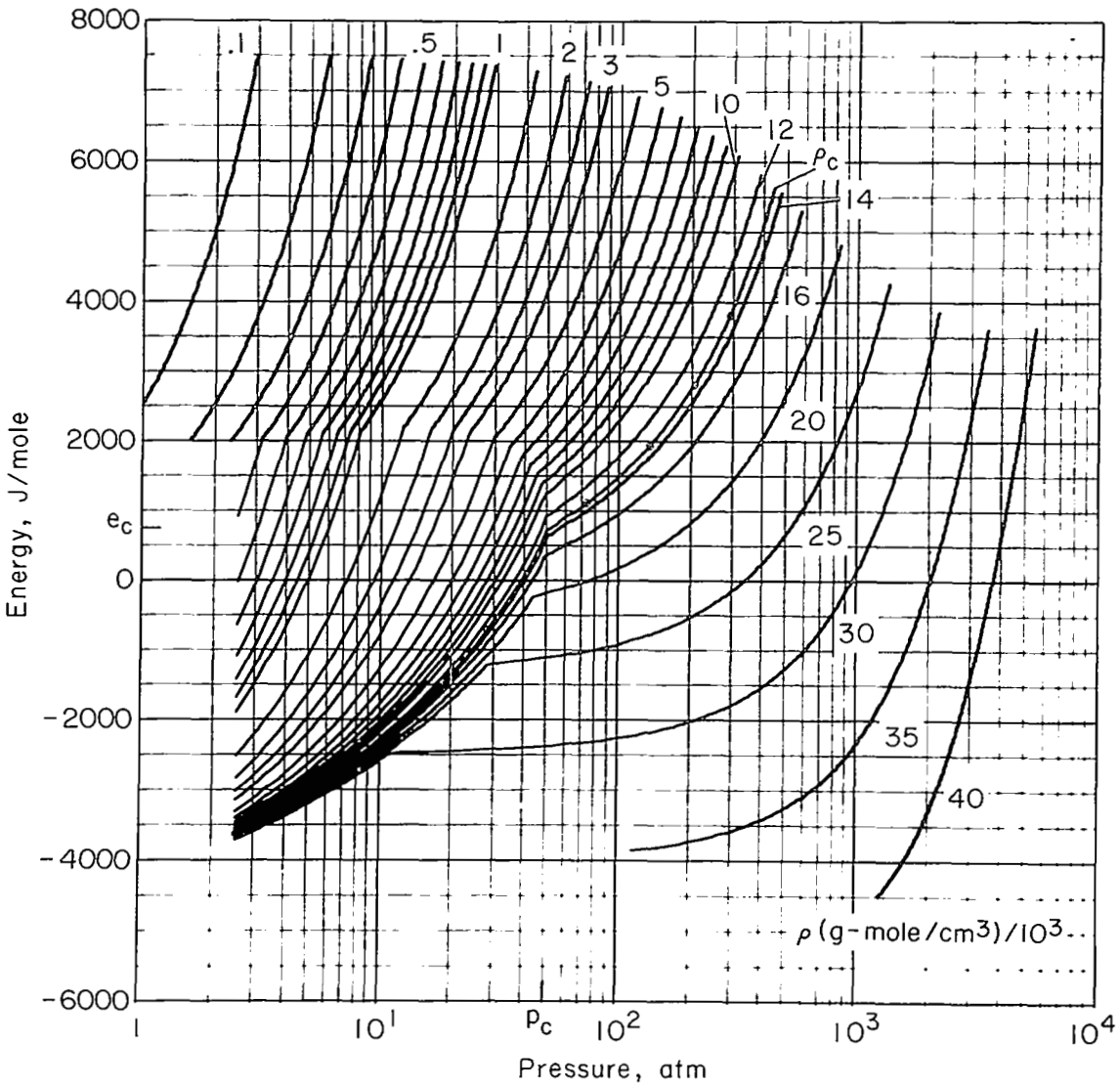

(a) Isochores.

Figure 4.6.– Internal energy versus pressure.

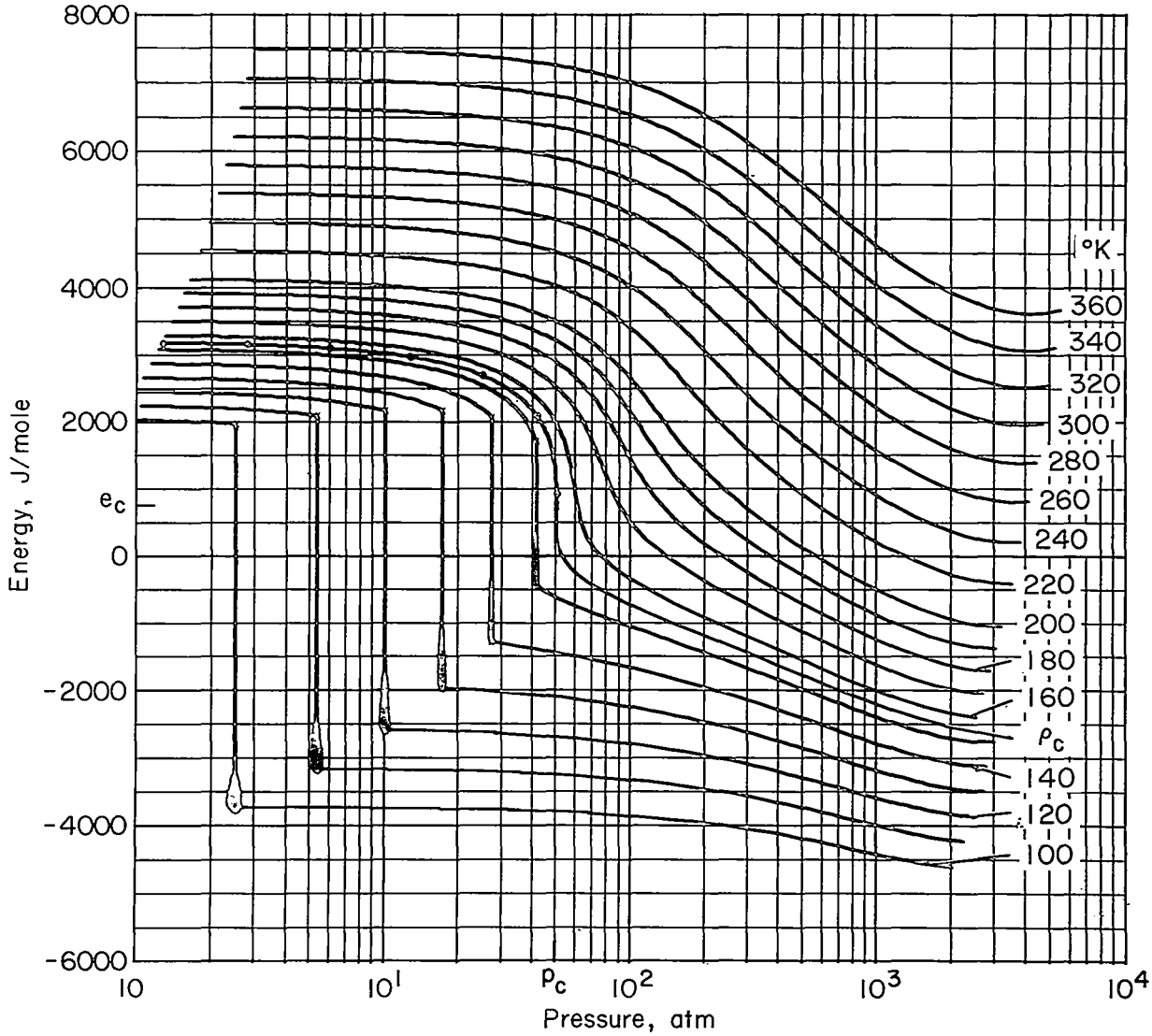

(b) Isotherms.

Figure 4.6.– Concluded.

5. ANALYSIS OF THERMODYNAMIC STATES RESULTING FROM SMALL-DENSITY-VARIATION APPROXIMATION OF FLUID MOTION IN CRYOGENIC OXYGEN TANKS

Barrett S. Baldwin, Walter A. Reinhardt, and Yvonne S. Sheaffer

SUMMARY

Methods are developed for analysis of the thermodynamic states predicted by a small-density-variation approximation of the fluid motion in a cryogenic storage tank. Relations are derived for evaluating variations in pressure and other thermodynamic quantities resulting from conduction and convection of heat. Methods are developed for simulating the heater in an Apollo oxygen tank in a manner compatible with the small-density-variation approximation of the fluid motion. Correction procedures are specified to account for compressibility effects and to suppress nonphysical behavior introduced by the numerical method used to determine the conduction and convection of heat.

INTRODUCTION

The integration procedure for evaluating the motion and temperature distribution of the fluid described in chapters 2 and 3 is based on several approximations. Although pressure gradients must be considered in the momentum equations, it can be shown that for the low-velocity cryogenic oxygen flows under consideration, pressure gradients can be neglected in the energy equation. Similarly, the variations in pressure with time do not affect the motion of the gas directly, but have only a cumulative effect in the energy equation. The most important coupling between the momentum and energy equations is through temperature gradients and convection of temperature variations. As a result, for the purpose of finding the motion of the gas, the density can be considered a function primarily of temperature, with pressure as a slowly varying parameter. If the temperature variations are sufficiently mild, the density and enthalpy can be approximated by the first several terms of series expansions in temperature with coefficients that vary slowly in time due to cumulative changes in pressure and temperature level.

In chapter 2 it is shown that to lowest order the flow equations can be cast in a form that is independent of pressure and density variations. The associated integration procedure described in chapter 3 requires as input a mean density $\bar{\rho}$ and thermal expansion coefficient β, each of which can be time-dependent to allow for cumulative changes in pressure and density level. A time-dependent temperature distribution results from this integration procedure. In this chapter, we indicate how this output can be used to determine the attendant slowly varying pressure as well as other thermodynamic variables such as the density distribution and the potential pressure decay that would result from adiabatic mixing. Methods for simulating the heater in an Apollo oxygen tank are developed. Correction procedures are also developed to account for compressibility effects and to counteract nonphysical behavior introduced by the numerical method (ch. 3) used to compute evolutions of temperature.

So far as the thermodynamic state of the gas is concerned, pressure gradients are negligible at the low velocities that occur in a cryogenic oxygen storage tank in a near zero gravitational environment. The pressure can therefor be considered uniform in the tank. The kinetic energy associated with the

motion of the gas and the dissipation term in equation (2.97) are also negligible compared to changes in the internal energy of interest. Thus the problem here is to evaluate the time-dependent thermodynamic state of a stationary stratified gas from a knowledge of the time-dependent mean density and temperature distribution. The degree of rigor brought to bear is independent of the means used to arrive at the input information on mean density and temperature distribution. The methods developed for this purpose therefore would be applicable to the results from more accurate higher order or three-dimensional analyses of the convection and conduction processes within the tank. Regarding the rigor of the analysis, we have considered the problem at two levels. In preliminary work, the van der Waals equations of state were used as described in the next section. In subsequent sections, we include results based on the more exact thermodynamic relations developed in chapter 4.

APPROXIMATE PROCEDURE BASED ON VAN DER WAALS EQUATIONS

The problem at hand is to find the pressure and other thermodynamic quantities when the mean density and temperature variation in the tank are known. In this section, we describe the procedure used to obtain preliminary values of these thermodynamic properties by an approximate method based on the van der Waals equations of state. The mean density $\bar{\rho}$ is known in terms of the total mass of oxygen M from the relation

$$\bar{\rho} = M/V_T \tag{5.1}$$

where V_T is the tank volume. The rate of change of mean density is found by differentiation

$$\frac{d\bar{\rho}}{dt} = \frac{dM/dt}{V_T} \tag{5.2}$$

where dM/dt is the rate of gas removal (typically 0 to 3 lbm/hr). Values of $\bar{\rho}$ are computed at each time step from the relation

$$(\bar{\rho})_{t+\Delta t} = (\bar{\rho})_t + \frac{\Delta t(dM/dt)}{V_T} \tag{5.3}$$

using input values of dM/dt and V_T.

At each time step the values of temperature T_{jk} at the computational grid points (see fig. 3.1) are determined from the integration procedure. The corresponding densities ρ_{jk} are computed to lowest order from the relation

$$\rho = \bar{\rho}[1 - \beta(T - \bar{T})] \tag{5.4}$$

where $\bar{T}$ is the volume average of the temperature variation T_{jk} and $\beta = (-1/\rho)(\partial\rho/\partial T)_p$ is the coefficient of thermal expansion corresponding to

the state $\bar{\rho}$, $\bar{T}$ (see eq. (2.16)). The van der Waals equation for pressure is

$$p = \frac{RT\rho}{1 - b\rho} - a\rho^2 \tag{5.5}$$

Differentiation leads to the relation

$$\beta = \frac{R(1 - b\rho)}{RT - 2a\rho(1 - b\rho)} \tag{5.6}$$

for the coefficient of thermal expansion. In our preliminary results reported at meetings of the Apollo Cryogenic Oxygen Tank Analysis Team at the NASA Manned Spacecraft Center, a constant value of β was used that was evaluated at the initial values of $\bar{\rho}$ and $\bar{T}$.

Since a uniform spacing of computational grid points is employed in the integration procedure, the volume average $\bar{T}$ can be computed according to the relation

$$\bar{T} = \frac{\sum_{j,k} T_{jk} W_{jk}}{\sum_{j,k} W_{jk}} \tag{5.7}$$

where W_{jk} is a weighting function (proportional to the volume associated with each grid point) that is taken equal to 1.0 at interior points, 0.5 at boundary points except in the corners, and 0.0 in the corners. The corners are excluded (zero weight) because in the integration procedure described in chapter 3 temperatures at the corners are not used and are not computed. The error introduced by this omission is negligible for the 17 × 17 array of grid points used in the calculations.

Substitution of the T_{jk} and ρ_{jk} into equation (5.5) would lead to pressures p_{jk} that are not all equal as they should be. Since the pressure should be uniform in the tank, it is expedient to evaluate an average pressure according to the relation

$$\overline{(p + a\rho^2)(1 - b\rho)} = R\overline{T\rho}$$

where the bar indicates a volume average of the same type as in equation (5.7). Substitution of equation (5.4) into this relation, use of the fact that $(T - \bar{T}) = 0$, and omission of $\overline{(T - \bar{T})^3}$ terms found to be negligible in the cases considered lead to the approximate expression

$$\bar{p} = \frac{R\bar{T}\bar{\rho}}{1 - b\bar{\rho}} - a(\bar{\rho})^2 + \frac{[a(\bar{\rho})^2(3b\bar{\rho} - 1)\beta^2 - R\bar{\rho}\beta]\overline{(T - \bar{T})^2}}{1 - b\bar{\rho}} \tag{5.8}$$

for the pressure in terms of average density, average temperature, and mean squared deviation of the temperature from the average value. The latter quantity is computed at each time step as in equation (5.7) according to the relation

$$\overline{(T - \bar{T})^2} = \frac{\sum_{j,k} (T_{jk} - \bar{T})^2 W_{jk}}{\sum_{j,k} W_{jk}} \tag{5.9}$$

In addition to the pressure, the potential pressure decay (pressure decay that would result from complete adiabatic mixing) is of interest. This quantity provides a conservative estimate of the maximum drop in pressure that could result from an abrupt spacecraft maneuver. This pressure drop could result in the tank fluid becoming a two-phase mixture, an undesirable state according to design criteria. The potential pressure decay that arises from nonuniform heating under various operating conditions is thus an important indication of the level of stratification of the fluid. In general, the procedure for evaluation of this quantity is as follows:

total mass	$M = \bar{\rho} V_T$
total internal energy	$E = \overline{e\rho} V_T$
specific internal energy of collapsed state resulting from complete adiabatic mixing	$e_{col} = E/M$
density of collapsed state	$\rho_{col} = \bar{\rho}$
temperature of collapsed state	$T_{col} = T(e_{col}, \rho_{col})$
collapse pressure	$p_{col} = p(T_{col}, \rho_{col})$
potential pressure decay	$(p - p_{col})$

where e is the specific internal energy at individual grid points and $\overline{e\rho}$ is a volume average. The functions $T(e_{col}, \rho_{col})$ and $p(T_{col}, \rho_{col})$ are to be found by inversion of the equations of state for specific internal energy $U(T,\rho)$ and pressure $p(T,\rho)$.

The above procedure for determination of the potential pressure decay can be carried out using approximate equations of state or the more exact relations given in chapter 4. Our preliminary results were based on the van der Waals equations of state, equation (5.5) and (ref. 1)

$$e = c_1 + c_v T - a\rho \tag{5.10}$$

Substitution of equation (5.5) into (5.10) to eliminate T yields

$$e = c_1 + \frac{c_v}{R\rho}(p + a\rho^2)(1 - b\rho) - a\rho$$

This relation can be used to evaluate $\overline{e\rho}$ and obtain an expression for e_{col} in terms of p, $\bar{\rho}$, $\overline{(\rho^2)}$, and $\overline{(\rho^3)}$ according to the foregoing general procedure for finding the potential pressure decay. Direct substitution in the above relation also yields an expression for e_{col} in terms of p_{col} and $\rho_{col} = \bar{\rho}$. Equating the two expressions for e_{col} then leads to the formula

$$p - p_{col} = \frac{ab[\overline{\rho^3} - (\bar{\rho})^3] - a[1 - (R/c_v)][\overline{\rho^2} - (\bar{\rho})^2]}{1 - b\bar{\rho}}$$

where $\overline{\rho^2}$ and $\overline{\rho^3}$ indicate volume averages. Substitution of the first-order density relation equation (5.4), rearrangement, and omission of $\overline{(T - \bar{T})^3}$ terms leads to the approximation

$$p - p_{col} = \frac{a(\bar{\rho})^2[3b\bar{\rho} - 1 + (R/c_v)]\beta^2\overline{(T - \bar{T})^2}}{1 - b\bar{\rho}} \tag{5.11}$$

which expresses the potential pressure decay in terms of the average density and mean squared deviation of temperature from the average value.

The specific heat at constant pressure is needed in the integration procedure described in chapters 2 and 3. The van der Waals equations of state (eqs. (5.5) and (5.10)) can be used to derive the relation

$$c_p = c_v + \frac{R}{1 - 2a\rho(1 - b\rho)^2/RT} \tag{5.12}$$

In our preliminary results a constant value of c_p is used that is evaluated at the initial values of $\bar{\rho}$ and $\bar{T}$. The values of the constants R, b, a, and c_v used in the van der Waals equations were chosen such that the critical pressure, temperature, and density are matched exactly according to relations given by Hirschfelder, Curtiss, and Bird (ref. 1).

PROCEDURE BASED ON EXACT THERMODYNAMICS

In this section a more exact method is developed for finding the pressure and other thermodynamic quantities when the mean density and temperature distribution in the tank are known. This method makes use of a temperature distribution function to save considerable computation time. A method for simulating the heater in an Apollo oxygen tank also is described, and correction procedures are developed to account for compressibility effects and to counteract nonphysical excursions of pressure introduced by the numerical method (ch. 3) used to compute evolutions of the temperature distribution.

Computation of Tank Pressure

When the mean density and temperature distribution are known, the uniform pressure in the tank can be computed. For this purpose it was found expedient to determine a temperature distribution function F_N of the type developed in chapter 4 (after eq. (4.18)), rather than considering thermodynamic quantities at each computational grid point. The procedure using a distribution function and computation of thermodynamic quantities at temperatures T_N replaces computation at grid temperatures T_{jk}. The advantage is that there are many more values of T_{jk} than of T_N, so many unnecessary repetitions of nearly identical calculations are eliminated. The temperature distribution function F is a function of temperature to be evaluated at a series of fixed, equally spaced temperatures T_N with $N = 1, 2, 3, \ldots, N_{max}$. The temperature dependence of F is here indicated parametrically by expressing F as a function of N, that is, F_N. The function F_N is defined to be a weighted number of computational grid points with temperatures between $T_N - \Delta T$ and $T_N + \Delta T$ where the T_N constitute a fixed array of temperatures with uniform spacing equal to ΔT. The weighting employed is proportional to the volume associated with each computational grid point. Interior points are given a weight $W_{jk} = 1.0$, for boundary points $W_{jk} = 0.5$, and the corner points are given zero weight since their temperatures are not computed in the integration procedure. For each value of j and k, W_{jk} is assigned to the two F_N between which its temperature lies in proportion to its proximity to each. That is, if $T_N < T_{jk} < T_{N+1}$, F_N is increased by an amount $W_{jk}(T_{N+1} - T_{jk})/\Delta T$, and F_{N+1} is increased by an amount $W_{jk}(T_{jk} - T_N)/\Delta T$. Thus the sum

$$\sum_{N=1}^{N_{max}} F_N$$

is equal to the total number of interior computational grid points plus half the number of boundary points, not counting corners. The quantity F_N is essentially equal to the total number of computational grid points with temperature between $T_N - (1/2)\Delta T$ and $T_N + (1/2)\Delta T$ except for a small readjustment corresponding to a linear interpolation. Figure 5.1 shows an example of a temperature distribution F_N plotted versus T_N. Additional examples and further discussion of the meaning of this distribution function are given in chapter 6.

An array of temperatures T_N is associated with the temperature distribution function F_N. Since the pressure is uniform in the tank, at a given tank pressure p, associated arrays of density ρ_N and internal energy e_N can be computed according to the relations

$$\rho_N = (p, T_N) \tag{5.13}$$

$$e_N = U(T_N, \rho_N) \tag{5.14}$$

The computation of the function $\rho(p,T_N)$ is described after equation (4.16) and $U(T_N,\rho_N)$ is given by (4.5). Since the F_N are proportional to the volume of gas in the temperature range $T_N - (1/2)\Delta T$ to $T_N + (1/2)\Delta T$ the volume averages $\overline{\rho}$ and $\overline{\rho e}$ can be computed according to

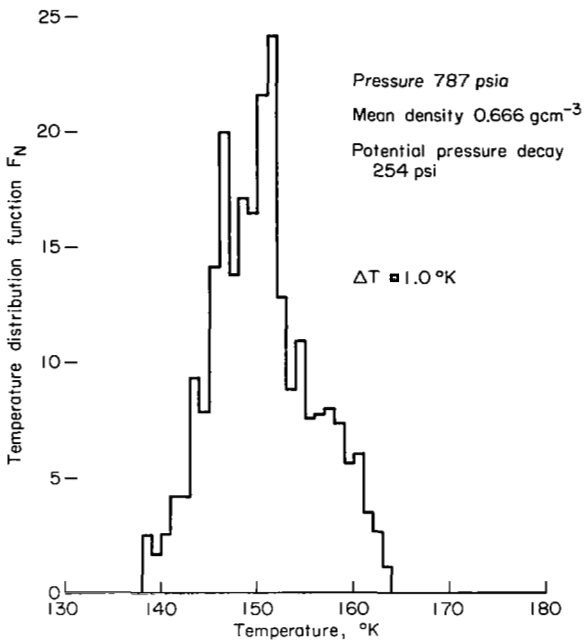

Figure 5.1.– Typical temperature distribution function.

$$\bar{\rho} = \frac{\sum_{N=1}^{N_{max}} F_N \rho_N}{\sum_{N=1}^{N_{max}} F_N} \tag{5.15}$$

$$\overline{\rho e} = \frac{\sum_{N=1}^{N_{max}} F_N \rho_N e_N}{\sum_{N=1}^{N_{max}} F_N} \tag{5.16}$$

At the beginning of an integration for the motion and temperature of the fluid a tank pressure p and values of temperature T_{jk} at the computational grid points are specified. The distribution function F_N is computed, and the above relations are used to determine the initial values of $\bar{\rho}$ and $\overline{\rho e}$. In the subsequent integration the variation of $\bar{\rho}$ is computed from equation (5.3) and depends on the specified rate of gas removal dM/dt. The values of T_{jk} resulting from the integration for the motion of the gas (see eqs. (3.2d) and (2.95a)) are used to compute F_N at the end of each time step. The problem then arises of computing the change in pressure Δp in each time step. It should be recalled that pressure p is uniform in the tank. By differentiation it can be seen that changes in the ρ_N are related to changes in pressure according to

$$\Delta\rho_N = \frac{\Delta p}{(\partial p/\partial\rho)_{T_N}} \tag{5.17}$$

since the values of T_N are held fixed throughout the integration. Substitution of this in the relation

$$(\rho_N)_{n+1} = (\rho_N)_n + \Delta\rho_N \tag{5.18}$$

yields

$$(\rho_N)_{n+1} = \frac{(\rho_N)_n + \Delta p}{(\partial p/\partial\rho)_{T_N}} \tag{5.19}$$

where the subscript n refers to the time step in the integration. Multiplication of the last equation by $(F_N)_{n+1}$, summation over N, and substitution of

$$\sum_{N=1}^{N_{max}} (F_N)_{n+1}(\rho_N)_{n+1} = \bar{\rho}_{n+1} \sum_{N=1}^{N_{max}} (F_N)_{n+1} \tag{5.20}$$

yield

$$\bar{\rho}_{n+1} \sum_{N=1}^{N_{max}} (F_N)_{n+1} = \sum_{N=1}^{N_{max}} (F_N)_{n+1} (\rho_N)_n + \Delta p \sum_{N=1}^{N_{max}} (F_N)_{n+1} (\partial\rho/\partial p)_{T_N} \quad (5.21)$$

Since $\bar{\rho}_{n+1}$ and $(F_N)_{n+1}$ are known at the end of the (n+1)th time step, this equation can be used to compute the change in pressure Δp associated with the time step. Once Δp is known, equation (5.19) can be used to compute the updated values of density $(\rho_N)_{n+1}$. As a check, $\bar{\rho}_{n+1}$ can be computed using equation (5.20) for comparison with the imposed value $\bar{\rho}_{n+1}$ from equation (5.3). Finally, the updated pressure is computed according to

$$p_{n+1} = p_n + \Delta p \quad (5.22)$$

The structure of equation (5.21) is such that the value of $\bar{\rho}_{n+1}$ computed from equation (5.20) will always be driven toward the imposed value from equation (5.3) so that cumulative drifts cannot occur. This follows from the fact that the first term on the right of equation (5.21) closely resembles the left side of equation (5.20). Cumulative drifts of the individual $(\rho_N)_{n+1}$ computed from equation (5.19) can take place, however. To avoid this, at every tenth time step, the ρ_N are recomputed according to equation (5.13). It has been found that the foregoing procedure is quite stable, and, for the sizes of time step imposed by stability criteria of the integration procedure, it is quite accurate with a 1° K spacing of the temperature elements T_N.

Once the pressure is determined the potential pressure decay can be computed by the procedure described in chapter 4 that utilizes the distribution function F_N. As a check the potential pressure decay can also be computed by the alternative method of chapter 4 for which the pressure p and temperatures at computational grid points are utilized. Figure 5.2 shows a comparison of potential pressure decays computed by the two methods for a linear temperature distribution. The dashed lines indicate the potential pressure decay for each case computed exactly by evaluation of the thermodynamic quantities at all computational grid points. The symbols indicate values of the potential pressure decay computed using the distribution function F_N for various values of the temperature array spacing ΔT. It can be seen from the results in figure 5.2 that the temperature array spacing ΔT = 1° K provides adequate accuracy for all the cases considered.

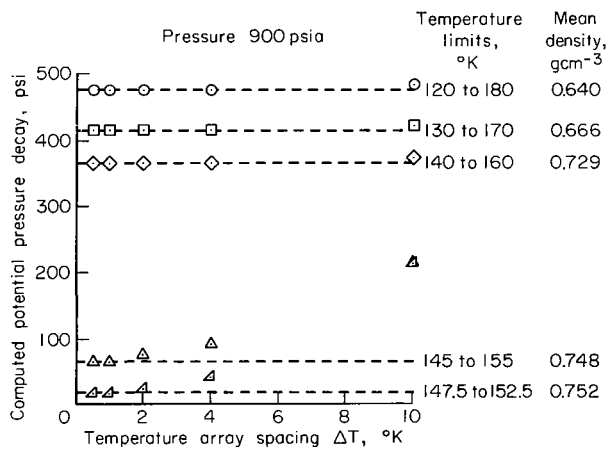

Figure 5.2.– Effect of temperature array spacing on computed potential pressure decay.

Method for Heater Simulation

An internal heater is used in the Apollo oxygen tanks to increase the pressure when it falls below 865 psia due to gas removal. In unpublished work of C. K. Forester, D. D. Rule, and H. W. Patterson reported at meetings of the Apollo Cryogenic Oxygen Tank Analysis Team, a segment of the wall was used to simulate such a heater. It was found that the boundary-layer flow in the neighborhood of the heater cannot be adequately resolved with a uniform grid spacing when the acceleration field is of order 10^{-6} g or greater. Methods can nevertheless be found that lead to physically reasonable and qualitatively correct results if attention is confined to energy conservation, and accurate values of heater temperature are not required.

In this section, a method for simulating the heater by assigning selected computational grid points as heater elements is described. When the heater is on, the temperatures of the grid points assigned as heaters are increased by an amount dependent on the heat capacity of the gas associated with each grid point. The heat capacity depends on the volume of gas V_H associated with a grid point, which is equal to the depth of the tank times the product of grid point spacings in the x and y directions. Adjustments in heater temperatures are made at the beginning and end of a time step in the integration for motion and temperature of the fluid described in chapter 3. The energy balance will be properly maintained if at the beginning of each time step the heater element temperatures are increased by an amount ΔT_H corresponding to a specified heater power dQ/dt added to the total gas volume V_{HT} associated with the heater element computational grid points; that is,

$$\Delta T_H = \frac{(dQ/dt)\Delta t}{\rho c_p V_{HT}} \tag{5.23}$$

before the integration step. The gas volume associated with each interior computational grid point is

$$V_H = \frac{V_T \, \Delta x \, \Delta y}{\ell_x \ell_y} \tag{5.24}$$

where Δx and Δy are the distances between grid points; the depth of the tank is equal to $V_T/\ell_x\ell_y$; V_T is the total tank volume; and ℓ_x, ℓ_y are the tank dimensions.

If the heater element computational grid points are interior points, the total heater gas volume V_{HT} is equal to the number of heater elements times V_H. But heater volume elements on the boundary are half the value given in equation (5.24) since the boundary passes through the grid points. When the heater elements are in the interior their temperatures will rise until a balance is reached between the temperature increase from equation (5.23) and the decrease due to convection and conduction computed in the integration procedure of chapter 3. When the heater elements are on the boundary, however, the integration procedure does not modify their values. In that case, it is necessary to allow for a decrease in temperature at the *end* of each time step according

to the amount of heat transferred to the interior grid points from the heater elements. For a heater on a wall parallel to the y axis the appropriate change in wall heater element temperatures is

$$\Delta T_H = - \frac{2k(T_H - T_{interior})\Delta t}{\rho c_p (\Delta x)^2} \tag{5.25}$$

after the integration step. When the heater is turned off ($dQ/dt = 0$) the increase ΔT_H computed in equation (5.23) is zero. If the heater is on a wall, the ΔT_H computed in equation (5.25) corresponds to an insulated wall boundary condition when the heater is off except for a small (physically correct) lag due to the heat capacity of the gas adjacent to the wall.

The same type of computation as that in equations (5.23) and (5.25) can be used at all boundary points to simulate the heat leak from the exterior of the tank. In that case dQ/dt in equation (5.23) is replaced by the heat leak rate dQ_L/dt.

The power radiated from the heater can be allowed for by means of the relation

$$\frac{dQ}{dt} = \frac{d\tilde{Q}}{dt} - Q_{rad} \tag{5.26}$$

where $d\tilde{Q}/dt$ is the specified input heater power and

$$Q_{rad} = \varepsilon \sigma_R (T_H^4 - \bar{T}^4) A_H \tag{5.27}$$

where ε is the emissivity (typically 0.32), σ_r the Stefan-Boltzmann constant, and A_H the heater area. According to reference 2, less than 10 percent of the radiated power is absorbed in the oxygen (usually much less depending on the heater temperature). Therefore, most of the radiation is absorbed in the tank wall, and Q_{rad} should be added to the heat rate dQ_L/dt. That is, radiation from the heater is absorbed in the wall and heats the fluid adjacent to the wall by conduction in the same manner as heat leaking to the interior of the insulated wall from the warmer outer wall of the tank.

CORRECTION FOR SPURIOUS INTERNAL SOURCES

The integration method for the motion and temperature of the fluid described in chapter 3 utilizes the so-called "conservative form" of the convective terms. The method is not strictly conservative in the sense of reference 3, although it may provide more accurate treatment of convection effects. Also the treatment of heater and wall computational grid points described in the preceding section is not strictly conservative. For that reason small spurious internal sources may lead to erroneous cumulative computed pressure variations. To avoid this the method can be made conservative overall by applying a correction to the temperatures T_{jk} at the end of each time step.

For that purpose integration of the energy equation over the tank volume, use of Gauss' theorem, and rearrangement lead to the expression

$$\frac{dE}{dt} = \frac{dQ_T}{dt} + h_o \frac{dM}{dt} \tag{5.28}$$

where

$$E = \overline{\rho e} V_T \qquad \text{total internal energy} \tag{5.29}$$

$h_o \approx h(\bar{\rho}, \bar{T})$ specific enthalpy of fluid at the exit orifice

$$\frac{dQ_T}{dt} = \frac{dQ}{dt} + \frac{dQ_L}{dt} \qquad \text{total power input} \tag{5.30}$$

$\frac{dM}{dt}$ rate of fluid removal (negative for outflow)

If a strictly conservative numerical method were used to integrate the exact conservation relations, equation (5.28) would be satisfied. A procedure for imposing equation (5.28) is developed in a later section. First, however, it is worthwhile to consider the corresponding energy conservation relation that applies to the approximate energy equation derived in chapter 2.

Integration over the tank volume, application of Gauss' theorem to the energy equation derived in chapter 2, and use of $M = \bar{\rho} V_T$ lead to the expression

$$Mc_p \frac{d\bar{T}}{dt} = \frac{dQ_T}{dt} + (h_o - c_p \bar{T}) \frac{dM}{dt}$$

If a strictly conservative numerical method were used to integrate the equations of chapter 2, the above equation would be satisfied. Conversely, overall energy conservation will result if this relation is imposed at the end of each time step by a uniform readjustment of the temperatures T_{jk} at the computational grid points. A uniform readjustment is chosen because we have no information on the spatial location of the error. For this purpose h_o can be taken equal to $c_p \bar{T}$ and

$$Mc_p \frac{d\bar{T}}{dt} = \frac{dQ_T}{dt} \tag{5.31}$$

Setting h_o equal to $c_p \bar{T}$ has the effect of removing the dM/dt term from equation (5.31). The meaning of this choice is that we take the enthalpy at the exit orifice to be equal to the average specific enthalpy in the tank rather than attempting to specify an exact location of the exit orifice. Imposition of this relation at the end of each time step ensures conservation of energy and removes pressure excursions resulting from small but cumulative spurious internal energy sources arising from the nonconservative numerical method described in chapter 3. A dimensionless temperature H is defined in equation (2.95a) and H_{jk} is evaluated at the computational grid points in the

numerical integration procedure of chapter 3 (eq. (3.2d)). The temperatures T_{jk} at the computational grid points are related to the dimensionless temperatures H_{jk} by the relation

$$T_{jk} = T_R + T_{dif} H_{jk} \tag{5.32}$$

where T_R is a reference temperature that can be time dependent and T_{dif} is an arbitrary constant temperature difference. The uniform readjustment of the T_{jk} at each time step can be effected by a change in the reference temperature T_R rather than modifying all elements of the computational matrix H_{jk}. For that purpose the volume average of equation (5.32)

$$\bar{T} = T_R + T_{dif} \bar{H} \tag{5.33}$$

is needed. At the end of each time step the volume average $\bar{H}$ is computed to determine the necessary correction of T_R. Integration of equation (5.31) over one time step yields

$$\bar{T}_{n+1} - \bar{T}_n = \frac{1}{Mc_p} \frac{dQ_T}{dt} \Delta t$$

Substitution of equation (5.33) leads to the relation

$$(T_R)_{n+1} - (T_R)_n + T_{dif}(\bar{H}_{n+1} - \bar{H}_n) = \frac{1}{Mc_p} \frac{dQ_T}{dt} \Delta t$$

from which it follows that the required correction $\Delta T_R = (T_R)_{n+1} - (T_R)_n$ is

$$\Delta T_R = \frac{1}{Mc_p} \frac{dQ_T}{dt} \Delta t - T_{dif}(\bar{H}_{n+1} - \bar{H}_n) \tag{5.34}$$

Correction to Account for Mean-Density Variations

Additional nonphysical cumulative excursions of pressure can result from the use of approximate thermodynamics in the integration procedure for determination of the motion and temperature of the fluid. If an exact compressible conservative method were used, equation (5.28) would be satisfied. Conversely, imposition of equation (5.28) by readjustment of dQ_T/dt will result in an overall energy balance and will restore the correct pressure variation with time. If this were done at every time step, the correction for spurious internal sources (eq. (5.34)) would be superfluous since it would be overridden. However, the computing time required for evaluating the necessary thermodynamic functions in their present form (described in ch. 4) is not negligible. Since the correction to account for compressibility effects is relatively small for short time periods, computing time can be saved by imposing it only at every tenth time step. In that case, since the computing time required for imposing

the correction for spurious internal sources at every time step is negligible, both corrections are worthwhile.

Substitution of equation (5.29) into (5.28) and integration over one time step yield

$$(\overline{\rho e})_{n+1} - (\overline{\rho e})_n = \frac{1}{V_T}\left(\frac{dQ_T}{dt} + h_o \frac{dM}{dt}\right) \Delta t$$

This relation may not be satisfied if a nonconservative numerical method is used. It will be satisfied if a correction power dQ_c/dt is added to the total input power dQ_T/dt such that

$$\frac{dQ_c}{dt} = \frac{V_T}{\Delta t}[(\overline{\rho e})_{n+1} - (\overline{\rho e})_n] - \frac{dQ_T}{dt} - h_o \frac{dM}{dt} \tag{5.35}$$

It is convenient to add this small correction to the wall heat leak power dQ_L/dt discussed after equation (5.25). Thus heat is added (or subtracted) at the tank walls to allow for the difference between accurate thermodynamics and the approximate thermodynamics used in the integration procedure. Physically realistic pressure variations will result for cases in which the convection and conduction processes within the tank are adequately approximated by the two-dimensional integration procedure for a square tank described in chapters 2 and 3.

Method for Including Effects of Tank Stretch and Variable Transport Properties

Since the Apollo oxygen tanks are thin-walled pressure vessels, the tank volume depends on the pressure according to the relation

$$V_T = V_{T_o}\left[1 + \frac{1}{V_{T_o}} \frac{dV_T}{dp} (p - p_o)\right] \tag{5.36}$$

where V_{T_o} and p_o are the initial volume and pressure, respectively. According to relations given in unpublished work of C. K. Forester, dV_T/dp can be considered constant and is given by

$$\frac{dV_T}{dp} = \frac{3r(1 - \sigma)V_{T_o}}{2b_1 E_y} \tag{5.37}$$

where

r/b_1 ratio of spherical tank radius to wall thickness

σ Poisson's ratio for tank wall material

V_{T_o} initial tank volume

E_y Young's modulus for tank wall material

The changes in tank volume due to changes in pressure are small, but they can have a large effect on the rate of pressure rise due to heating and on the potential pressure decay. To account for such effects it is necessary to replace equation (5.28) with

$$\frac{dE}{dt} = \frac{dQ_T}{dt} + h_o \frac{dM}{dt} - p \frac{dV_T}{dt}$$

which is a form of the first law of thermodynamics. This relation is applicable to the entire volume of stratified fluid because pressure gradients are negligible. Differentiation of equation (5.36) with V_{T_o}, dV_T/dp, and p_o held constant, and substitution in the last relation yield

$$\frac{dE}{dt} = \frac{dQ_T}{dt} + h_o \frac{dM}{dt} - \frac{1}{2} \frac{dV_T}{dp} \frac{dp^2}{dt}$$

Integration of this equation leads to the expression

$$E = E_o + \int_o^t \left(\frac{dQ_T}{dt} + h_o \frac{dM}{dt} \right) dt - \frac{1}{2} \frac{dV_T}{dp} (p^2 - p_o^2) \qquad (5.38)$$

for the total internal energy in the tank.

To ensure conservation of energy in each time step a procedure similar to that leading to equation (5.21) can be applied to the relation

$$(\rho_N e_N)_{n+1} = (\rho_N e_N)_n + \Delta p \left(\frac{\partial \rho e}{\partial p} \right)_{T_N}$$

to obtain

$$(\overline{\rho e})_{n+1} \sum_{N=1}^{N_{max}} F_N = \sum_{N=1}^{N_{max}} F_N (\rho_N e_N)_n + \Delta p \sum_{N=1}^{N_{max}} F_N \left(\frac{\partial \rho e}{\partial p} \right)_{T_N}$$

where F_N is evaluated at n+1. Since $\overline{\rho e} = E/V_T$, substitution of equations (5.36) and (5.38) into the last relation yields

$$\frac{\left\{E_o + \int_o^{t_{n+1}} \left(\frac{dQ_T}{dt} + h_o \frac{dM}{dt}\right) dt - \frac{1}{2}\frac{dV_T}{dp}\left[(p_n + \Delta p)^2 - p_o^2\right]\right\} \sum_{N=1}^{N_{max}} F_N}{V_o\left[1 + \frac{1}{V_{T_o}}\frac{dV_T}{dp}(p_n + \Delta p - p_o)\right]}$$

$$= \sum_{N=1}^{N_{max}} F_N(\rho_N e_N)_n + \Delta p \sum_{N=1}^{N_{max}} F_N \left(\frac{\partial \rho e}{\partial p}\right)_{T_N} \qquad (5.39)$$

Similarly, use of $\bar{\rho} = M/V_T$ and substitution of equation (5.36) into equation (5.21) yield

$$\frac{M_{n+1} \sum_{N=1}^{N_{max}} F_N}{V_{T_o}\left[1 + \frac{1}{V_{T_o}}\frac{dV_T}{dp}(p_n + \Delta p - p_o)\right]} = \sum_{N=1}^{N_{max}} F_N(\rho_N)_n + \Delta p \sum_{N=1}^{N_{max}} F_N \left(\frac{\partial \rho}{\partial p}\right)_{T_N} \qquad (5.40)$$

In this derivation F_N is evaluated at the (n+1)st integration step. If equations (5.39) and (5.40) are satisfied at each time step, overall conservation of energy and mass is assured. At the end of an integration step all quantities appearing in these equations are known except Δp and ΔT_R, the change in reference temperature imposed by the effect of tank stretch on the total energy. Note that equations (5.39) and (5.40) can be solved for Δp and ΔT_R at each time step so that energy and mass are conserved.

The temperatures T_{jk} at the computational grid points are related to the dimensionless temperatures H_{jk} computed in the integration procedure of chapter 3 by equation (5.32). Substitution of that equation into the expression for the distribution function F_N, equation (5.28) of chapter 4 yields

$$F_N = \sum_{j,k} W_{jk}\left[1 - \left|\frac{T_{dif}H_{jk} + T_R - T_N}{\Delta T}\right|\right]\left\{S\left[\frac{T_{dif}H_{jk} + T_R - (T_N - \Delta T)}{\Delta T}\right]\right.$$
$$\left. - S\left[\frac{T_{dif}H_{jk} + T_R - (T_N + \Delta T)}{\Delta T}\right]\right\}$$

The W_{jk} are constant weighting values discussed previously. The T_N are an array of fixed temperatures with uniform spacing ΔT and T_{dif} is an arbitrary temperature difference. At the end of an integration step according to the method of chapter 3, the dimensionless temperatures H_{jk} are known. Therefore, all quantities needed to compute F_N for use in equations (5.39) and (5.40) are known except the reference temperature T_R. However, T_R is known at the previous time step. Therefore, F_N is evaluated by means of the relation

$$F_N = F_N[(T_R)_n] + \Delta T_R \frac{\{F_N[(T_R)_n + \Delta T] - F_N[(T_R)_n]\}}{\Delta T} \tag{5.41}$$

where ΔT is the spacing between the T_N, that is, $\Delta T = T_{N+1} - T_N$. Substituting equation (5.41) into (5.39) and (5.40) yields a pair of equations too lengthy to be written out conveniently. However, the important point is that the resulting equations can be solved (by iteration) for Δp and ΔT_R at each time step. In this procedure no additional corrections for spurious internal sources or changes in mean density are required since energy and mass are already conserved. The structure of the relations in this section is such that the computed values of $\overline{\rho}$ and $\overline{\rho e}$ are automatically driven toward the correct values and significant drifts do not occur.

At the end of each time step, and also at the start of the calculation, when p and T_R are known a number of quantities needed for calculation at the next time step are evaluated at the fixed temperatures T_N and pressure p. Each element of the fixed double arrays

$$\rho_{MN} = \rho(p_M, T_N) \tag{5.42}$$

$$e_{MN} = U(p_M, T_N) \tag{5.43}$$

used in these evaluations is computed and stored during the calculation the first time it is needed, using the thermodynamic relations of chapter 4. The stored values are used, if they have been previously computed, to minimize the computing time. It has been determined that a uniform spacing of 10 psi between the p_M and 1° K spacing between the T_N provide adequate accuracy.

The densities ρ_N and derivatives $(\partial\rho/\partial p)_{T_N}$ and $(\partial\rho e/\partial p)_{T_N}$ are evaluated according to

$$\rho_N = \left(\frac{p - p_M}{p_{M+1} - p_M}\right)\rho_{M+1,N} + \left(\frac{p_{M+1} - p}{p_{M+1} - p_M}\right)\rho_{MN} \tag{5.44}$$

$$\left(\frac{\partial\rho}{\partial p}\right)_{T_N} = \frac{\rho_{M+1,N} - \rho_{M,N}}{p_{M+1} - p_M} \tag{5.45}$$

$$\left(\frac{\partial\rho e}{\partial p}\right)_{T_N} = \frac{(\rho_{M+1,N} e_{M+1,N} - \rho_{MN} e_{MN})}{(p_{M+1} - p_M)} \tag{5.46}$$

where M is chosen such that $p_M \le p < p_{M+1}$. Additional derivatives needed in the calculation are

$$\left(\frac{\partial\rho}{\partial T}\right)_p = \frac{\rho_{M,N+1} - \rho_{MN}}{T_{N+1} - T_N} \tag{5.47}$$

$$\left(\frac{\partial e}{\partial T}\right)_p = \frac{e_{M,N+1} - e_{MN}}{T_{N+1} - T_N} \tag{5.48}$$

Again M is chosen such that $p_M \le p < p_{M+1}$ and these derivatives are evaluated at all N so that the quantities

$$\beta_N = -\frac{[(\partial\rho/\partial T)_p]_N}{\rho_N} \tag{5.49}$$

$$(c_p)_N = \frac{[(\partial e/\partial T)_p]_N + \beta_N p}{\rho_N} \tag{5.50}$$

can be computed and stored for all N. Arrays ν_N (kinematic viscosity) and k_N (thermal conductivity) are also computed and stored at the end of each time step for use in the next integration step. The relations used are

$$\nu_N = \nu(\rho_N, T_N) \tag{5.51}$$

$$k_N = k(\rho_N, T_N) \tag{5.52}$$

where the functions $\nu(\rho,T)$ and $k(\rho,T)$ are evaluated according to an unpublished recommendation of H. M. Roder. Equations (5.49) through (5.52) indicate the evaluations used to impose variable coefficients in the equations of chapter 2. The value of N used at each computational grid point is chosen such that $T_N \le T_{jk} < T_{N+1}$.

The tank stretch effect also modifies the relations for potential pressure decay listed after equation (5.9). The total mass of the collapsed state is unaffected, but the total energy and volume are given by

$$E_{col} = E + \frac{1}{2}\frac{dV}{dp}(p^2 - p_{col}^2) \tag{5.53}$$

$$V_{col} = V_o\left[1 + \frac{1}{V_o}\frac{dV}{dp}(p_{col} - p_o)\right] \tag{5.54}$$

Then

$$\rho_{col} = M/V_{col} \tag{5.55}$$

$$e_{col} = E_{col}/(\rho_{col}V_{col}) \tag{5.56}$$

The equations of state

$$p_{col} = p(\rho_{col}, T_{col}) \tag{5.57}$$

$$e_{col} = U(T_{col}, \rho_{col}) \tag{5.58}$$

are also needed. Iterative solution of these relations is required to find the collapse pressure p_{col}.

At the beginning of an integration for the motion and temperature distribution of the fluid the initial pressure p_o, tank quantity, and dimensionless temperature distribution H_{jk} are specified. The tank quantity is defined to be the ratio of fluid mass in the tank to the fluid mass when the tank is full. Thus, the mass of oxygen in the tank is computed according to

$$M = M_{full} \times \text{Quantity} \tag{5.59}$$

Then

$$\bar{\rho} = M/V_o \tag{5.60}$$

The distribution function F_N is a function of T_R; see the discussion following equation (5.40). Therefore, the relations

$$\rho_N = \rho(p_o, T_N) \tag{5.61}$$

$$\bar{\rho} \sum_{N=1}^{N_{max}} F_N = \sum_{N=1}^{N_{max}} F_N \rho_N \tag{5.62}$$

can be solved for T_R by iteration. Once T_R is known

$$\overline{\rho e} = \frac{\sum_{N=1}^{N_{max}} F_N \rho_N}{\sum_{N=1}^{N_{max}} F_N} \tag{5.63}$$

and

$$E_o = \overline{\rho e} V_{T_o} \tag{5.64}$$

can be evaluated.

Suppression of Nonphysical Excursions of Temperature and Vorticity

At an early stage in this investigation it was noted that the numerical integration method described in chapter 3 results in small excursions of temperature outside the range of values imposed in the boundary conditions. This probably occurs because of the use of a coarse grid that does not adequately resolve the heater boundary layer. We have described methods for ensuring overall conservation of mass and energy. An additional remedy has been adopted to suppress nonphysical excursions of temperature.

In simulating a heater, heater temperatures are computed at the beginning of an integration for each time step. Similarly, wall temperatures are

computed to account for heater radiation absorbed by the walls and heat leak through the walls. After these computations the highest and lowest temperatures in the entire temperature matrix are found. These limits are then imposed on the entire temperature matrix at the end of each integration step since they are valid physical limits.

A similar type of nonphysical behavior can occur in the computation of vorticity due to the failure of the coarse grid to resolve boundary layers. Therefore, upper and lower limits were imposed on the vorticity matrix at the end of each time step in the same manner as for the temperature. When this was not done, much larger values of vorticity occurred at the boundaries and produced oscillations in the flow unless the time step was decreased. Imposition of vorticity limits stabilized the flow and allowed long computations to be made. Fixed limits of plus or minus four times the magnitude of the uniform vorticity corresponding to a rotation reversal starting at three revolutions per hour were imposed. These limits were chosen because they are beyond the extreme values observed at interior points in the flow for the cases investigated. There is no physical justification for vorticity limits as there is for temperature limits. There is a physical interpretation of the effect, however. Disturbances that extend over several computational grid points can be computed correctly, but small-scale disturbances that cannot be computed correctly with a coarse grid in any case are filtered out. The flow in thin boundary layers and near the corners of the rectangular enclosure will not be computed correctly. However, the mixing action that occurs in the main body of the fluid for times up to several hours can be computed and should provide a conservative estimate of the mixing that would take place in a spherical tank without corners.

Effect of Changes in Parameters

Chapter 6 presents results from a series of calculations based on the methods of this and the preceding chapters. A 17 × 17 computational grid was used in those calculations as well as fixed values of several other parameters. It is of interest to consider the effect of changing the total number of mesh points and other parameters.

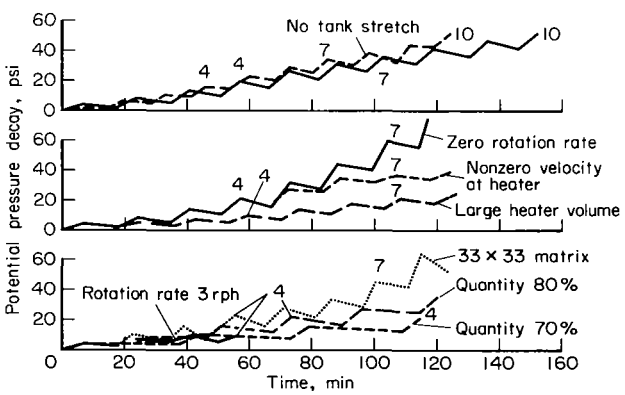

Figure 5.3.— Effect of changes in parameters (in all cases, flow rate = 1.5 lbm/hr, heat leak = 10 W, heater power = 115 W, rotation rate = 0.4 rph except where noted, quantity = 90 percent except where noted).

Figure 5.3 contains plots of potential pressure decay versus time during heater cycling. In all of the calculations represented the heater is turned on when the pressure falls below 870 psia due to gas removal and the heater is turned off when the pressure rises above 910 psia. A flow rate of 1.5 lbm/hr, a heat leak rate of 10 watts, and a heater power of 115 watts were

imposed in all of the calculations. A steady spacecraft rotation rate of 0.4 revolutions per hour was used, except where noted, and the tank quantity (required in eq. (5.59)) was 90 percent except for two cases at 80 and 70 percent. The quantity decreases by about 1 percent in 2 hr when the mass-flow rate is 1.5 lbm/hr.

The potential pressure decay rises when the heater is on and subsides when the heater is off, but there is a cumulative increase as the level of temperature stratification increases. It can be seen in figure 5.3 that the heater is turned on and off a number of times in each of the calculations shown. The positions of the fourth, seventh, and tenth peaks are labeled in the figure as an indication of the effect of changes in parameters on the rate of pressure rise. Since the pressure fluctuates linearly between 870 and 910 psia in all cases, the time required for 10 peaks in the potential pressure decay is inversely proportional to the rate of pressure rise. This is illustrated in sketch (a), which shows pressure and potential pressure decay versus time for two heating cycles. Note that the rate of pressure rise due to heating is reduced by the tank stretch effect. The amount of the reduction is inversely proportional to the ratio of times required to complete a given number of cycles. Calculations with and without the tank stretch effect are compared in the plot at the top of figure 5.3. The ratio of times required to reach the tenth peak indicates that the tank stretch effect decreases the rate of pressure rise by a factor of 1.225 relative to the rate of rise for a rigid container. In unpublished work of the Propulsion and Power Division, NASA Manned Spacecraft Center, results were obtained showing that with uniform heating at 90 percent quantity the corresponding ratio of rise rates is 1.563. Thus, we find the tank stretch correction to be smaller for nonuniform stratified heating than it is for uniform heating. It can also be seen in the plots at the top of figure 5.3 that the tank stretch effect tends to suppress the cumulative rise in potential pressure decay but does not counteract it completely. Additional information on this point is supplied by comparison of potential pressure decays with and without tank stretch for an assumed linear temperature distribution across the tank. In a representative calculation at 90 percent quantity with a temperature spread of 20° K, the values of potential pressure decay computed were 135 psi with tank stretch and 208 psi for a rigid container. Thus, tank stretch becomes more effective at higher levels of stratification in counteracting the buildup of potential pressure decay that would be present in a rigid container.

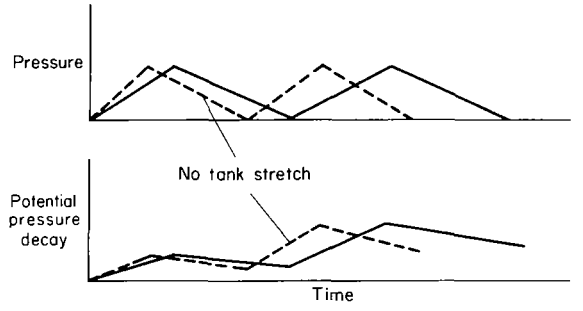

Sketch (a)

Effects of changes in other parameters can be noted in figure 5.3. Rotation rate refers to the steady rate of rotation of the spacecraft used in the calculation. In each case, the calculation was started with a uniform temperature and with the fluid at rest relative to the rotating tank. In all calculations the heater was located at an off-center position described more

completely in chapter 6 (fig. 6.10). Five computational grid points forming a + were used as heater elements. At the end of each time step in the integration, the stream function at these five points was set equal to the average of the values computed at the five points by the numerical method of chapter 3. This was done for the purpose of imposing zero velocity at the center of the heater. "Nonzero velocity at heater" in figure 5.3 refers to a calculation in which the stream function was not readjusted at heater elements. "Large heater volume" indicates a calculation in which 13 points were used as heater elements rather than five points. It can be seen in figure 5.3 that use of 13 points decreased the computed potential pressure decay by only a factor of about two. Most of the calculations in this report were computed using 17 × 17 uniformly spaced matrix points. In figure 5.3 results are given for a 33 × 33 matrix that are to be compared with the standard calculation represented by the solid curve in the top plot. For tank quantities less than 90 percent the rate of pressure rise and the cumulative rise in potential pressure decay are smaller as shown in the plots at the bottom of figure 5.3.

REFERENCES

1. Hirschfelder, J.; Curtiss, C. F.; and Bird, R. B.: Molecular Theory of Gases and Liquids. John Wiley & Sons, Inc., 1954, pp. 237, 250-252, 256.

2. Borucki, W. J.: Absorption of Infrared Radiation by High-Density Oxygen. Letter to the Editor, J. Spacecraft and Rockets.

3. Forester, C. K.: Numerical Integration of the Conservation Equations for the Storage and Expulsion of Single-Phase Cryogens. M.S. Thesis, Dept. of Mech. Engr., Univ. of Washington, 1969.

6. RESULTS FROM NUMERICAL COMPUTATIONS SIMULATING FLOWS IN AN APOLLO OXYGEN TANK

Barrett S. Baldwin, Walter A. Reinhardt, and Yvonne S. Sheaffer

SUMMARY

The effectiveness of vehicle maneuvering as a means for producing necessary mixing in the Apollo oxygen tanks is investigated. Results are presented from numerical simulation of flow in the tanks showing the effect of reversal of rotation after a prolonged period of rotation at a constant rate. Results are given from calculations corresponding to spin up of the vehicle after a prolonged period at zero rotation rate and near-zero acceleration. Both maneuvers lead to a reduction in potential pressure decay by a factor of 2 or more. Photographs of a cathode ray display tube are presented illustrating the convection currents and cumulative buildup of potential pressure decay that result from intermittent operation of the heater.

INTRODUCTION

In this chapter, results are presented from a series of calculations utilizing the methods developed in preceding chapters. Preliminary results based on the van der Waals equations of state were presented at meetings on the Apollo oxygen system held at the Manned Spacecraft Center prior to the Apollo 14 flight.

Following the failure of an oxygen tank during the Apollo 13 flight and the subsequent diagnosis of the cause, intensive efforts in the areas of design, development, analysis, and testing were conducted to assure the timely redesign of the Apollo cryogenic oxygen storage and supply system. After the Apollo 14 flight a symposium was organized at the NASA Manned Spacecraft Center for the purpose of disseminating the information acquired. Seventeen papers were presented under five categories: hardware development, stratification analyses, system models, test programs, and flight performance. The papers were collected in an unpublished document, MSC Cryogenics Symposium Papers. The relationship of the present investigation to the overall effort is outlined in chapter 1.

The recommendation of the Apollo 13 Review Board that the mixing fans be removed from the oxygen tanks was adopted. This decision and the subsequent redesign studies were aided by data acquired from the Apollo 12 flight during which the fans were not used for an appreciable part of the flight. Analysis of that data was reported in unpublished work of C. K. Forester, D. D. Rule, and H. W. Patterson. Of particular interest was a period from 4 to 8 hr after the launch during which the fans were not operated. During most of this time very little spacecraft maneuvering occurred, and the effective acceleration field was of order 10^{-7} earth gravity. It was found that a number of pressure decays took place that were correlated with accelerations due to maneuvering, which caused spikes of acceleration of order 10^{-4} g lasting for several seconds. After a prolonged period of low acceleration a pressure decay of 140 psi was observed at the time of an acceleration spike that reached a level of 10^{-3} g. A stratification analysis based on a two-dimensional square-tank simulation reproduced these effects reasonably well.

The analyses of Apollo 12 data indicated that no serious stratification problems were to be expected from operation of the oxygen tanks with the mixing fans removed. It was concluded that normal vehicle maneuvering could be relied on to produce the necessary mixing. Nevertheless, several investigations were made of emergency procedures that could be used if the performance fell below an acceptable level. The question was raised whether reversal of the rotation rate starting at three revolutions per hour (rph) would provide useful mixing action in the oxygen tanks. An analysis of the stratification using a two-dimensional model for this problem is difficult because prolonged motion of the fluid leads to the requirement of a small time step to achieve stability in the numerical method. Therefore, approximate methods were used initially to reduce the required computing time. From our preliminary results based on the van der Waals equations it was concluded that spacecraft rotation reversals would indeed provide effective backup means for mixing the oxygen if normally occurring maneuvers proved to be insufficient. That conclusion is of continuing interest for future Apollo flights in which vehicle maneuvering is relied on to produce the necessary mixing in the oxygen tanks.

In this chapter we present results based on the accurate thermodynamic relations developed in chapter 4. The effects of tank stretch analyzed in chapter 5 are accounted for. The equations for the fluid motion and convection of heat used in the analysis are derived in chapter 2. The numerical method employed in the integration of the fluid mechanical equations is described in chapter 3. Special methods for suppressing cumulative errors that were used in the calculations are described in chapter 5. Our preliminary conclusions on the mixing effectiveness of rotational spacecraft maneuvers are verified and put on a firmer basis by the results in this chapter. The effects of changes in the rate of spacecraft rotation on additional types of stratification are investigated. Calculations showing the buildup of potential pressure decay (the pressure decay that would result from complete adiabatic mixing) during heater cycling are presented.

MIXING EFFECTIVENESS OF ROTATION REVERSAL

Calculations were made in which the vehicle was taken to be rotating initially at 3 rph. A series of initial stratified states were imposed with the temperature varying linearly across the tank. The hot fluid was placed in the stable position toward the center of rotation, which was outside the tank. Such stratification can be expected to develop after many heater cycles while operating with a steady vehicle rotation rate. In the absence of other vehicle maneuvering and with the heater turned off, the calculations show a very slow decrease in potential pressure decay and no motion of the fluid relative to the tank. The decrease in potential pressure decay in this case is due to conduction arising from the mild temperature gradient. When the direction of rotation is abruptly reversed, however, a swirling motion of the fluid ensues, leading to mixing and enhanced temperature gradients. Figure 6.1 depicts the velocity field in the flow that results. It comprises photographs of a cathode ray display tube on which were plotted the velocity vectors at the computational grid points. Sketch (a) shows the dimensions and orientation of the

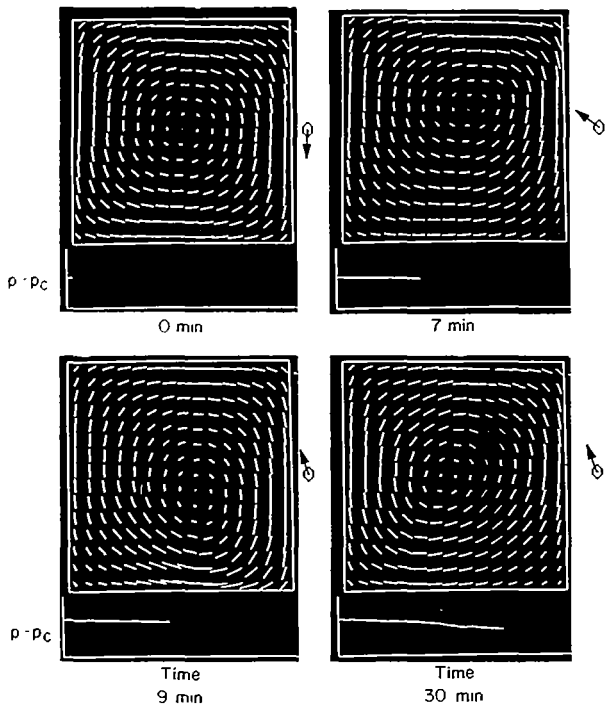

Figure 6.1.– Velocity vectors after rotation reversal.

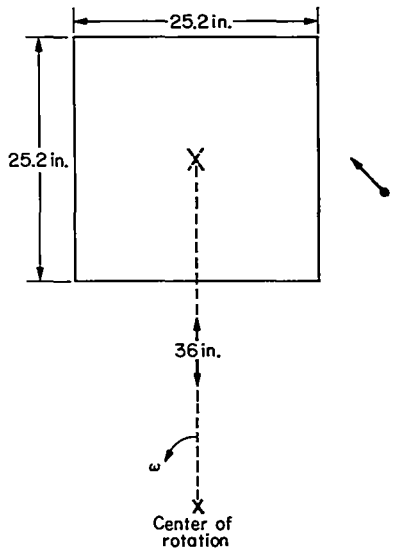

Sketch (a)

two-dimensional square-tank model. As indicated, the tank rotates counter-clockwise in the plane of the page about a center located at the center of the spacecraft. However, in the calculations a coordinate system is used that is fixed with respect to the tank and the center of rotation remains fixed at a position 1.5 tank diameters below the center of the tank. In all the photographs of figure 6.1 and later figures, the center of rotation is thus below the tank as indicated in the sketch. The arrow on the right in the photographs represents the position of a fixed star, such as the sun, with respect to the rotating tank. Thus when the rotation rate is steady, the arrow provides an indication of the passage of time. This feature was useful in viewing the cathode ray tube during calculations or in motion pictures of the displays. The upper left photograph in figure 6.1 shows the fluid velocity vectors in the tank immediately after rotation reversal. The magnitude of the velocity near the tank boundaries is about 0.02 ft sec^{-1}. The clockwise swirling motion shown results in part from the rotational inertia of the fluid, which tends to retain the motion it possessed before the rotation reversal of the vehicle. A lateral acceleration, present during the reversal, acts differentially on the stratified layers resulting in a significant contribution to the swirling motion. The other photographs in figure 6.1 show the velocity vectors at later times. The off-center swirl develops as a result of the stratification present and moves continuously in the clockwise direction, which is also the direction of motion of the fluid.

The graph at the bottom of each photograph in figure 6.1 is a plot of the potential pressure decay versus time from the beginning of the calculation. The scale is automatically decreased when the plot becomes overextended. In

the lower right photograph the time scale has been decreased by a factor of 2 relative to that in the other photographs.

Figure 6.2 shows the evolution of temperature distribution in the tank. For temperatures greater than the average, the deviations from the mean temperature are represented by vertical lines. As an aid to visualization, for temperatures less than average the deviations from the mean are shown as horizontal lines. In either case, the length of the lines indicates the relative magnitude of the temperature deviation from the mean at each computational grid point. The upper left photograph in figure 6.2 shows the initial assumed linear temperature distribution. The hot gas is toward the center of rotation. The remaining photographs show temperature distributions at later times after mixing has resulted from the swirling motion.

In figure 6.3 thermal stratification is viewed differently. The temperature distribution function described in chapter 4 (following eq. (4.24)) and in chapter 5 (preceding eq. (5.13)) is displayed in the form of histograms that indicate the number of computational grid points with temperatures within 1° K intervals. The unfilled histogram represents the initial linear temperature distribution. Gaps appear between the bars due to the discretization used in the numerical method. That is, every other 1° K interval did not happen to contain temperatures occurring at the computational grid points in the imposed linear temperature variation across the tank. The bars at 130° and 170° K are half the size of the others because the computational grid points at the tank boundaries are given half the weight of interior points, which represent twice as much fluid volume. During a calculation the temperatures change due to convection and conduction of heat. The heights of the bars change and the gaps are filled in. The shaded histogram in figure 6.3 shows the temperature distribution 40 min after a rotation reversal maneuver when considerable mixing has taken place and the steep temperature gradients that developed have reduced the temperature deviations from the average. If complete mixing were to take place, the temperatures at all computational grid points would fall within the same 1° K interval and the histogram would become a single bar at that temperature. As a supplement to the potential pressure decay, histograms of this type provide additional quantitative information on the stratification present in the tank.

In a preliminary unpublished paper we have shown that under certain conditions the decrease in potential pressure decay due to a rotation reversal according to a calculation based on the van der Waals equations is in rough agreement with results based on more exact thermodynamic relations. However, such agreement is not obtained in all cases of interest, as illustrated by a comparison of figures 6.4 and 6.5. Figure 6.4 shows plots of potential pressure decay versus the magnitude of linear temperature variations for several tank pressures according to the van der Waals equations. Figure 6.5 shows results for the same conditions based on the accurate thermodynamic relations of Stewart as described in chapter 4. It is easily seen that the van der Waals results disagree grossly with those based on Stewart's equations at both low and high levels of stratification. Our preliminary conclusions on the mixing effectiveness of a spacecraft rotation reversal although qualitatively correct are put on a firmer basis by the calculations utilizing accurate thermodynamics in this chapter.

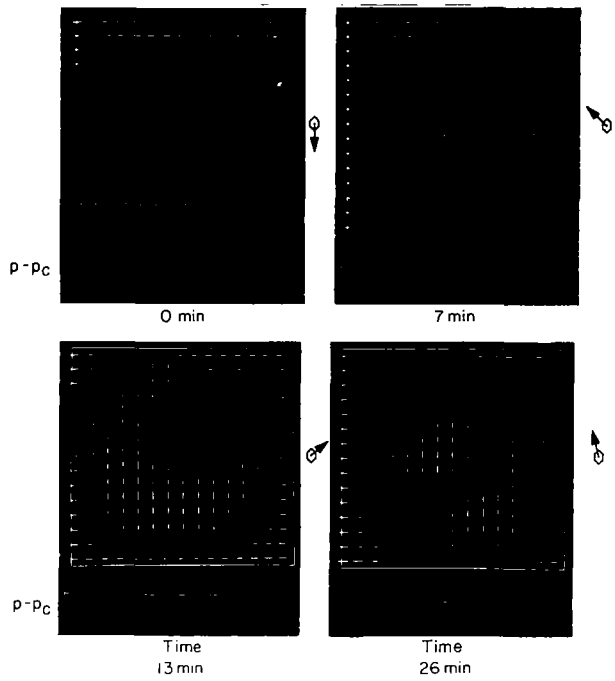

Figure 6.2.– Temperature distributions after rotation reversal.

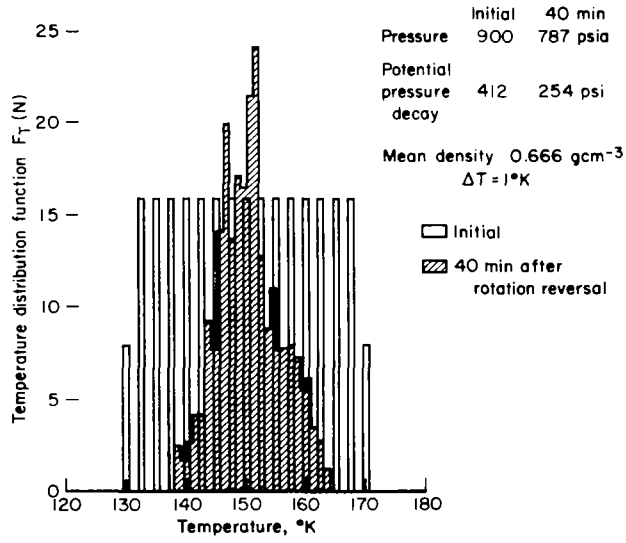

Figure 6.3.– Temperature distribution functions.

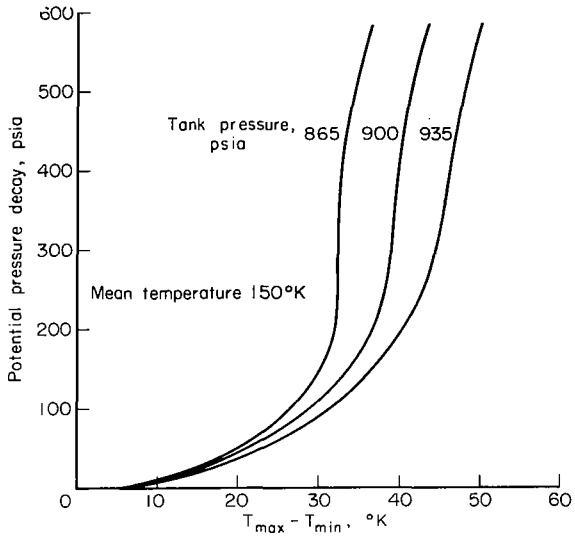

Figure 6.4.– Potential pressure decay for linear temperature variations; van der Waals equations.

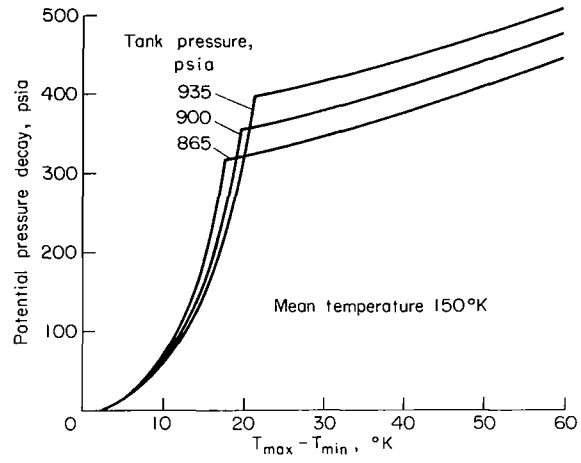

Figure 6.5.– Potential pressure decay for linear temperature variations; Stewart's equations.

The sharp bends in the curves contained in figure 6.5 are of interest. The flattening out takes place when a level of stratification is reached for which the collapsed state that would result from complete adiabatic mixing contains a two-phase mixture of liquid and vapor. Many other interesting aspects of the behavior of cryogenic oxygen are illustrated in the thermodynamic property plots presented in chapter 4.

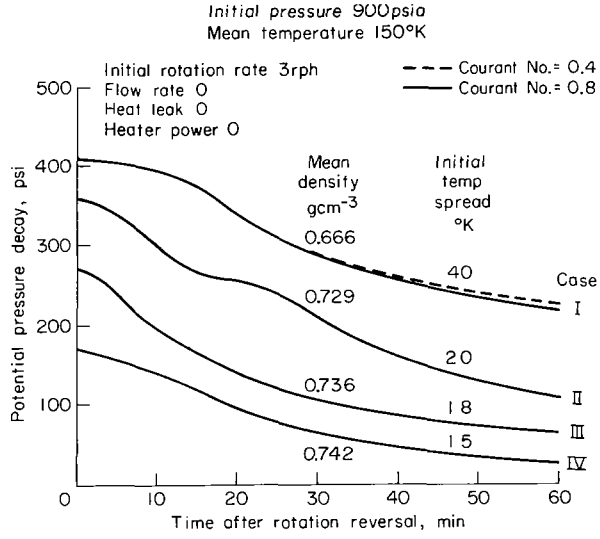

Figure 6.6.– Potential pressure decay after rotation reversal.

Figure 6.6 shows plots of potential pressure decay versus time after rotation reversal for four initial levels of stratification. The starting values of potential pressure decay in these plots can be obtained from figure 6.5. Decreases in potential pressure decay by a factor of about 2 or more result from a change in rate of spacecraft rotation from 3 rph to -3 rph.

The Courant number applicable to the numerical integration procedure used in the present calculations given in equation (3.28) can be written

$$\alpha = \frac{|U|\ \Delta t}{\Delta x} \tag{6.1}$$

where $|U|$ is the maximum speed present in the flow, Δt the time step, and Δx the spacing between computational grid points in both x and y directions. As discussed in chapter 3, the Courant number is a measure of the stability and

accuracy of the numerical integration procedure. Most of the calculations in this report were made with a value of $\alpha = 0.8$. Case I of figure 6.6 was also computed with $\alpha = 0.4$ (and smaller time steps according to eq. (6.1)) as indicated by the dotted line. Comparison of the dotted and solid line curves for case I in figure 6.6 shows that the predicted variation of potential pressure decay with time is insensitive to such a change in the Courant number. Appreciable variations in the flow variables extend over several computational grid points except in the boundary layer at the wall, which remains relatively thin during computation times considered here. Therefore, changes in the boundary layer do not significantly affect the evolution of the potential pressure decay, which depends on conditions in the main bulk of the fluid, in the rotation reversal problem. For this reason, the results are insensitive to a change in grid spacing from a 17 × 17 matrix to a 33 × 33 matrix. To save computing time, the latter computations were also made with a Courant number $\alpha = 0.8$.

MIXING EFFECTIVENESS OF SPINUP AFTER ATTITUDE HOLD

In the previous section, initial stratified states were considered that could be expected to result after many heater cycles with the spacecraft rotating at a steady rate (the so-called "passive thermal control mode"). Another case of interest is the type of stratification that would result after many heater cycles in a nonrotating state (attitude hold mode). In the absence of vehicle maneuvering, no convection currents would develop and the heat from the heater can spread into the gas only by conduction. A localized hot spot around the heater somewhat diffused by conduction and essentially zero fluid velocity are to be expected in this case. It is of interest to determine the mixing effectiveness of a spinup to a steady rotating state from such an initial stratified state. In the coordinate system fixed with respect to the tank, changes in rotation rate cause a rotating motion of the fluid. The velocity field that occurs as a result of spinup is similar to that shown in figure 6.1. Figure 6.7 illustrates the effect of spinup on the temperature distribution. It should be recalled that positive temperature deviations (from the mean temperature) are shown as vertical line segments and negative deviations are shown as horizontal line segments. The upper left photograph shows the initial assumed distribution. Subsequent distortions and dissipation resulting from the swirling motion are shown in the remaining photographs.

Figure 6.8 is a plot of potential pressure decay versus time after spinup. For comparison, a plot is included showing the very slow decrease in potential pressure decay that occurs as a result of conduction when the attitude hold condition is maintained. Again it is found that a change in vehicle rotation rate provides effective mixing action.

HEATER CYCLE

A pressure sensor is installed in the Apollo oxygen tanks and is used to automatically turn the heater on when the pressure drops below a lower limit of

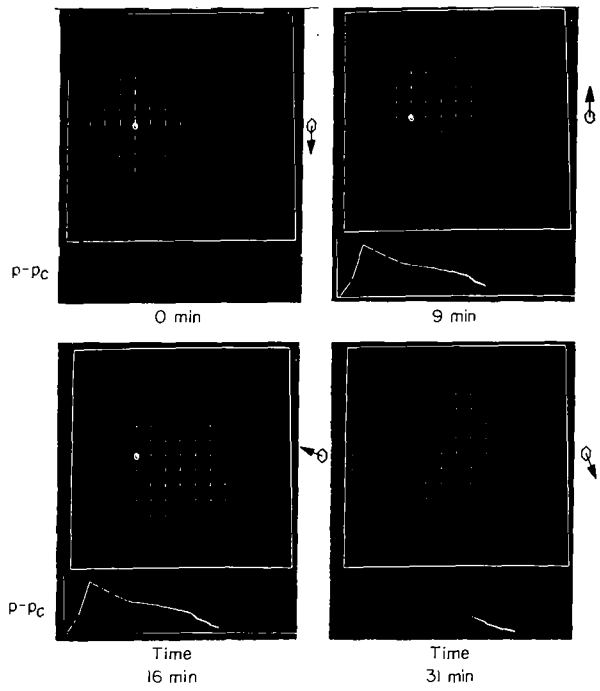

Figure 6.7.– Temperature distributions after spinup.

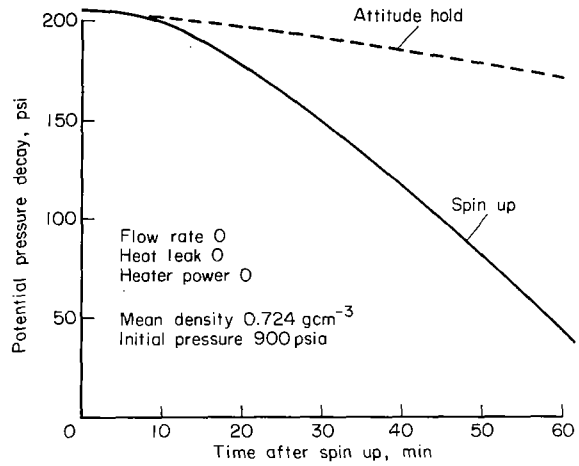

Figure 6.8.– Reduction in potential pressure decay due to spinup.

about 870 psia as a result of gas removal or pressure decay due to mixing. The heater is automatically turned off when the pressure rises above an upper limit of about 930 psia due to heating. As discussed in chapter 5 our machine program contains options for simulating the heater in either of two ways. One method utilizes a segment of the tank wall as a heater. In the other method, selected internal computational grid points can be utilized as heater elements to more nearly correspond to the actual position of the heater in an Apollo oxygen tank.

The photographs of figure 6.9 show the velocity and temperature distributions produced by cyclic operation of the two types of heater. The plots at the bottom of each photograph show the variations in potential pressure decay that have taken place since the beginnings of the calculations. When the heater is on, the potential pressure decay rises, and when the heater is off, it subsides, but there is a cumulative increase. About 2 hr (real time) have elapsed since the start of the calculation at the time of the photographs. During that time about six heater cycles have been completed. Additional information on the parameters of the calculations is given in the discussion of subsequent figures.

The upper left photograph in figure 6.9 shows the velocity vectors resulting from operation of a heater on the left wall. The upper right photograph shows the temperatures at the computational grid points. The temperature of hot fluid is represented by vertical line segments and the temperature of fluid cooler than average is indicated by horizontal lines. In either case, the

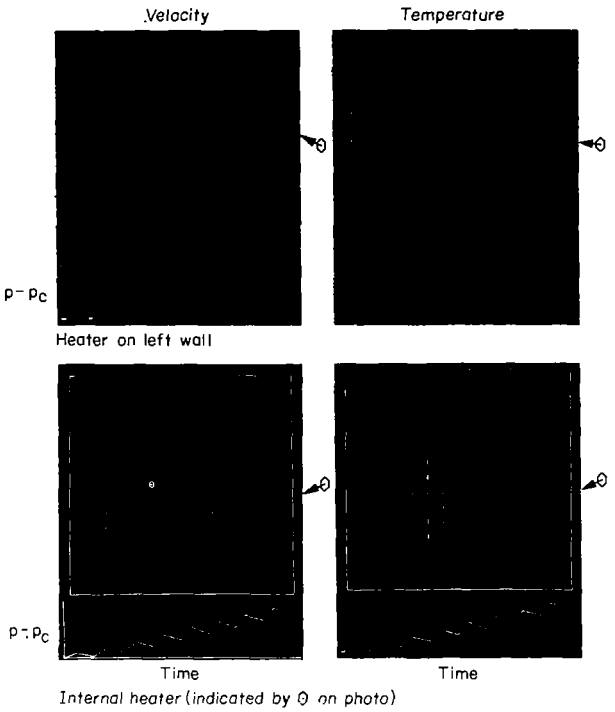

Figure 6.9.– Velocity and temperature distributions resulting from heater operation (0.4 rph).

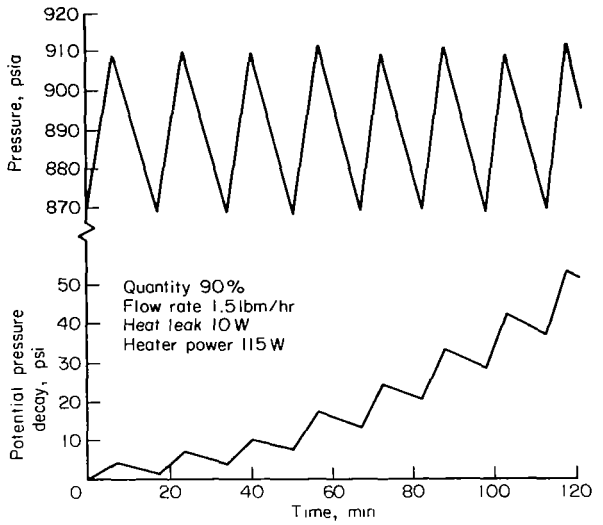

Figure 6.10.– Pressure cycles for square tank with wall heater (0.4 rph).

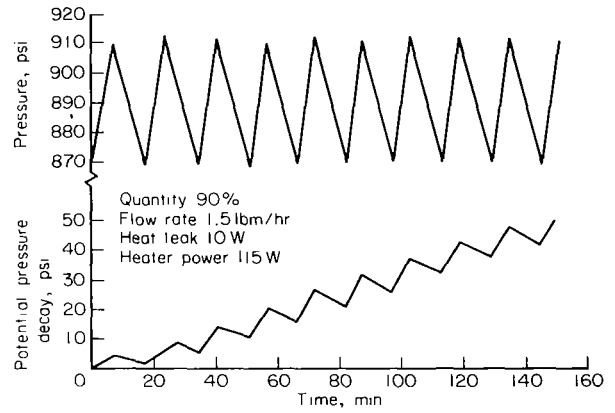

Figure 6.11.– Pressure cycles for square tank with internal heater (0.4 rph).

length of the line segment represents the deviation of the temperature from a reference value. Each time the heater is turned off, the reference temperature used in the display is readjusted to the value of the mean temperature in the tank. This is done so that hot fluid can be easily distinguished from cold fluid in the displays shown. For comparison, the velocity and temperature distributions arising from operation of an internal heater are shown in the lower two photographs of figure 6.9.

Figures 6.10 and 6.11 contain plots of pressure and potential pressure decay for the two heater positions. A steady spacecraft rotation rate of 0.4 rph was imposed. Additional parameters of the calculations are indicated on the figures. The notation QUANTITY = 90 percent indicates that the tank contains 90 percent of the amount of fluid it contained when full. FLOW RATE = 1.5 lbm/hr refers to the rate of fluid removal from the tank. HEAT LEAK - 10 W indicates that heat is leaking into the fluid from the exterior of the tank at the rate of 10 W. When the heater is on it produces heat at the rate of 115 W. The pressure rises due to heating when the heater is on and falls due to gas removal when the heater is off. Upper and lower pressure limits were imposed corresponding to data from

portions of the Apollo 14 flight. The results in figure 6.10 were generated using a wall heater, and the calculation represented by figure 6.11 was identical except for the use of an internal heater position. Comparison of the two figures shows that there are no gross differences arising from the position of the heater for the conditions of these calculations.

Figure 6.12 contains photographs showing velocity and temperature fields produced by prolonged heater cycling of an internal heater with the spacecraft rotating at a steady rate of 0.4 rph. The upper photographs were taken at a time corresponding to about 8 hr after the start of the calculation and the time of the lower photograph is 10 hr. The velocities remained small (less than 10^{-4} ft/sec) so that the stability criteria of the numerical method allowed a large time step (0.5 min) in the integration. The total computing time on an IBM 360-67 computer was 46 min. The photographs of temperature distribution on the right of figure 6.12 are somewhat similar to the assumed initial linear distributions used for previous calculations in this article. With prolonged heater cycling during steady spacecraft rotation, it is seen that there is a tendency for the hot gas (represented by vertical line segments) to collect at the bottom of the tank in the direction of the center of rotation. On the plots of potential pressure decay at the bottom of each photograph in figure 6.12, in the lower two frames the time scale has been halved relative to that in the upper two frames. These plots show that the cumulative rise in potential pressure decay does not continue indefinitely when the spacecraft is rotating. Instead a plateau is reached when the velocity past the heater has built up sufficiently that the incoming heat is convected to other regions of the tank rather than continuing to accumulate in a small region near the heater. As this natural convection effect continues to grow, there is a decrease in the level of the potential pressure decay. In the lower two frames of figure 6.12, it can be seen that near the end of the calculation the cumulative increase in potential pressure decay has resumed. This is probably due to the accumulation of hot gas at the bottom, which tends to counteract the driving force of the natural convection and reduce the velocity of flow past the heater. The highest level of potential pressure decay reached in this calculation was about 80 psi.

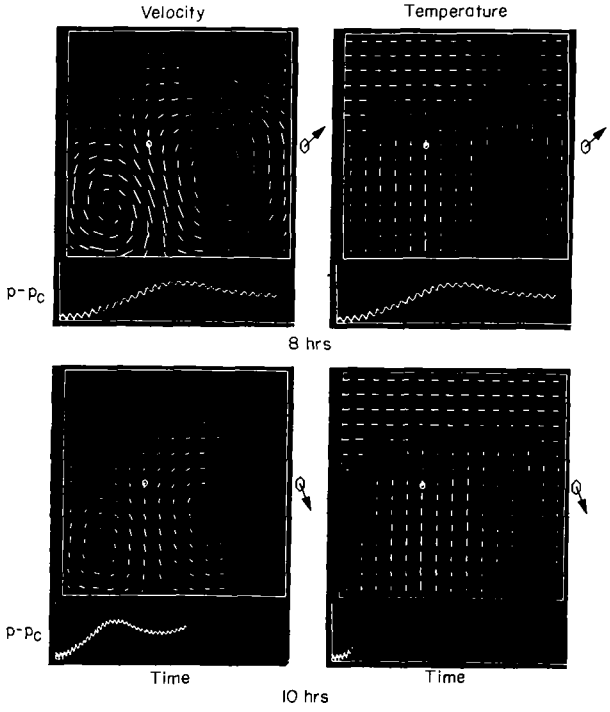

Figure 6.12.– Velocity and temperature distributions after prolonged heater cycling at 0.4 rph.

Figure 6.13 shows the effect of a change in spacecraft rotation rate on the cumulative rise in potential pressure decay. In this calculation the spacecraft was not rotating initially. The cyclic heater operation resulted

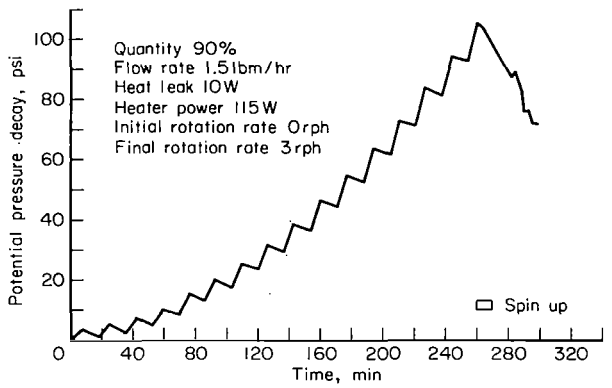

Figure 6.13.– Effect of spinup on cumulative rise in potential pressure decay.

in a rise of potential pressure decay to a level above 100 psi. At a real time 260 min after the start of the calculation, a spinup to 3 rph was initiated and completed in about 10 min. The rotation rate was held steady thereafter. Figure 6.13 shows that the change in spacecraft rotation rate resulted in an appreciable decrease in the potential pressure decay. The forced convection introduced by the maneuver entails larger fluid velocities than those arising from natural convection in the previous case considered. Furthermore, these larger velocities persist rather than being suppressed by accumulations of hot fluid on the side of the tank toward the center of rotation. Consequently, the potential pressure decay would be expected to continue to decrease if the calculation had been continued to longer times. The machine computing time on this run was 64 min. About two-thirds of that time was spent in the part of the calculation after the change in rotation rate. As a result of the maneuver the velocities became relatively large (~0.005 ft/sec), and the size of time step required for numerical stability decreased by more than an order of magnitude.

DISCUSSION

It is appropriate to discuss the probable effect of several approximations that were employed in this investigation. Two-dimensional simulation of the flow in a spherical tank was necessitated by the limited speed and storage capacity of the currently available computational facilities. If a highly stratified state is present in the tank with an appreciable fraction of the oxygen at a temperature 10° or more above the average temperature, a small temperature gradient will develop. Due to the low thermal diffusivity of cryogenic oxygen, such a nonuniform condition can persist for many hours if the flow velocity is negligible. The fluid velocity induced by spacecraft maneuvering will lead to penetration of the hot fluid by cold streams and lengthen the boundary between hot and cold regions. The enhanced temperature gradients and lengthened regions of heat exchange promote a more rapid trend toward a uniform temperature. The extent to which this occurs in a two-dimensional simulation should be indicative of the same trend in the actual three-dimensional flow if the driving force is in the direction of the two dimensions considered. There is no apparent reason to expect a large order-of-magnitude error in the estimate of mixing effectiveness from the two-dimensional calculations.

It was not possible to adequately resolve the thermal and viscous boundary layers that would occur in a real flow. Estimates based on the viscous flow over a flat plate indicate that the boundary layer at the tank wall due to

changes in rate of spacecraft rotation would be laminar. Also the boundary layer would not encompass an appreciable fraction of the fluid in the tank for periods up to 2 hr after a change in rate of rotation, if the fluid were initially at rest relative to the tank. During such times, the calculations show appreciable mixing in the main body of the fluid due to interaction of the acceleration field with the nonuniform density distribution in the stratified field. Therefore, it is not expected that accurate treatment of the boundary layer at the wall would appreciably alter our predictions of the response of the potential pressure decay to spacecraft maneuvers. The thermal and viscous boundary layer that develops at the heater was also not adequately resolved in our calculations. However, the nonuniform temperature distributions produced by the approximate heater simulation provide worthwhile tests of the mixing effectiveness of spacecraft maneuvers.

An objection can perhaps be raised to the use of a coarse computational grid spacing. Physical instabilities may develop in the boundary between hot and cold regions of a moving fluid. Generally, it is not possible to distinguish such an occurrence from a numerical instability. Special methods that have been used to control the numerical stability may therefore have eliminated physically real effects. In that case, the calculations should provide a conservative estimate of the mixing effectiveness of a spacecraft maneuver.

Because of the previous existence of numerical methods for computation of fluid flows in rectangular enclosures, it was expedient to consider first the flow in a rotating tank of square cross section. The coarse grid spacing and the special methods employed to control stability may have obscured physically real effects that would occur near the corners in an actual fluid flow in a rotating enclosure of square cross section. The error from such effects would be expected to grow with time and could be appreciable for long computation times. For the present purpose, omission of such corner effects is not objectionable since our purpose is to simulate the flow in a spherical tank without corners. We have developed a machine program for computing the two-dimensional flow in a rotating tank of circular cross section. Preliminary results from that program were presented in unpublished reports at the MSC Cryogenics Symposium. No gross differences were found in predictions of the mixing effectiveness of changes in spacecraft rotation rate based on calculations for square or circular cylindrical tank geometries.

The present investigation has been confined to large tank quantities (large values of the ratio of fluid mass to the mass when the tank is full). Unpublished work of C. K. Forester, D. D. Rule, and H. W. Patterson has shown that the levels of potential pressure decay to be expected decrease rapidly with decreasing tank quantity for values of tank quantity below about 70 percent. This occurs because of the departure of the fluid state from the proximity of the critical point as fluid is removed from the tank and the fluid density decreases. At a tank quantity of 10 percent the properties of oxygen are approximately those of a thermally and calorically perfect gas for which the potential pressure decay is zero regardless of the degree of stratification. For this reason, from the operational point of view, the response of the fluid states to spacecraft maneuvers is of greater interest when the tank quantity is large.

CONCLUDING REMARKS

The effectiveness of rotational spacecraft maneuvers as a means for producing necessary mixing in the Apollo oxygen tanks has been investigated. Photographs of a cathode ray display tube have been presented illustrating the convection currents resulting from changes in rate of rotation and from natural convection. Results have been presented showing the cumulative buildup of potential pressure decay that occurs due to intermittent operation of the heater used to maintain the pressure in the tank during removal of fluid.

There are several significant contributions from the present investigation toward a better understanding of conditions in the Apollo oxygen tanks during flight. We find that the mixing due to interaction of fluid density gradients with the acceleration field from rotational spacecraft maneuvers takes place in times that are short compared to those required for mixing due to viscous effects. For example, unpublished results from water tank simulation experiments of J. F. Lands, Jr., and R. C. Ried, Jr., indicate that times of order 4 to 20 hr are required for the effects of a spacecraft rotation reversal to spread throughout the bulk of the fluid. In contrast, our results, which include the effects of density gradients, show considerable mixing throughout the fluid volume in less than 1 hr. For reasons previously discussed, our calculations represent a conservative estimate of the amount of mixing to be expected in actual flight.

The levels of potential pressure decay to be anticipated according to our calculations are in reasonable agreement with previous estimates from Apollo 12 data and stratification analyses. We concur in the conclusion that dangerous levels of stratification will not occur with mass flow rates and acceleration fields corresponding to past and anticipated Apollo operational practices. If as a result of departures from usual practice, an unacceptable level of stratification is believed to exist during flight, we find that return to a safe level can be achieved by mild changes in the rate of spacecraft rotation. A change in rotation rate of three revolutions per hour produces a reduction in potential pressure decay by a factor of 2 or more in 1 hr. Again, this represents a conservative estimate.

In the event of future space-flight applications that require scaling of the Apollo design with respect to time or size, the computational methods of this report are applicable for estimating the levels of stratification and the response to spacecraft maneuvers to be anticipated.

NASA-Langley, 1972 — 12 A-4224

"The aeronautical and space activities of the United States shall be conducted so as to contribute . . . to the expansion of human knowledge of phenomena in the atmosphere and space. The Administration shall provide for the widest practicable and appropriate dissemination of information concerning its activities and the results thereof."

—NATIONAL AERONAUTICS AND SPACE ACT OF 1958

NASA SCIENTIFIC AND TECHNICAL PUBLICATIONS

TECHNICAL REPORTS: Scientific and technical information considered important, complete, and a lasting contribution to existing knowledge.

TECHNICAL NOTES: Information less broad in scope but nevertheless of importance as a contribution to existing knowledge.

TECHNICAL MEMORANDUMS: Information receiving limited distribution because of preliminary data, security classification, or other reasons.

CONTRACTOR REPORTS: Scientific and technical information generated under a NASA contract or grant and considered an important contribution to existing knowledge.

TECHNICAL TRANSLATIONS: Information published in a foreign language considered to merit NASA distribution in English.

SPECIAL PUBLICATIONS: Information derived from or of value to NASA activities. Publications include conference proceedings, monographs, data compilations, handbooks, sourcebooks, and special bibliographies.

TECHNOLOGY UTILIZATION PUBLICATIONS: Information on technology used by NASA that may be of particular interest in commercial and other non-aerospace applications. Publications include Tech Briefs, Technology Utilization Reports and Technology Surveys.

Details on the availability of these publications may be obtained from:

SCIENTIFIC AND TECHNICAL INFORMATION OFFICE

NATIONAL AERONAUTICS AND SPACE ADMINISTRATION

Washington, D.C. 20546